

LIBRARY Michigan State University

This is to certify that the

dissertation entitled

COUPLED MULTIOBJECTIVE OPTIMIZATION OF CRASHWORTHINESS AND MODAL FREQUENCIES IN STRUCTURES USING GENETIC ALGORITHMS

presented by

David J. Eby

has been accepted towards fulfillment of the requirements for

Ph.D. degree in Mechanics

major protessor

Ronald C. averill

Date December 5, 2000

MSU is an Affirmative Action/Equal Opportunity Institution

0-12771

PLACE IN RETURN BOX to remove this checkout from your record. TO AVOID FINES return on or before date due. MAY BE RECALLED with earlier due date if requested.

DATE DUE	DATE DUE	DATE DUE
NOV 0 4 20C3		
0013		
	7	

11/00 c:/CIRC/DateDue.p65-p.14

COUPLED MULTIOBJECTIVE OPTIMIZATION OF CRASHWORTHINESS AND MODAL FREQUENCIES IN STRUCTURES USING GENETIC ALGORITHMS

Ву

David J. Eby

AN ABSTRACT OF A DISSERTATION

Submitted to
Michigan State University
in partial fulfillment of the requirements
for the degree of

DOCTOR OF PHILOSOPHY

Materials Science and Mechanics Department

2000

Professor Ron C. Averill

ABSTRACT

COUPLED MULTIOBJECTIVE OPTIMIZATION OF CRASHWORTHINESS AND MODAL FREQUENCIES IN STRUCTURES USING GENETIC ALGORITHMS

By

David J. Eby

This dissertation presents an approach to concurrent optimization of structures by using an island injection Genetic Algorithm for: 1) crash energy management, 2) modal vibration frequency response, 3) peak crush force, 4) weight reduction, and 5) manufacturability, while considering stochastic variability of design variables and loading conditions. Existing automated design technology has never simultaneously addressed all of these competing mechanisms. In addition, this dissertation presents the development of a geometrically nonlinear first-order zig-zag sublaminate theory and finite element model which accounts for moderately large displacements and moderate rotations using a Total Lagrangian formulation. The accuracy of the model is demonstrated by comparing its structural response predictions with results from previous experimental investigations and with numerical tests. Finally, the optimal design of sandwich panels was approached with a simple Genetic Algorithm and the developed geometrically nonlinear first-order zig-zag sublaminate finite element model.

Copyright by David J. Eby 2000

DEDICATION

I would like to dedicate this body of work to all of my family and friends.

This includes my mother, father, three brothers, two sisters and many friends. In particular, Karen Kneibes for her love, patience, and understanding.

ACKNOWLEDGMENTS

I would like to express my gratitude to Dr. Ron Averill, Dr. Erik Goodman, Dr. William Punch III, Dr. Alejandro Diaz, and Dr. Baisheng Yan for serving on my defense committee. Also, John Madakacherry of General Motors provided insurmountable insight and leadership during the duration of this work. I would also like to acknowledge the support of the Computational Mechanics Research Group and the Genetic Algorithms Research and Application Group at Michigan State University for all of their patience and advise. I would like to thank my advisor, Professor Ron Averill, for helping me develop the tools needed to overcome the many challenges of life and research - without his guidance, understanding, and foresight none of this work would have been completed.

TABLE OF CONTENTS

List of Tables	vii
List of Figures	
Chapter 1: Introduction	
1.1 Introduction	1
1.2 Literature Review	
1.3 Present Study	
Chapter 2: The Mechanics of Genetic Algorithms	• •
2.1 Introduction.	16
2.2 Simple Genetic Algorithms	
2.3 Pros and Cons of Genetic Algorithms	
2.4 Island Injection Genetic Algorithms	
Chapter 3: Optimization of Crashworthiness and Modal Frequencies	
of Automotive Structures	
3.1 Introduction.	28
3.2 Optimization Problem Statement	
3.3 Optimization Objective Functions	
3.4 Optimization Constraints	
3.5 Application of Island Injection Genetic Algorithm	
3.6 Results	
3.7 Conclusions	41
Chapter 4: Development of a Geometrically Nonlinear First Order Zig-Zag	
Finite Element Model	
4.1 Introduction	65
4.2 Basic Ingredients Needed For The First-Order	
Zig-Zag Plate Theory	68
4.3 Virtual Work	
4.4 Finite Element Model	75
4.5 Newton-Raphson Method	78
4.6 Finite Element Approximations	80
4.7 Numerical Results	82
4.8 Conclusions	89
Chapter 5: Optimization of Sandwich Panels using Genetic Algorithms	
5.1 Introduction	
5.2 Optimization Problem Statement	
5.3 Results	112
5.4 Conclusions	
Chapter 6: Summary and Conclusions	121
Appendix A	122
References	

T

LIST OF TABLES

Table 3.1.	Target values of inequality constraints for fitness function 62	2
Table 3.2.	Weight values used for fitness function 62	2
Table 3.3.	Genetic operator rate for each island in the island injection Genetic Algorithm62	2
Table 3.4.	Primitive and thickness design variable information 63	3
Table 3.5.	Crush evaluation times per island and load case63	3
Table 3.6.	Number of full and partial design evaluations63	3
Table 3.7.	Thickness design variables for each best design63	3
Table 3.8.	Objective and constraint data for the best design found in three different independent runs64	1
Table 3.9.	Stochastic variability of internal energy for the best designs found (20 independent evaluations) with respect to thickness64	
Table 4.1.	Material properties for square single-layer orthotropic plate 10)7
Table 4.2. l	Material properties for square cross-ply laminated plate (0/90/90/0)10)7
Table 4.3. l	Material properties for sandwich panel10)7
Table 4.4. l	Lamination scheme for sandwich panel10)7
Table 4.5.	The effect of transverse refinement considering small displacements10)8
Table 5.1. l	Ply material properties11	19
Table 5.2.	Core material properties12	20
Table 5.3. l	Baseline and optimized sandwich panel design variables. All material names are in reference to Tables 5.1 and 5.212	20
Table 5.4.	Baseline and GA optimized sandwich panel objectives and constraints	20

LIST OF FIGURES

Figure 2.1. S	Simple Genetic Algorithm Structure	.27
Figure 2.2. A	simple iiGA topology that simultaneously searches various levels of resolution of the design space on three separate computational nodes (islands)	.27
Figure 3.1 B	iasing of cross sectional primitives along the length of a rail structure	.43
Figure 3.2 S	Surface of rail structure is developed with a linear blending of the cross sectional primitives. The surface was smoothed at each of the cross sectional primitive locations.	44
Figure 3.3. F	Potential thickness changes occurred at the placement of each cross sectional primitive	.45
Figure 3.4. C	Cross sectional primitive library that contains a set of knowledge-based manufacturable cross sections	. 46
Figure 3.5. I	Finite element model and of rail structure running into a stationary rigid wall for the first load case. A lumped mass was placed directly behind the rail structure	47
Figure 3.6. I	Finite element model and of rail structure running into a stationary rigid wall for the second load case. An eccentric lumped mass was placed behind the rail structure	48
Figure 3.7. A	In iiGA topology that breaks down the design space into three levels of design variable and evaluation time based resolutions with multiple load cases	. 49
Figure 3.8. A	an iiGA topology that monitors islands the performance of the best designs for the two objectives defined by two structural load cases	50
Figure 3.9. C	Crush zone internal energy as a function of generation number for load case 1, island 9	51
Figure 3.10.	Normalized constraints as a function of generation number for island 9. A feasible design has normalized mass, force, and manufacturability constraints which are less than or equal to unity. A feasible design also has normalized first and second modal frequency constraints which are greater	

F

Fi

Fi

Fi

	than or equal to unity 52
Figure 3.11.	Crush zone internal energy as a function of generation number for load case 2, island 1853
Figure 3.12.	Normalized constraints as a function of generation number for island 18. A feasible design has normalized mass, force, and manufacturability constraints which are less than or equal to unity. A feasible design also has normalized first and second modal frequency constraints which are greater than or equal to unity
Figure 3.13.	Crush zone internal energy as a function of evaluation number for load cases 1 and 2 from monitoring island55
Figure 3.14.	Normalized constraints as a function of evaluation number for monitor islands. A feasible design has normalized mass, force, and manufacturability constraints which are less than or equal to unity. A feasible design also has normalized first and second modal frequency constraints which are greater than or equal to unity
Figure 3.15.	Animation of deformation for the best design found (load case 1)
Figure 3.16.	Animation of deformation for the best design found (load case 2)58
Figure 3.17.	Surface models for best design found, run 159
Figure 3.18.	Surface models for best design found, run 2 60
Figure 3.19.	Surface models for best design found, run 361
Figure 4.1. S	chematic of ply stacking and coordinate system used in first-order sublaminate theory90
Figure 4.2. E	lement topology for the eight-noded brick and the six-noded wedge finite elements based on first order zig-zag sublaminate theory90
Figure 4.3. L	oad versus deflection for a square simply-supported single-layer orthotropic plate under uniform pressure at various levels of in-plane and through-thickness refinement 91
Figure 4.4.L	pad-deflection curves for the clamped square cross ply

F

F

Fi

Fi

Fi

Fig

Fig

Figi

Figu

Figu

Figu

Figur

	plate (0/90/90/0) under uniform pressure at various levels of in-plane and through-thickness refinement92
Figure 4.5. L	inear and nonlinear load versus deflection at the top of a simply-supported square sandwich panel under uniform pressure using first-order zigzag sublaminate theory
Figure 4.6. L	inear and nonlinear load versus deflection at the bottom of a simply-supported square sandwich panel under uniform pressure using first-order zigzag sublaminate theory94
Figure 4.7. T	Through-thickness variation of total X1-displacement at the plate midspan and X1=095
Figure 4.8. T	Through-thickness variation of total X2-displacement at the plate midspan and X2=096
Figure 4.9. T	Through-thickness variation of the normal Cauchy stress (in the X1-direction) at the Gauss points nearest to the center of the plate
Figure 4.10.	Through-thickness variation of the normal Cauchy stress (in the X2-direction) at the Gauss points nearest to the center of the plate
Figure 4.11.	Through-thickness variation of the normal Cauchy stress (in the X1-direction) for the top five layers of the sandwich panel at the Gauss points nearest to the center of the plate99
Figure 4.12.	Through-thickness variation of the normal Cauchy stress (in the X2-direction) for the top five layers of the sandwich panel at the Gauss points nearest to the center of the plate100
Figure 4.13.	Through-thickness variation of the normal Cauchy stress (in the X3-direction) at the Gauss points nearest to the center of the plate
Figure 4.14.	Through-thickness variation of transverse normal strain (ϵ_{33}) at the Gauss points nearest to the center of the plate 102
Figure 4.15.	Through-thickness variation of the transverse Cauchy stress (σ_{23}) at the Gauss points nearest to the center of the plate103
Figure 4.16.	Through-thickness variation of the transverse Cauchy stress (σ_{13}) at the Gauss points nearest to the center of the plate104

Figure 4.17.	Through-thickness variation of the in-plane Cauchy stress (σ_{12}) at the Gauss points nearest to the center of the plate	105
Figure 4.18.	Measurement points for the displacements, strains, and stresses for the sandwich panel	106
Figure 5.1. F	inite element mesh including applied boundary conditions. Location of maximum transverse displacement and failure index. The sandwich panel is 24 inches wide and 84 inches long	115
Figure 5.2. T	he mass of the best design found as a function of generation number	116
Figure 5.3. N	lormalized constraints of the best design found as a function of generation number	117
Figure 5.4. L	inear and geometrically nonlinear load deflection response curves for the baseline and simple GA optimized sandwich panels	118

1.

gr va

cr

ba

the

ur

op

to ap

ех

rec

spa

COF

sea

res

Chapter 1

INTRODUCTION

1.1 Introduction

Current automated design technology generally requires computation of gradients of the objective functions and constraints with respect to the design variables in order to identify a better design. Due to the noisy, chaotic nature of crash problems, gradients of objectives and constraints with respect to typical structural design variables are difficult, if not impossible, to attain. A gradient-based optimization approach assumes that the objectives and constraints are unimodal with respect to the design variables, and will seek extremal portions of the design space where the gradients are equal to zero. A gradient-based optimization approach experiences difficulties in multimodal design spaces due to the fact that many local extrema may exist, making it difficult for such an approach to escape a local minimum. Typically, many real-life design spaces are extremely multimodal.

A Genetic Algorithm (GA) is a global search technique that does not require the computation of gradients for the minimization of objectives or constraint violations, with the ability to consider stochastic behavior of the design space. An Injection Island Genetic Algorithm (iiGA) can help increase the computational efficiency of a simple GA with a divide-and-conquer approach by searching a discretized design space simultaneously at various levels of resolution in a heuristic hierarchical fashion (Goodman, 1996).

prot Lan she This

opti

and in fr

mat

loca can

stati

then

mate

The beco

sequ

Fiber reinforced laminated composites have a natural ability to be optimized. Additional design variables are introduced into the optimization problem statement when laminated fiber reinforced composites are considered. Laminated composites are orthotropic in the plane with low ratio of transverse shear modulus to in-plane modulus and are laminated through-the-thickness. This allows for a rich design space when compared to standard monolithic materials. Fiber reinforced laminated composites also have high specific strength and stiffness when compared to conventional monolithic materials. This increase in freedom and flexibility is not free; the cost is complex structural behavior at local and global levels. Fiber reinforced laminated composite lamination schemes can be specifically constructed to optimally perform under complex loads (large static loads and large dynamic impact loads). Fiber reinforced composite material behavior is unique and complex at both the local and global level and therefore difficult to predict, especially when considering geometric nonlinearities. The task of manually designing an optimal laminated composite structure becomes staggeringly hindersome when a large number of discrete lamination sequences is coupled with complex geometric nonlinear structural behavior.

•

st

ar

Cl

W

str

line str

dov

app

pert

litera

struc of G

litera reinfo

are si

stocha

1.2 Literature Review

The purpose of this literature review will be to give an overview of the current level of automated design and composite technology while setting the stage to define the uniqueness and overall contribution of this research. A huge amount of research has been performed in the area of structural optimization. With such a broad area of research, it is impossible to review all aspects of structural optimization. Since the focus of this dissertation is the optimization of structures considering nonlinear behavior, this literature review will not include a broad view of optimization problems where the structure is considered to behave linearly. Very few researchers have been successful in the area of optimization of structures while considering nonlinear behavior. The literature review is broken down into five major parts. The first part will contrast various optimization approaches. In the second part of the literature review, relevant papers pertaining to classical optimization will be discussed. The third part of the literature review will present papers regarding the optimization of robust structures. The fourth part of the literature review will contain recent applications of GAs in appropriate areas of structural optimization. Finally, the fifth part of the literature review will refer to papers dealing with the development of fiber reinforced laminated composite finite elements.

Optimization approaches include hill climbing, stochastic search, directed stochastic search and hybrid methods. Hill climbing or gradient-based methods are single-point search methods that have been applied successfully to many

; ; ;

> nı re

> > ev: thu

rec

et a

was The

the r

Point

shape optimization problems (see Soto and Diaz, 1993, and Suzuki and Kikuchi, 1991). Gradient-based methods are less applicable to problems in which the design space is nonconvex and multimodal (see Sangen, 1990). search methods simply evaluate randomly sampled designs in the search space, and are therefore generally limited to problems that have small search spaces, if practical search times are required. A directed random search method, such as a Genetic Algorithm (GA), is a multiple-point, directed stochastic search method that can be an effective optimization approach to a broad class of problems (Goldberg, 1988). The use of GA's for optimal design requires that a large number of possible designs be analyzed, even though this number generally still represents only a miniscule fraction of the total design space. When each evaluation is computationally intensive, a traditional simple or parallel GA can thus be difficult to apply. Injection Island Genetic Algorithms (iiGA's) can help reduce the computational intensity associated with typical GA's by searching at various levels of resolution within the search space (see Eby et al., 1999, Mallot et al., 1996).

Application of gradient-based topological optimization for crashworthiness was attempted with success using homogenization (see Mayer, et al., 1996). The objective of the optimization problem was to maximize the internal energy of the rear rail of an automobile with a single inequality constraint on total mass. The objective function was a weighted sum of the internal energy at specified points in time. The crash analysis was performed with LS-DYNA, an explicit finite

ļ

e

0

W

m. Th

ele

gra

bo pro

poi pre

spe spa

beg

element code. A homogenization method was used to compute the elastic and plastic moduli as a function of the density of the material. The technique begins searching from a "baseline" design, where gradients of the objective and constraint are computed with respect to the density of the material for each finite element. These gradients directed a search algorithm which determined a set of design variables (material densities) to find a better design in terms of the objective and constraint. The final design had a 47% increase in internal energy when compared to the original "baseline" design. The paper makes reference to a stiffer structure, without specifying the actual peak crush force. No constraints were placed on: peak crush force, modal response, packaging or manufacturability. Stochastic variation of gage thickness was not considered. The paper did show that an optimality condition exists, requiring that each finite element must have a constant strain energy.

The construction of response surfaces can provide information needed for gradient-based optimization. Roux et. al (1996) constructed response surfaces of nonlinear structural analysis considering material, geometric and contact boundary conditions for a semi-solid tire. The objective of the optimization problem was to minimize the mass of the design while minimizing strain at a point. Constraints were placed on the deflection of a point on the design under a prescribed load. The design variables included the thickness of the tire at specified regions and the number of "webs" in the design. "Webs" determine the spacing of material inside the tire which contains air chambers. The authors began the optimization procedure with a crude finite element model to represent

ſ

ot

٧á

va ap

inc

gra Vie

clas

(19) stat

resp

to un

Sund

the initial design. Final design iterations in the optimization procedure were performed using a refined finite element model. This optimization process represents an attempt to perform a reasonable approximation of the behavior of the design early in the optimization process while refining the finite element model later in the optimization run to capture more complex structural behaviors.

A design can be considered robust when small changes in the design variables and/or loadings produce little or no effect on the behavior of the objective function and constraints. It is often desirable to desensitize the objective function and constraints with respect to small changes in the design variables. Kushel and Rackwitz (1998) formulated a classical gradient-based approach to reliability-based structural optimization. This was accomplished by incorporating a smooth differentiable failure probability function into the classical gradient-based optimization problem statement as a set of constraints. Similarly, Vietor (1997) approached a stochastic distribution of design variables with a classical optimization approach as a set of constraints. Gausser and Schuller (1997) considered optimization of a geometrically nonlinear truss structure with statistical uncertainties for loading and structural properties through the use of response surfaces.

The idea of robust optimization through desensitizing engineering systems to uncertainties, such as manufacturing errors and operational variances has been the subject of much research (see Belegundu, 1992, Khot, 1991, and Sundaresan, 1992). Traditionally, the sensitivities of optimal designs are

r

a١

01

m

Wi

op Qu

199

str

Mai

Has

199

GAs cras

neur

the s

minin

The o

recorded after the products are manufactured. G. Taguchi (1985) developed a method to measure sensitivity of a system during the initial design process. The method was first developed at a time when little computer simulation was available, so most data was gathered from actual experiments. Taguchi used orthogonal arrays for approximating the expected design sensitivity to be efficient with respect to the number of evaluations, due to the lack of compute power.

Many researchers are currently investigating application of GAs for the optimal design of structures using various numerical methods (Genta, 1995 and Queipo, 1994). Most papers apply GAs to optimization problems that assume the structure behaves in a linear fashion (see Chapman, 1996; Eby, 1999; Fabbri, 1997; Flynn, 1995; Foster, 1997; Furura, 1993; Furura, 1995; Genta, 1995; Haslinger, 1996; Keane, 1995; Kosigo, 1993; Le Riche, 1993; Mallot, 1996; Mares, 1996; Parmee, 1997; Punch, 1995; Punch, 1994; Rajan, 1995; Sangren, 1990 and Wolfersdorf, 1997)

Optimization of structures considering nonlinear structural response using GAs has been applied successfully by Hajela and Lee (1997). Hajela considered crashworthiness of rotorcraft subfloor structures with a GA in conjunction with a neural network. A crash model was developed to capture the overall behavior of the structure through the use of lumped masses, nonlinear beam elements and nonlinear spring elements. The objective of the optimization problem was to minimize the accelerations experienced by the occupants for multiple load cases. The objective was minimized by determining the optimal load-deflection behavior

ol tra ne se ar

> fur inte

de

loca obje

Obje

surf

sequ

serio dem

was i

of energy absorbing elements while simultaneously finding their optimal location in the structure. The neural network constructed a response surface of the objective function (acceleration experienced by the occupant) based on a set of training data points (in terms of design variables). The surface from the neural network seeks to approximate the behavior of the structure in a least squares sense from the data points, and can be viewed as a form of nonlinear regression analysis. It was shown, for this problem, that the neural network adequately represented the actual response of the objective function with respect to the design variables. The load-deflection curves were defined as piecewise linear functions. An energy balance of the initial kinetic energy of the system and the internal energy of the structure at rest was performed to produce realistic bounds on peak force of the load-deflection curves. The second set of design variables was the topological placement of the energy absorbing components at discrete locations. The acceleration levels for two load cases were weighted in the objective function. Multiple independent runs with different weights placed on the objectives were performed to obtain a Pareto front. A Pareto front is a tradeoff surface of the objectives (acceleration level for two load cases).

Furuya et al. (1993 and 1995) used a simple GA to optimize the stacking sequence of a laminated composite plate for buckling load maximization. A serious problem with GAs occurs when a single analysis is computationally demanding. In light of this, the objective of the work was to reduce the computational intensity associated with GAs. One step made in this direction was the use of a binary tree. A binary tree was used to store all previous

ana ana red

eva the

pre

con

Buo

ope by a

the

tech

stru

find

amo

appr was

reso

islan

islan

first

analyses performed in the optimization to be retrieved later if an exact duplicate analysis was reiterated, avoiding costly repeat analyses. A binary tree can reduce computational costs when a high computational price is paid for each evaluation (compared to the time used to search the binary tree). A drawback of the binary tree is the need for a large amount of available memory to store previous design information. A second step made in the direction of reducing the computational intensity of GAs was the approximation of certain buckling loads. Buckling loads were computed exactly for each design string created by genetic operators. The set of all possible combinations of design strings is approximated by a linear least squares fit based on bending lamination parameters. The best of these combinations replaced the nominal design in the population. This technique searches a small neighborhood of designs for a local optimum.

Punch et al. (1994 and 1995) also used GAs to find optimal composite structures. They searched for optimal laminated composite beams with a coarse-grained island injection Genetic Algorithm (iiGA). The objective was to find stacking sequences for a laminated composites beam that maximized the amount of mechanical energy absorbed by the beam before fracture. The goal of approaching the problem with an iiGA was to reduce computational effort. This was accomplished with an iiGA by searching at various levels of spatial resolution on separate computational nodes. Structured migration amongst islands allowed good individuals at low spatial resolution to be injected into islands of higher spatial resolution. The fitness of the beam was evaluated with first order zig-zag finite element model developed for composite laminate

analysis. The new finite element model accounted for layerwise variations of displacements and stresses by assuming a piecewise linear through-the-thickness in-plane displacement distribution. A clamped-clamped graphite-epoxy composite layered beam had a point load applied at its midspan. The GA was allowed to place either a 0 or 90 degree ply in each element in the discretized beam. First, a symmetric beam with a small search space was explored with the island injection GA. The final results from the island injection GA were confirmed to be the global optimal solution by enumerating (exhausting) the search space. Next, larger search spaces that did not assume beam symmetry were explored with the island injection GA with promising results.

Mallot, et al. (1996) used an island injection GA to optimize an idealized airfoil. The objective of the problem was to find composite stacking sequences of sandwich plates that maintain an appropriate opposite twist to compensate for inflight aerodynamic loads that cause adverse airfoil twisting, while minimizing weight under stiffness and ply clustering constraints. Displacements and stresses were predicted with a finite element model based on a cubic zig-zag plate theory. The iiGA approach was able to find designs which reduce weight by 66%, increase minimum in-plane stiffness values by 33% and increased the twist by a magnitude of 77 times the baseline design, but in the opposite direction. In comparison with a variety of search methods tested, the iiGA approach was the most efficient in terms of computational time.

ļ

fä

th di:

di: Re

de

Mil tha

def

thro

to s

pred struc

stres

defor

Out-of-plane loading of a laminated composite can cause appreciable transverse stresses with respect to other components of stress. Central and edge delaminations are the primary damage mode in laminated composites. Often, central delaminations are caused by impact loading while an edge delamination can often be attributed to the free edge effect (see Liu, 1988). The correct prediction of transverse stresses is crucial since the interlaminar stresses play a major role in the energy absorption capability of the laminated composite during failure.

The first plate theory developed is referred to classical laminate plate theory and is based on the Kirchoff-Love hypothesis that the in-plane displacements vary in a linear fashion through-the-thickness while the transverse displacement remains constant and the transverse shear strain is zero (see Reddy, 1993). First order shear deformation theory (FSDT) was independently developed by Reissner and Mindlin, and is typically referred to as Reissner-Mindlin theory. The theory relaxed the Kirkoff-Love hypothesis which enforced that the normals to the mid-plane of the plate must remain normal throughout deformation (see Reddy, 1993). This deformation mode implies a constant through-thickness transverse shear stress. Shear correction factors are needed to satisfy equilibrium conditions (see Reddy, 1993). FSDT theory accurately predicts displacements and stresses of thin and moderately thick isotropic structures. FSDT theory does not satisfactorily predict displacements and stresses in some laminated composites (see Cho, 1997). High-order shear deformation theories (HSDT) have been developed to account for more accurate

la the lay int Nui lan ano Was disp con degi Cho prim, varia

al

19

displacements and stresses (especially the transverse stresses) in laminated composites (Averill, 1992). The through-thickness displacement field is based on higher order polynomial functions. The higher order polynomials enforce smooth and continuous variation of displacements. This smooth continuous variation of displacement causes double valued stresses at inter-laminar interfaces. With abrupt changes of material properties at ply interfaces, the displacements and strain field through-the-thickness are not smooth and continuous (see Cho. 1997). Rather, the displacements can "zig-zag" through-the-thickness of the laminated composite. With this "zig-zag" variation in mind, the goal of layerwise theories is to describe each laminated composite as an assembly of individual layers and then impose one or more continuity condition(s) at the laminate interfaces. Accurate displacements and stresses are predicted, but the total number of degrees of freedom is proportional to the total number of layers in the laminated composite. In view of the strengths and weaknesses of the high order and laverwise theories, an accurate efficient theory is highly sought.

A new class of laminate theories called first order zig-zag theories (FZZT) was first developed by DiSciuva (1985). Zig-zag theories use a presumed displacement field for each layer while analytically enforcing interlaminar continuity of transverse shear stress while maintaining an independent number of degrees of freedom per layer. Later, many researchers (see DiSciuva, 1993, Cho, 1993, Averill, 1996 and Yip 1996) improved the accuracy of FZZT, the primary improvement was achieved by superimposing a piecewise linear variation of in-plane displacements on a cubic function of the through-thickness

coordinate, which is commonly referred as higher order zig-zag theories (HZZT). This improved capturing the kinematics associated with warping of unsymmetric laminates but required C¹ continuity of the approximation of transverse displacement, thus Hermitian-type interpolation functions are required. This introduced additional rotational degrees of freedom which are gradients of the through-thickness displacement. These additional degrees of freedom make it inconvenient, if not impossible, to implement into a commercial finite element code that allows only six degrees of freedom per node (three displacements and three rotations).

Averill and Yip (1995) developed a generalized FZZT and a HZZT that eliminated the requirement of C¹ continuity of the through-thickness displacement with an interdependent element (anisoparametric) scheme and the penalty method for beams with a two-noded element. These elements still required additional degrees of freedom associated with the gradient of the transverse displacement. Yip and Averill (1996) approached this problem by combining the strengths of discrete-layerwise theory and zig-zag theory. The new theory permits the laminate to be subdivided into a set of sublaminates. Each sublaminate can contain many layers. Each sublaminate is modeled with zig-zag kinematics. The FZZT in-plane displacement field in each sublaminate is assumed to be a piecewise linear function through-the-thickness (Cho, 1997). The finite element was cast as an eight-noded brick with three translations and two rotations as degrees of freedom. Yip (1996) expanded the HZZT to include von Karman geometric nonlinear Green's strains with the Total Lagrangian

1.3

ap

fu

fini

ap

con

str

stoc

atter

any

geor

will b

variat develo

will be

finite

metho

approach. Lee (1998) developed C¹ continuity zig-zag plate elements with the full set of nonlinear Almansi strains with an Updated Lagrangian formulation.

1.3 Present Study

The overall objective of the present study was to develop tools and approaches for optimization of structures using GA's. Combining a GA with the finite element method is by now a familiar approach in the optimization of structures. Using an Injection Island Genetic Algorithm to perform optimization considering crashworthiness, modal response, mass, manufacturability, stochastic variability of design variables and load cases has never been attempted. Accurate, efficient evaluation tools are necessary when performing any type of optimization, this is especially true when attempting to predict the geometrically nonlinear response of composite structures.

For reader familiarization, the mechanics of GA's and Injection Island GA's will be reviewed. An optimization problem involving crashworthiness, modal frequency response, mass, manufacturability, stochastic variability of design variables and load cases will be approached with an Injection Island GA. The development of a geometrically nonlinear first order zig-zag finite element model will be presented. Verification of the geometrically nonlinear first order zig-zag finite element model will be confirmed with experimental and computational methods. Lastly, the optimization of composite sandwich panels will be

approached with a GA considering geometrically nonlinear response of sandwich panels using the first order zig-zag finite element model.

Chapter 2

THE MECHANICS OF GENETIC ALGORITHMS

2.1 Introduction

The goal of this chapter is to review the mechanics of simple Genetic Algorithms and island injection Genetic Algorithms. First, the mechanics of simple Genetic Algorithms are described. Next, the benefits of approaching an optimization problem with an island injection Genetic Algorithm are discussed. Finally, the "pros" and "cons" of Genetic Algorithms are presented.

2.2 Simple Genetic Algorithms

Genetic Algorithms (GAs) are a powerful technique for search and optimization problems, and are particularly useful when the design space is large and complex. Many design spaces are discontinuous, nonconvex and multimodal. These design space characteristics bring strong possibilities that many local suboptimal solutions exist, which limit the applicability of gradient-type approaches. The main downfall of a simple GA is the potentially large number of design evaluations required to obtain a set of satisfactory solutions.

A GA is a search procedure based on the mechanics of natural selection. Specific knowledge is embedded in a chromosome which represents the overall design with a set of design variables. The fidelity of each design variable is determined by the number of bits in the string defining each locus, or position on the chromosome. These design variables are the building blocks used to

ir

w op

inv

pe no

larg

help The

Рори Рори

displa

initial

rando

construct a particular design. Typically, each design variable has the potential to be mapped from the chromosome to a physical attribute of the actual design.

Designs are created and destroyed by the process of decoding chromosomes. Natural selection is the connection between a chromosome and the performance of the chromosome and is a process that causes superior performing chromosomes to have a higher probability of reproduction, while inducing poorly performing chromosomes to have a lower probability for reproduction. During reproduction, two genetic operators are commonly modeled which can produce new chromosomes: crossover and mutation, a third genetic operator, inversion is sometimes added. The amount of crossover, mutation and inversion are all controlled by the user. A high crossover rate will produce new organisms quickly, but will also have a high probability to disregard higher performing chromosomes. A low crossover rate could stagnate search, producing no new chromosomes. Many mutation operators exist, and their main purpose is largely to aid search by introducing new design variables during search. Mutation helps maintain diversity and reduces the probability of premature convergence. The inversion operator was not used in this study.

A set of co-existing chromosomes defines a population, while successive populations are termed generations. A large genetic pool increases diversity in a population, which in turn improves the ultimate results of the GA. Figure 2.1 displays the structure of a simple GA. The simple GA begins by creating a single initial population, wherein chromosomes of different design variables are randomly created. At this point the "goodness" of each design is measured.

Biased by the evaluations obtained, the GA uses unary and binary operators on these designs to create another population. This population probabilistically maintains the previously "good" designs while discarding poorly performing designs. The program evaluates the new population members and continues with additional rounds of generation and selection. This is repeated until satisfactory solution(s) are obtained (see Goldberg, 1988). Incorporating these processes in a computer algorithm will produce an algorithm that solves problems in a manner reminiscent of natural evolution.

2.2.1 Representation of Design Variables within a Chromosome

A chromosome of "p" potential design variables (x_i) can be represented in vector form as: $\{x_1, x_2, x_3,, x_p\}$. Each design variable is typically referred to as a field or locus on the chromosome. The size of each field on the chromosome will define the number of choices for each design variable. If a coarse representation of a continuous design variable is sought, then the field size of the continuous design variable should have a small number of choices between the lower and upper bounds of the design variable. A larger number of choices between the lower and upper bounds of a continuous design variable can be defined to refine the representation of the continuous design variable. Each design variable (field) on the chromosome can have an independent field size. If a design variable is truly discrete in nature, then the field size of the discrete design variable should be set at the number of choices in the discrete set.

2.2.2 Initial Population Generation

First, the GA must perform initialization and evaluation of the initial population. The GA stochastically creates a population of chromosomes composed of a randomly chosen allele at each locus. A measure of "goodness" or fitness is assigned to each individual based on the fitness function.

2.2.3 Selection

The next process the GA must perform is selection. The selection mechanism for GAs is simply the process that favors the selection of fit individuals to be placed in a mating pool. The fitness function provides a means of comparing individuals and the selection process determines how the individuals are compared. Selection mechanisms determine which chromosomes are placed in the mating pool. Roulette wheel, stochastic remainder and rank based are all common selection mechanisms. Tournament selection was used exclusively in this study due to its low selection pressure. Tournament selection allows for a group of individuals that are chosen stochastically to gather and compete in a tournament, the individual with the highest fitness is placed in the mating pool. A low selection pressure lessens the pressure to converge by disallowing any "super" individual to dominate the reproduction cycle, promoting diversity. The mating pool is comprised of the individuals that will create the next generation through genetic operators. Selection is the GA search catalyst that works by mimicking natural selection.

2.2.4 Crossover

Crossover is a genetic operation performed by a GA that recombines building blocks from two chromosomes to create new chromosomes. Pairs of chromosomes that were placed in the mating pool through the selection process are combined through crossover. Uniform order-based, cycle, partially matched, one-point, two-point and uniform crossover are commonly used procedures. One-point crossover was used exclusively in this study and is explained in detail. Consider the two chromosomes below that have five design variables:

$$\{ x_1, x_2, x_3, \underline{x_4}, \underline{x_5} \}$$

 $\{ y_1, y_2, y_3, y_4, y_5 \}$

One-point crossover only occurs between two loci. One-point crossover occurring between the third and fourth loci would result in the following new individuals:

$$\{ y_1, y_2, y_3, \underline{x}_4, \underline{x}_5 \}$$

 $\{ x_1, x_2, x_3, y_4, y_5 \}$

This new set of designs have simply been created through recombination of the original two chromosomes by swapping their fourth and fifth design variables between the two chromosomes.

2.2.5 Mutation

Mutation is another genetic operator that aids GAs in search and optimization. The mutation operator helps maintain diversity during search by introducing new alleles. A mutation operator that acts upon a field-by-field basis

of

de

Th

Th va

OC

2.2

def

wa

Wher

the j

of the chromosome was used in this study. A field-by-field mutation of this type is demonstrated in the following example at the first locus on the chromosome:

$$\{ \underline{X}_1, X_2, X_3, X_4, X_5 \}$$

The new chromosome would be:

$$\{ \underline{x}_1', x_2, x_3, x_4, x_5 \}$$

The field-by-field mutation would randomly change the value of the first design variable (bounded by the field size). Typically, low rate of field-by-field mutation occurs for each field on the chromosome.

2.2.6 Fitness Function

For the problems investigated in this study, the "goodness" of each design was represented with a single scalar value called the fitness function. The formal definition of the type of optimization problems addressed in this work is:

Find: $\{x_i\}$ i=1,..., Number of Design Variables

Such that: Minimize $F(x_i)$

Subject to:

 $h_j(x_i) \le 0$ j=1,..., Number of Inequality Constraints

 $\overline{h}_k(x_i) = 0$ k=1,...,Number of Equality Constraints

 $x_i' \le x_i \le x_i''$ i=1,..., Number of Design Variables

State Equations

where $\{x_i\}$ is a vector of design variables, $F(x_i)$ is the objective function, $h_j(x_i)$ is the j^{th} inequality constraint, $\overline{h}_k(x_i)$ is the k^{th} equality constraint while x_i^l and

 x_i^u represent the lower and upper bounds on the ith design variable. The state equations relate the behavior of the objective function and constraints to the vector of design variables.

For all problems investigated in this study, the "goodness" of each design was represented with a single scalar value called the fitness function. Within the fitness function the objective(s) are either maximized or minimized, for this research, the fitness, thus the objective(s), are maximized. All constraint violations are minimized with the penalty method. To evaluate the fitness of a design, the objectives and constraints are normalized and aggregated. The formal optimization statement can be rewritten as:

Find: $\{x_m\}$ m = 1,...,Number of Design Variables

Such that: Maximize: Fitness (x_m)

Subject to:

$$x_m^l \le x_m \le x_m^u$$

State Equations

The "fitness" of a candidate design can be defined as:

Fitness=A+
$$\sum_{i=0}^{n-obj} B_i \frac{Obj_i}{Norm_i} - \sum_{j=0}^{n-ineq} C_j \left(\frac{ineq_j - t_ineq_j}{t_ineq_j} \right)^n j - \sum_{k=0}^{n-eq} D_k \left(\frac{eq_k - t_eq_k}{t_eq_k} \right)^n k$$
 2.1.)

where "n_obj" is the number of objectives to be maximized, "n_eq" is the number of equality constraints and "n_ineq" is the number of inequality constraints. "A" is a large coefficient which insures that the fitness is positive. "B_i", "C_j" and "D_k" are weights associated with the ith objective, jth inequality constraint and the kth

equality constraint, respectively. C_j are penalty coefficients which are set to zero when the associated inequality constraint is satisfied.

For a candidate design: "Obji" is a scalar value representing the ith objective, ineq_i is a scalar value of the jth inequality constraint and "eq_k" is a scalar value of the kth equality constraint. "Norm_i", "t_eq_i", and "t_ineq_k" are target values used as scalars that normalize the objectives, equality constraints and inequality constraints with respect to their target values. "n_k" and "n_j" are penalty parameters which are chosen such that a violation of a constraint reduces the overall fitness of the design. Typically take on values of 2 or greater. This guarantees the fitness of an infeasible design is penalized in at least a quadratic fashion with respect to the violation of any constraint. This technique ensures the fitness rapidly decreases when the candidate design violates any constraint. Often, optimal solutions lie near or at a constraint boundary, so the penalty method can help maintain solutions that nearly or slightly violate a constraint.

2.3 Pros and Cons of Genetic Algorithms

A good optimization algorithm should not necessitate excessive computational costs while progressively finding better solutions. Unfortunately, no single approach is best for all problems. Fortunately, certain optimization approaches work better for a specific class of problems. Calculus based hill-climbing methods work well for an explicit class of problems whose objectives and constraints change in a smooth, well-behaved manner with respect to the design variables. Most real life design spaces do not have a convex unimodal

n cl Sil pr aı ob, rec rep obj pro med that thou spac muct numt optim addit design space. If a design space is known to be convex, a calculus based hill-climbing approach should be applied. Calculus based hill-climbing will tend to proceed to local sub-optimal solutions when extended to problems with complex, noisy design spaces. This handicaps the applicability of calculus based hill-climbing methods to many nontrivial problems.

To the other extreme, one technique to alleviate these problems is to simply enumerate the design space. Exhausting the design space is not practical if the space is large and or if a single computational evaluation requires a moderate amount of compute time.

GAs do not require the existence or computation of gradients of the objective and or constraint functions to perform optimization. Rather, a GA requires that the fitness of each design can be evaluated. The fitness should represent a design's "goodness", or overall performance in terms of the objectives and constraints. This makes GAs applicable to a large set of problems. A GA is a multi-point search procedure modeled specifically on the mechanics of natural selection. A simple GA is a multi-point search procedure that occurs within isolated surroundings, interacting with nothing else. Even though a GA requires fitness evaluation for only a fraction of the total design space, the total number of evaluations to find an optimal solution can still be much too large for practical applications. This requirement represents the number one downfall of a GA. This is true for GA applications in structural optimization using computational methods such as the finite element method. An additional downfall to a simple GA is its propensity to converge to suboptimal

solutions. Parallel GAs attempt to mitigate both of these issues by allowing search to happen on a set of multi-point searches (often on separate computational nodes) with various topological structures allowing structured migration amongst the search sets.

2.4 Island Injection Genetic Algorithms

An island injection Genetic Algorithm (iiGA) also uses structured migration of search points amongst a group of search sets, but allows for the exploration of various levels of resolution of the search space to reduce the overall computational time required to arrive at a given set of well performing solutions. iiGAs search at various levels of resolution to quickly find building blocks at low levels of spatial resolution to inject into higher levels of resolution. iiGAs can independently search for optimal solutions considering multiple objectives concurrently while handling stochastic variabilities. An island injection Genetic Algorithm (iiGA) represents an approach to search at various levels of resolution within a given space in a structured hierarchical fashion (see Eby, 1996, Goodman, 1996). This includes first searching at low levels of resolution on different nodes (islands) and then injecting the high performing individuals into islands of higher resolution to "fine-tune" the design. If the formal definition of the fitness is known to change when migrating individuals, the receiving subpopulation must reevaluate the migrants performance. Figure 2.2 displays a typical island injection topology that has an island that searches at a low level of resolution and migrates good designs to islands of higher resolution. The search

space is fundamentally divided into hierarchical levels with well defined overlap (the search space of the parent is contained in the search space of the child). The rate and structure of migration can be set for each island. Each island could independently represent the problem in terms of design variables, objectives, constraints, fitness definition and fitness evaluation. The design variables, objectives and constraints on each island could be considered stochastic or deterministic. The rates of each genetic operator could be independently set for each island. Each island could be evaluated on separate computational nodes. Many variations on the island topology in Figure 2.2 can easily be performed for problem dependent custom tailoring. iiGAs embody a divide-and-conquer and partitioning strategy which has been applied to many problems (see Eby et al., 1999 and Mallot et al., 1996). The simple GA and iiGA applied in this dissertation were developed by Goodman (1996).

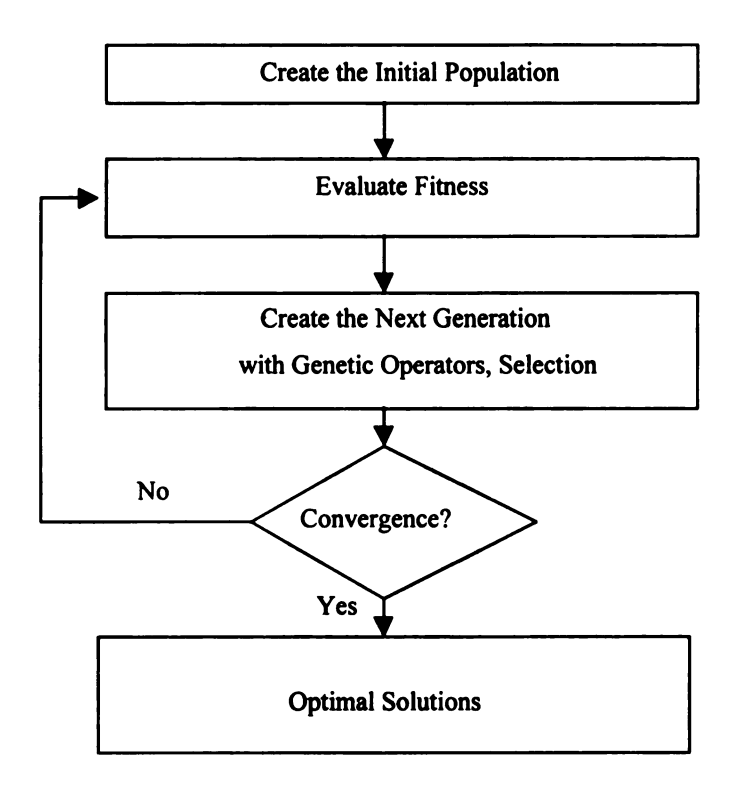


Figure 2.1. Simple Genetic Algorithm Structure.

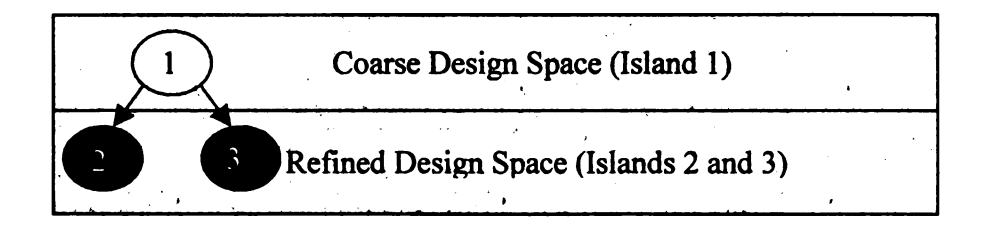


Figure 2.2. A simple iiGA topology that simultaneously searches various levels of resolution of the design space on three separate computational nodes (islands).

Chapter 3

OPTIMIZATION OF CRASHWORTHINESS AND MODAL FREQUENCIES OF AUTOMOTIVE STRUCTURES

3.1 Introduction

The goal of this chapter is to demonstrate an island injection Genetic Algorithm's ability to perform optimization of crash type problems while concurrently satisfying a set of conflicting constraints considering stochastic variability of design variables and load cases. The traditional optimization statement for this problem will be developed in terms of the objective functions, constraints and design variables with respect to an island injection Genetic Algorithm. Results display an island injection Genetic Algorithm's ability to maximize multiple objectives while concurrently satisfying multiple conflicting constraints. A beam-type structure typically referred to as an automotive lower front motor compartment rail will be the particular automotive structure considered during this research. The front motor compartment rail is considered the main mechanism that governs mechanical transfer of energy during a crash event. The front motor compartment rail connects the front bumper to additional beam-type structures along the front of dash of an automobile.

3.2 Optimization Problem Statement

In order to define the optimization problem this section describes 1) optimization design variables, 2) optimization objective functions, and 3) optimization constraints. The optimization problem can be stated as: find the

cross sectional shape and thickness varying along the length of a rail structure to maximize the energy absorbed by a specific region within the structure subject to inequality constraints on the first and second modal frequencies, peak crush force, mass and manufacturability while considering multiple load cases with stochastic variability of loads and design variables. The objectives were decomposed by simultaneously (but independently) seeking deterministic optimal solutions for each load case in hierarchical heuristic levels of refinement. Concurrently, the objectives were stochastically represented with stochastic variation of the design variables. An objective function can be considered stochastic when non-unique objective values are possible for a unique design. The stochastic nature of the objective functions can be defined by the stochastic nature of the design variables.

3.3 Optimization Design Variables

Every design variable in structural optimization can be thought of as being either discrete or continuous in nature while behaving in either a deterministic or stochastic manner. A design variable behaves stochastically when the mapping of the intended design variable to the actual design is non-unique. A design variable acts stochastically when a design is produced multiple times and the produced designs are not necessarily identical. Each time the design is produced, a slightly modified design could be created. This inherently occurs in many processes - each time a design is manufactured, slight differences in the manufacturing process will produce slightly different design variables. A design

lin

fid

Crit

bel are

variable behaves deterministically when a unique mapping from the intended design variable to the actual design occurs. Given a set of deterministic design variables, a unique design will be repeatedly produced, irrelevant of the process that creates them. Many real life design variables are stochastic in nature. Stochastic variability of design variables should not be disregarded for problems that involve noisy chaotic objectives. Nonlinear response of structures is often very sensitive to small changes in the design variables.

The cross sectional shape of the structure was viewed as a discretized composition of cross section *primitives* or structural elements. With this in mind, the first set of design variables was defined as a deterministic discrete set of cross sectional primitive shapes. The cross sectional primitives allow variation of the shape of the cross section along the axis of the structure, see Figure 3.1. A total of five cross sectional primitives biased towards the front of the rail defined the overall surface of the design, using interpolation from cross section to cross section with a linear blending function (see Figure 3.2). The surface was smoothed with a fourth order Bezier surface at the cross sectional primitives to avoid sharp changes in geometry that would be artificially generated from the linear blending of the primitive cross sections.

Biasing of the design variables was performed to increase the model fidelity in critical portions of the structure. Refinement of the design variables in critical regimes of the structure was performed to control complex localized behaviors. Coarsening of the design variables was performed in non-critical areas of the structure where localized behavior was of a lesser concern. Since a

progressive crush is sought, the crush of the front of the rail is crucial. Therefore, the placement of primitive cross sections was biased towards the front of the rail in the "crush-zone". Figure 3.2 and 3.3 display biasing of the design variables towards the front of the rail structure.

The second set of design variables was the thickness of each section of the rail, which was considered a continuous stochastic design variable. The manufacturing process of the rail structure was considered stochastic – each time a target design was created the thickness of the rail structure would change within ten percent of the target thickness. The stochastic noise in thickness was considered to play an important role in the objective functions. Thickness changes occurred between the placement of each cross sectional primitive, see Figure 3.3. Since the surface of the design was generated with five primitive cross sections, there were four design variables describing the thickness of the rail structure. The rail structure was made out of aluminum.

As depicted in Figures 3.1 and 3.2, the cross sectional shape of the rail was allowed to vary as a function of the rail axis by choosing a set of primitive cross sections. The choice of primitive cross sections was bounded by a discrete set of manufacturable primitive cross sections. The iiGA could choose any combination of cross sectional shapes from a predefined library of manufacturable primitives. This library of cross section primitives is not arbitrary – rather, it is knowledge based. Figure 3.4 displays a primitive library that contains a set of knowledge-based manufacturable cross sections. A design volume constrained the rail structure to have a smaller width compared to the

height of the rail cross section. Each cross section in Figure 3.4 was scaled up to 1.5 times the dimension of the original perimeter to define the upper and lower bounds for each cross section design variable.

The representation of the design variables within the chromosome was set up in an order that staggered the primitive cross sections with the thickness of each section. The order of the design variables on the chromosome was constructed to reflect the physical attributes for a given design which has been known to aid search within a GA (see Holland, 1975, Goldberg, 1988).

3.4 Optimization Objective Functions

The optimization objective function is the maximization of the internal energy of a specific region of the structure termed the "crush-zone" for multiple load cases. The internal energy of the crush-zone was computed by LSDYNA, (see LSTC/KBS2, 1999). The objective function for a single load case can be stated as:

$$I.E. = \frac{1}{2} \int_{\Omega} \int_{0}^{\varepsilon_{ij}} S_{ij} d\varepsilon_{ij} d\Omega |_{\tau = \tau_{f}}$$
3.1.)

where Ω is the volume of interest called the "crush-zone", S_{ij} is the second Piola-Kirchoff stress tensor and ε_{ij} is Green's strain tensor. The equations of motion were simulated with LS-DYNA (see LSTC/KBS2, 1999) to obtain the objective functions. LS-DYNA is an explicit nonlinear finite element code.

The upper bound of the internal energy of a feasible design was computed by considering the inequality constraint on the maximum crush force and the

maximum distance the rail could displace during crush. This value was used to normalize the objectives.

Load cases considered were meant to simulate a component of a front end of an automobile during various crash events. During frontal crash events, the lower front rail is often designed to be the main mechanism to govern crash energy. The crash event was modeled by defining an initial velocity for the lower front rail structure and allowing it to move into a stationary rigid wall. A lumped mass (with identical initial velocity as the rail) was constrained at the end of the rail structure to simulate inertial effects that would drive the rail into the rigid barrier. Different crash events were modeled with various load cases. The first load case was meant to simulate a rail structure traveling at 35 mph colliding with a rigid barrier. For the first load case, a lumped mass was placed directly behind the rail structure as depicted in Figure 3.5. The second load case was meant to simulate a rail structure traveling at 40 mph colliding with a rigid barrier with additional moments into the system. The second load case placed an "eccentric" lumped mass behind the rail at an offset to create additional moments into the system as shown in Figure 3.6.

3.5 Optimization Constraints

The first and second inequality constraints in this optimization problem were to ensure that the first two modal frequencies were greater than or equal to predetermined target values. The cross sectional properties of the structure were computed and the modal response of the structure was based on a beam

analysis performed by ADINA (see ADINA, 1999). It is well documented that an optimization problem that considers at least two modal frequencies is non-convex and multimodal with portions of the design space that have undefined gradients (See Haftka and Gurdal, 1993, and Gurdal, 1999) due to the possibility that order of modal frequencies may switch as search occurs.

The third inequality constraint was that the maximum force experienced during crush be less than or equal to the target force. The peak crush force was computed at the rigid barrier by LSDYNA, (see LSTC/KBS2, 1999). A definition of work is the "dot" product of force and distance, while energy can be defined by integrating work through time. With this in mind, there are two ways to increase the objective function for a specific load case: the internal energy of a structure can be maximized by increasing either the force or distance vectors during crush. The Euclidean length of the force vector was constrained. To this end, we can conclude that the constraint placed on the maximum crush force will play a major role in limiting the amount of energy absorbed during crush.

The fourth constraint in the optimization problem was to insure that the total mass was less than or equal to a target value. Equation 3.1 defines the objective function of a single load case as the internal energy of a specific volume of the rail structure. An increase in volume would obviously increase the total mass of the rail structure. For a given design, the total energy of the system will remain constant. Kinetic energy will be the only form of energy that is input into the system. An increase in volume (mass) will slightly increase the initial (kinetic) energy of the system. The internal energy absorbed by a design is

bounded by the total energy into the system (kinetic energy), which in turn is bounded by the volume (mass) of the design.

The last constraint measured is the manufacturability of the design. Manufacturability constraints were enforced by ensuring good designs had a maximum "local-taper" less than or equal to a target value. The "local-taper" of a design was the maximum amount of change in the size of the perimeter of the rail as a function of the rail axis. This constraint limits the amount of load that the structure could carry in localized bending. Localized bending is often required to initiate crush.

All constraints were evaluated prior to a "full" crush analysis. The maximum force experienced during crush often occurs shortly after the instant of contact of the rigid barrier with the rail substructure. If all constraints were satisfied within 30 percent of the target values, then a full crush evaluation was performed to determine total internal energy of the crush zone and the actual maximum force experienced during full crush. If a design severely violated any of the constraints, then the fitness was penalized by assuming the internal energy of the crush-zone was zero. This technique reduced the total number of crush evaluations of "poor" designs that harshly violated constraints.

The fitness for each design was computed using equation 2.1. Target values for all constraints are given in Table 3.1. All coefficients used in the fitness function are given in Table 3.2. The weights for the fitness function are all equal except for the manufacturability weight. The optimization process should not be dominated by manufacturability constraints.

3.6 Application of an Island Injection Genetic Algorithm

An iiGA approaches an optimization problem by simultaneously searching at various levels of resolution within the design space in a heuristic hierarchical fashion. The following paragraphs present the framework of the iiGA applied within the context of the current application.

Figure 3.7 shows an iiGA topology that breaks down the total design space into three levels of design variables and time-based resolutions. The overall iiGA topology seeks designs which maximize the internal energy for the two load cases discussed previously. Each island independently searches on one of nineteen separate computer nodes (termed *islands*) while simultaneously sharing information in an ordered fashion. Each computer node had 400MHz processing speed, on a P586 architecture. Table 3.3 gives genetic operator rates for all the islands in Figure 3.7.

Each level of resolution was defined by the discretization of the design variables (rail section thickness and cross sectional primitives) and crush evaluation time. Islands 0 through 2 have a low level of design variable representation with a small duration of simulated crush, islands 3 through 8 have a medium level of design variable representation with a larger crush evaluation time, while islands 9 through 18 have the highest level of design variable representation and largest crush evaluation time. The total number of possible designs grows with an increase in the level of resolution (discretization) of the design variables. Each cross section depicted in Figure 3.4 was bounded by 35

t to to to do do

id

isi pr

2, an

lur

by 127 and 55 by 200 millimeter design areas. Each primitive had an equal number of choices scaled uniformly between the upper amd lower bounds of the design areas. Table 3.4 contains the total number of cross sectional primitive and thickness choices. The lower and upper bounds on the thickness were 2.5 and 6.5 millimeters.

Figure 3.7 also displays the structured rules of migration within the iiGA topology. The coarse design spaces were constructed to map into the refined design spaces in a hierarchical fashion. In general, a unique mapping from a high to low level of design variable resolution cannot be defined, so designs cannot be shared from a high to low level of design variable resolution. The best design plus a randomly chosen design was injected according to the iiGA structured migration rules as depicted in Figure 3.7 at the end of every generation.

The evaluations performed with LS-DYNA are dynamic, thus time dependent. An evaluation that measures the performance of design over a small amount of time is computationally cheaper when compared to evaluating the identical design over a longer period of time. This fact can be taken advantage of by allowing the iiGA to search with evaluation times that can vary from one set of islands to another. This can also benefit the development of a design that progressively crushes. Table 3.5 contains evaluation times for all islands.

Many islands have stochastic design variables and load cases. Islands 0, 2, 3, 8, 9 and 18 evaluate a single deterministic objective function. Islands 0, 3 and 9 evaluate designs based on the first load case. The first load case placed a lumped mass directly behind the rail with an initial velocity of 35 MPH. Islands 2,

8 and 18 evaluate designs based on the second load case. The second load case placed an eccentric lumped mass at an offset behind the rail with an initial velocity of 40 MPH. Islands 1, 4 through 7, and 10 through 17 considered stochastic variability of load case and rail section thickness. For these islands, the load case was randomly chosen for each evaluation. Each load case had an equal probability to be chosen for these islands. The thickness of each finite element was allowed to vary within 10% of the original variable.

The iiGA topology in Figure 3.7 was also dynamic in nature: islands 0 through 2 evaluated 30 generations of designs and then were reinitiated to monitor the overall progress of the topology, see Figure 3.8. Upon re-initiation, the islands evaluated the best designs from the highest level of resolution from the iiGA topology in terms of each load case. This set of islands were meant to monitor the overall performance of the iiGA topology, not to perform additional search. No genetic operations were performed on the designs injected into the monitoring islands.

3.7 Results

The performance of the iiGA topology is represented in Figures 3.7 - 3.8 for each deterministic objective (load case). The overall performance of the iiGA topology will be measured by viewing the behavior of the objectives and constraints for a monitoring island in Figure 3.8.

Figure 3.9 displays a progressive increase in the deterministic objective function of internal energy of the crush zone for the first load case of the best

Π

а

C m

CC 3.

co

the as

dis

40

fun

3.1

ma

fun

design found as a function of generation number for island 9 in Figure 3.8. Figure 3.10 displays the deterministic normalized constraints for the best design found as a function of generation number for island 9 in Figure 3.8. It is important to realize that a feasible design has normalized mass, force, and manufacturability constraints which are less than or equal to unity. A feasible design also has normalized first and second modal frequency constraints which are greater than or equal to unity.

Figures 3.9 and 3.10 display a search that allowed for tradeoffs in constraint violations in order to maximize the deterministic objective of maximizing the internal energy of the crush zone for the first load case. Many constraints are violated throughout the evolutionary process depicted in Figure 3.10, but the final design satisfies all the constraints except for the force constraint, which violates the target force by only 2%.

Figure 3.11 shows the deterministic objective function of internal energy of the crush zone, for the second load case, increasing for the best design found, as a function of generation number for island 18 in Figure 3.8. Figure 3.12 displays the deterministic normalized constraints for the best design found, as a function of generation number for island 18 in Figure 3.8. The run lasted a total of 40 generations and the best design of the run was found at generation 35.

Similar to the results portrayed in Figure 3.9 and 3.10, Figures 3.11 and 3.12 display a search that allowed for tradeoffs in constraint violations in order to maximize its deterministic objective for island 18. The deterministic objective function of island 18 was the internal energy of the crush zone for the second

load case. Figure 3.11 shows a slight decrease in internal energy of the crush zone for the second load case from generations 9 to 10 and 19 to 20. This is can be explained in Figure 3.12 by inspecting where the constraints were violated. A sudden drop in overall constraint violations occurred over generations 9 to 10 and 19 to 20. This was reflected in the measure of fitness of the designs by enforcing the constraints with the penalty method.

Figures 3.13 and 3.14 depict the overall performance of the iiGA topology considering each stochastic objective and constraint. Figures 3.13 and 3.14 show the objectives increasing along with the behavior of the normalized constraints. It should be stressed that the monitoring islands in Figure 3.8 were initiated after islands 0 through 2 completed 30 generations of search, which spanned about three days. During this initial time, the entire iiGA topology was performing search seeking good solutions for each load case with stochastic variabilities — in other words, a huge amount of work was performed before the monitoring islands were spawned. Figures 3.13 and 3.14 plot the objectives and constraints as a function of evaluation number due to the fact that the monitoring islands did not perform any search. The iiGA topology compute time was six and a half days. Table 3.6 contains the number of evaluations and full crush evaluations. If a design did not satisfy the constraints, then the objective function was not evaluated, eliminating the LSDYNA nonlinear finite element evaluation. A full nonlinear finite element evaluation took about 13 minutes of compute time for a single load case.

Figures 3.15 and 3.16 animate the deformation of the best design found for the first and second load cases, respectively. The design crushes progressively from the front to rear of the crush zone for both load cases. Two additional independent runs were performed to verify that the algorithm converges to a similar best design. The three best designs found in the three independent runs are depicted in Figures 3.17 through 3.19. Table 3.7 contains the thickness of each section for all three designs. All three designs closely resemble each other in overall shape and thickness - this is an important fact because it displays the iiGA topology repeatedly converged to similar solutions even though the algorithm started with different initial search sets. The objective and constraint function values are listed in Table 3.8 for all three designs. All three designs have near identical objective and constraint function values. To verify that the objectives are not highly sensitive to stochastic variability of thickness, twenty additional independent evaluations were performed on the best designs depicted in Figures 3.17-3.19. It was found that the standard deviation of internal energy was small compared to the average internal energy. Table 3.9 contains the average and standard deviation of the internal energy for the design portrayed in Figures 3.17-3.19.

3.5 Conclusions

The study developed an approach that overcame the shortcomings of available optimization techniques by allowing concurrent optimization of structures with an island injection Genetic Algorithm for: 1) crash energy

management, 2) modal vibration frequency response, 3) peak crush force, 4) weight reduction, and 5) manufacturability, while considering stochastic variability of design variables and loading conditions. Existing automated design technology has never simultaneously addressed all these competing mechanisms.

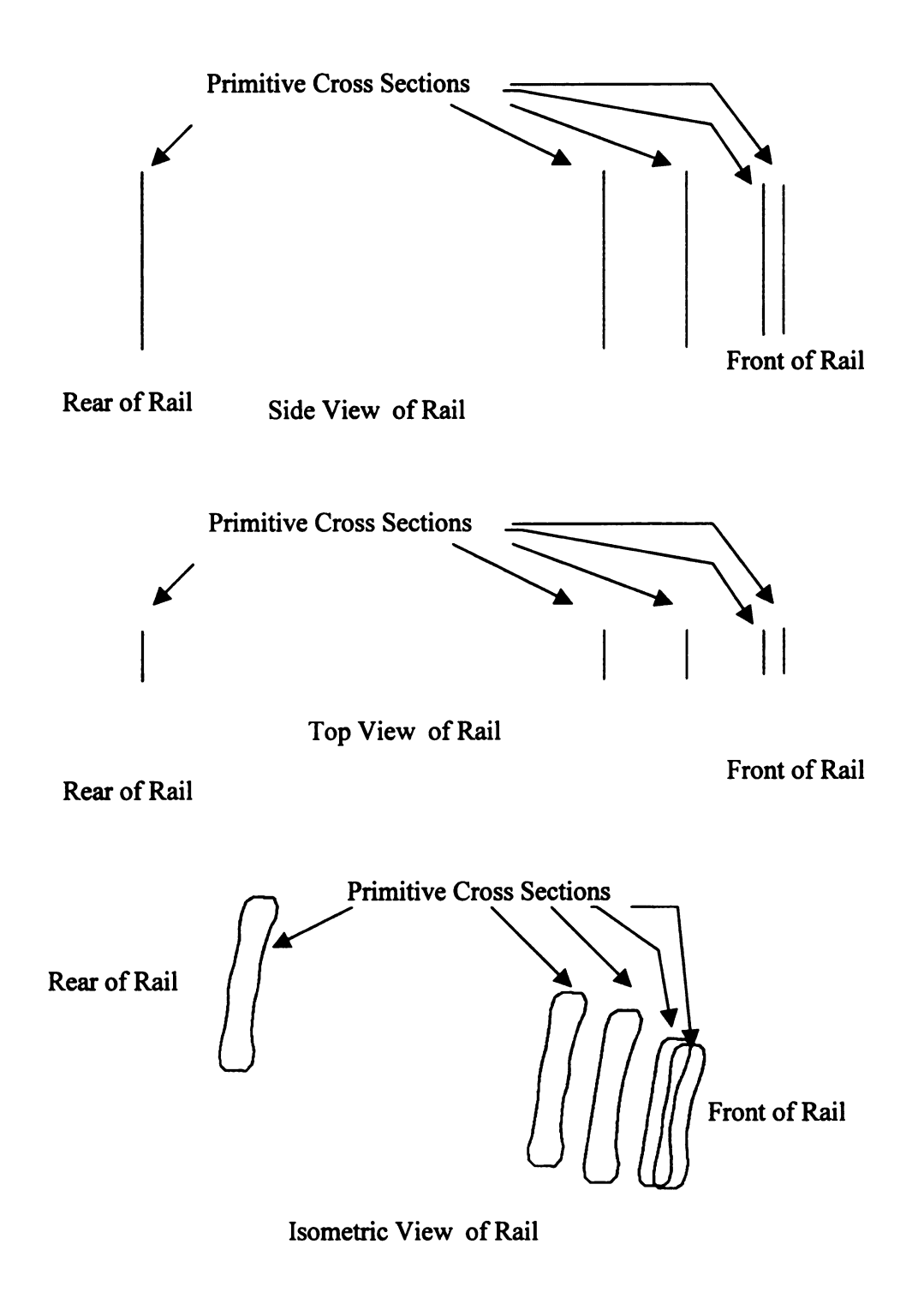


Figure 3.1 Biasing of cross sectional primitives along the length of a rail structure.

Fig sect

Prir

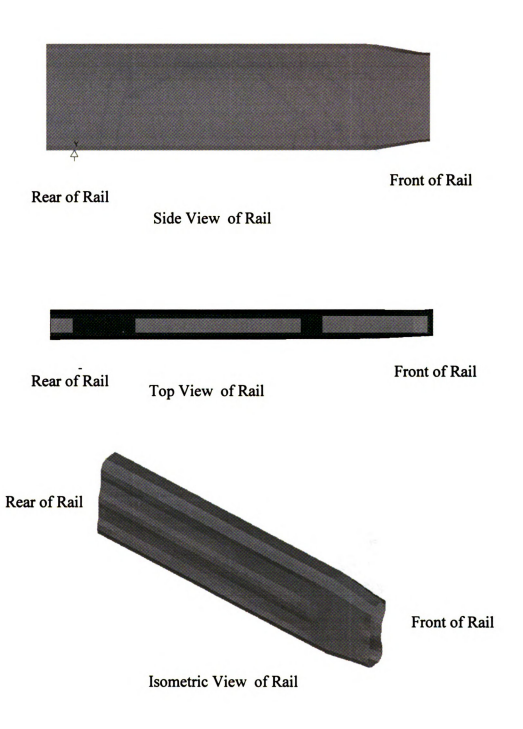
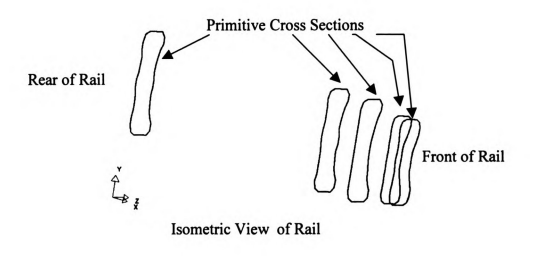


Figure 3.2 Surface of rail structure is developed with a linear blending of the cross sectional primitives. The surface was smoothed at each of the cross sectional primitive locations.



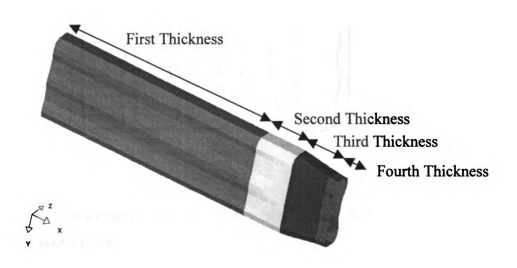


Figure 3.3. Potential thickness changes occurred at the placement of each cross sectional primitive.

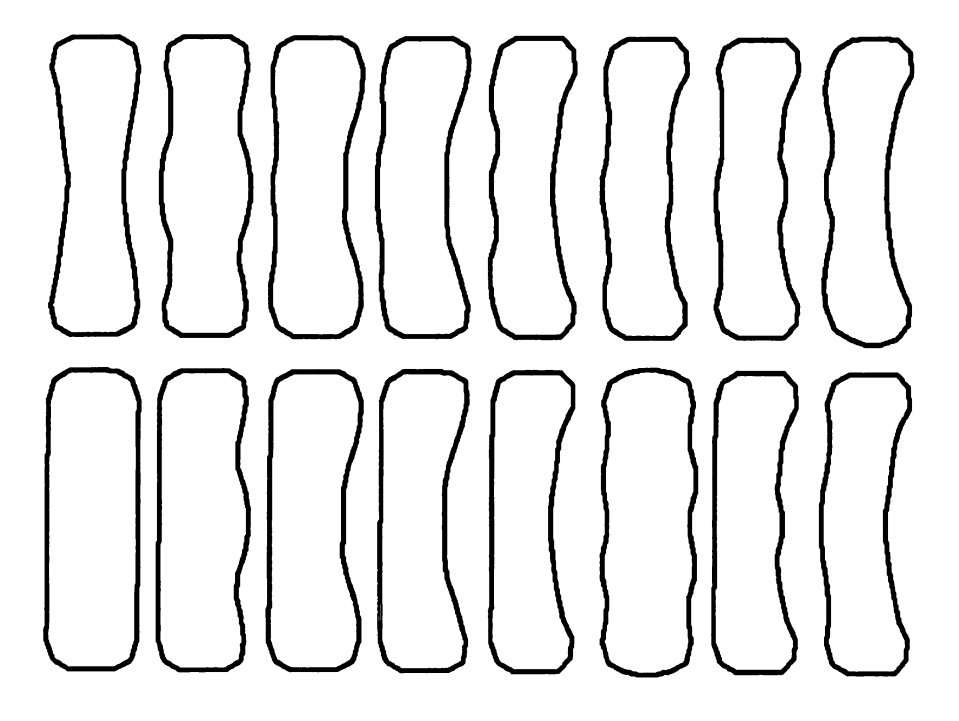


Figure 3.4. Cross sectional primitive library that contains a set of knowledge-based manufacturable cross sections.

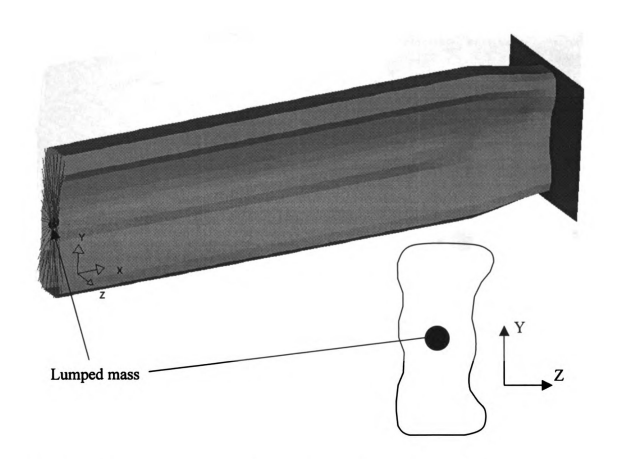


Figure 3.5. Finite element model and of rail structure running into a stationary rigid wall for the first load case. A lumped mass was placed directly behind the rail structure.

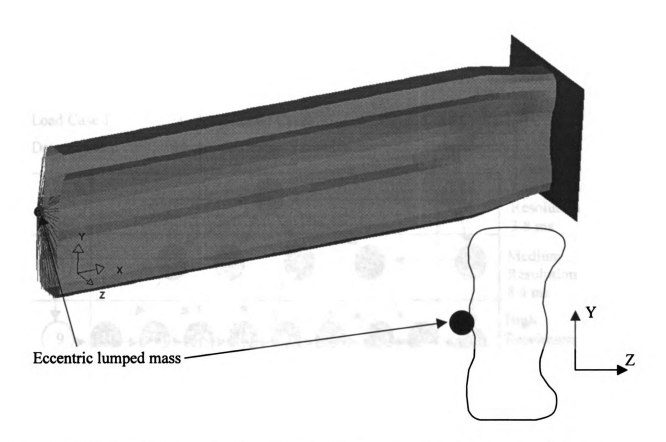


Figure 3.6. Finite element model and of rail structure running into a stationary rigid wall for the second load case. An eccentric lumped mass was placed behind the rail structure.

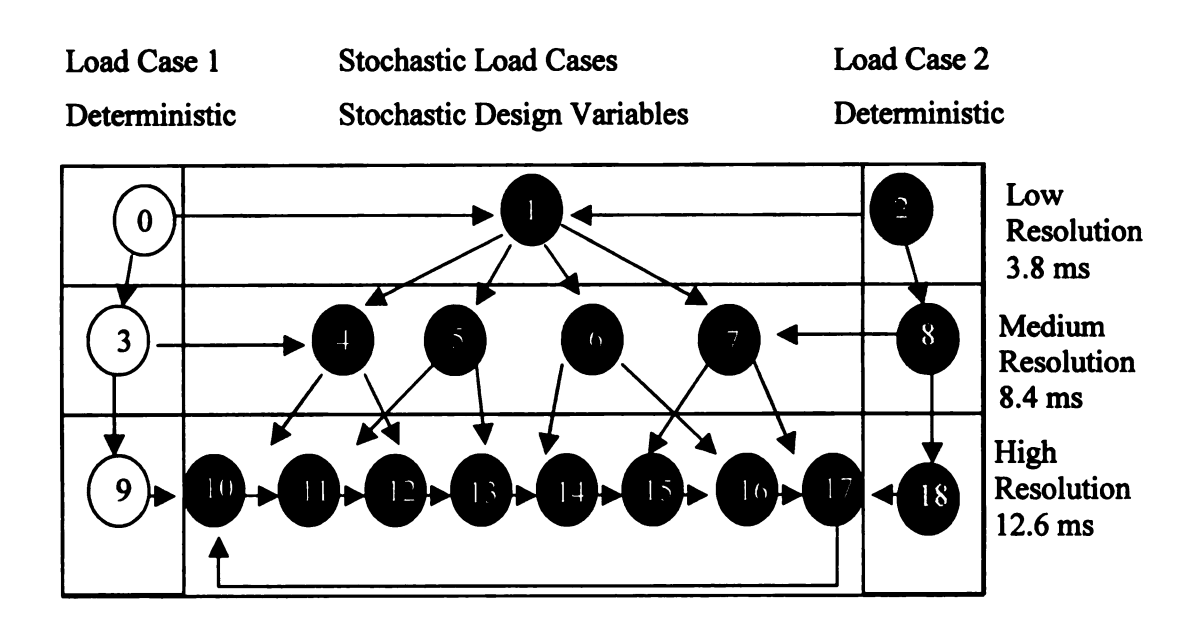


Figure 3.7. An iiGA topology that breaks down the design space into three levels of design variable and evaluation time based resolutions with multiple load cases.

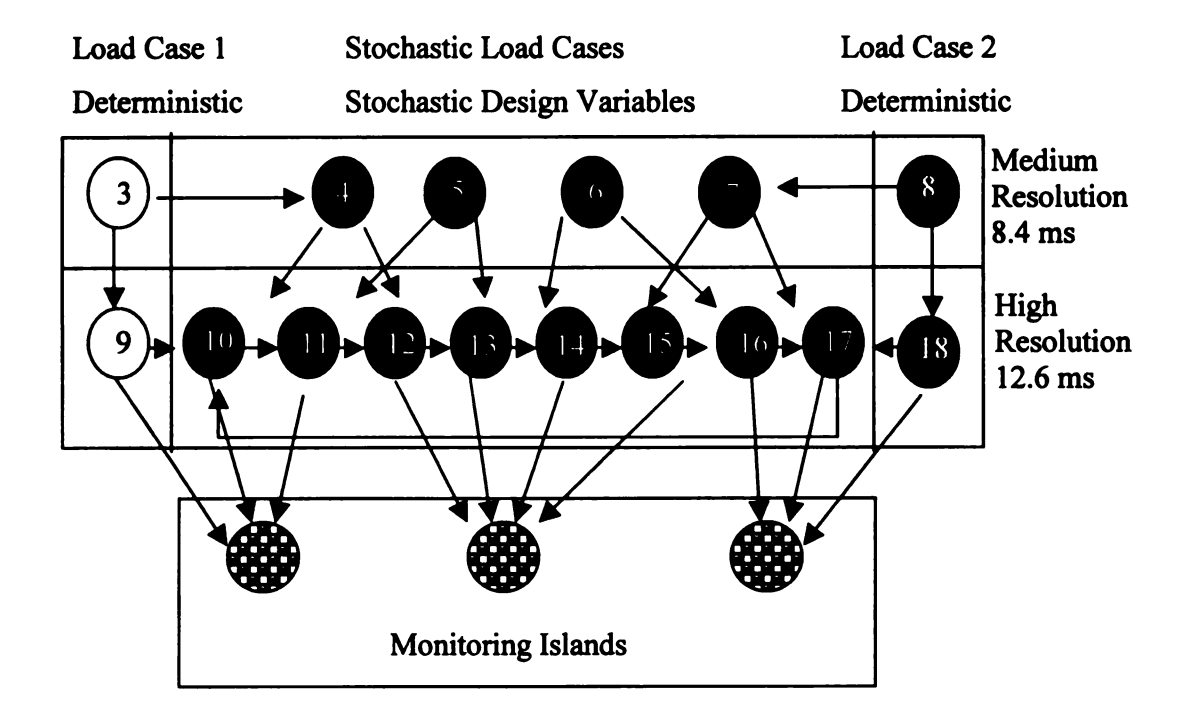


Figure 3.8. An iiGA topology that monitors islands the performance of the best designs for the two objectives defined by two structural load cases.

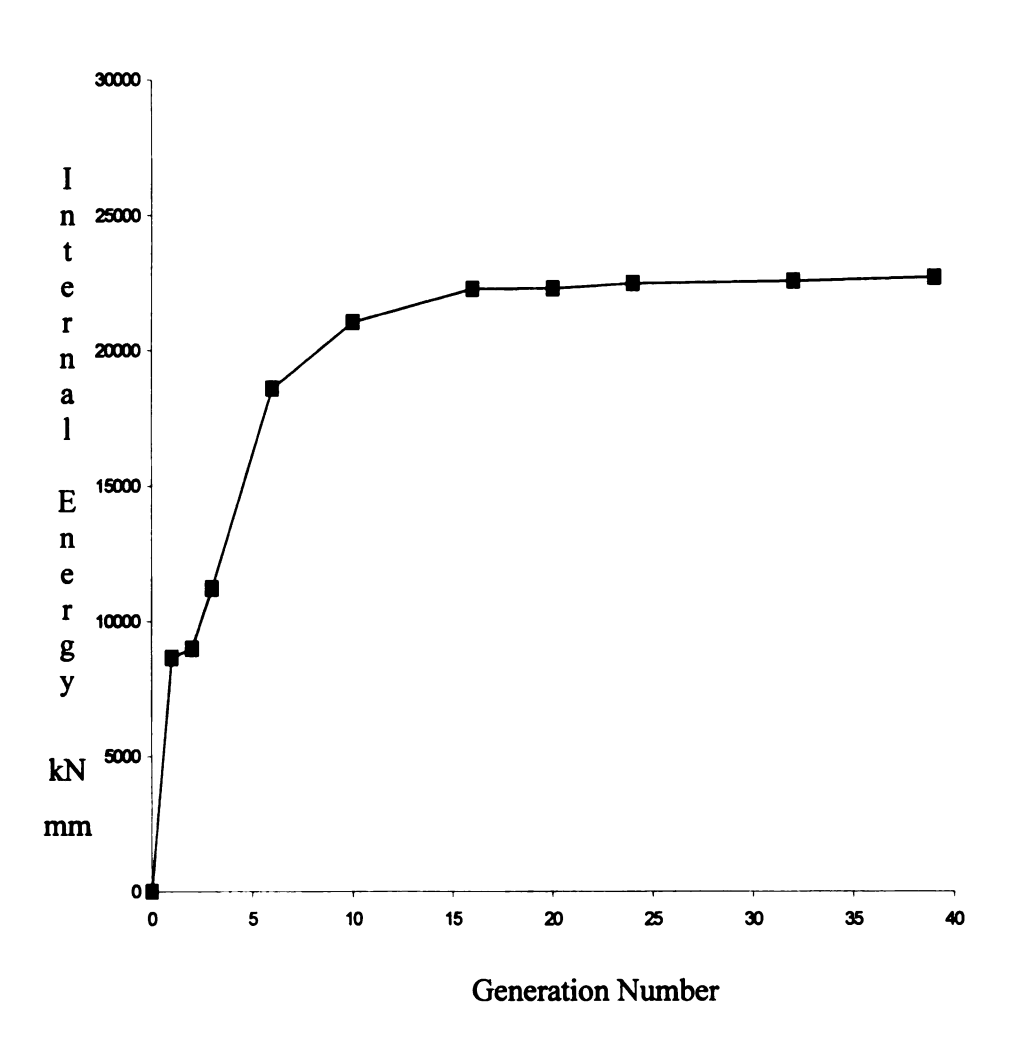


Figure 3.9. Crush zone internal energy as a function of generation number for load case 1, island 9.

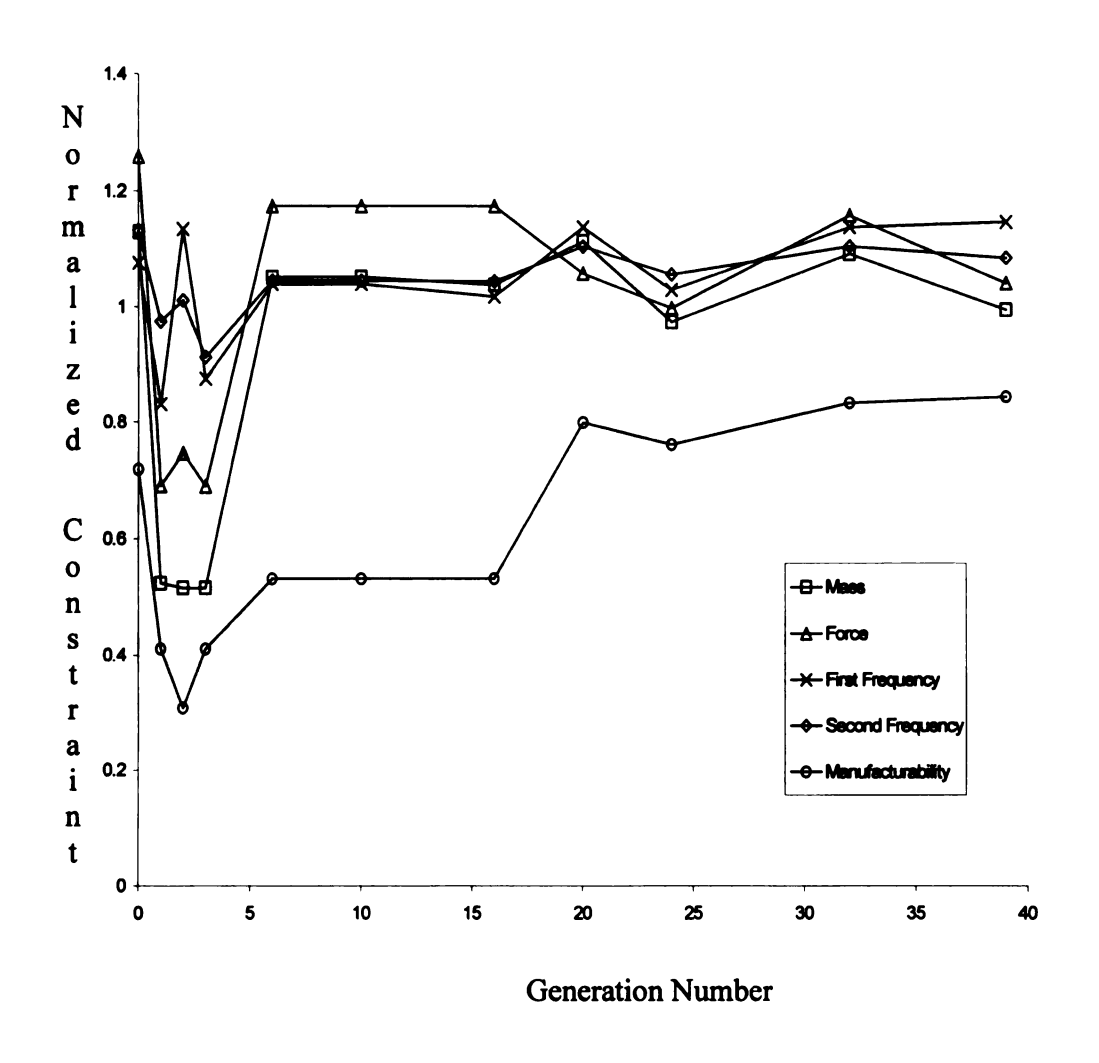


Figure 3.10. Normalized constraints as a function of generation number for island 9. A feasible design has normalized mass, force, and manufacturability constraints which are less than or equal to unity. A feasible design also has normalized first and second modal frequency constraints which are greater than or equal to unity.

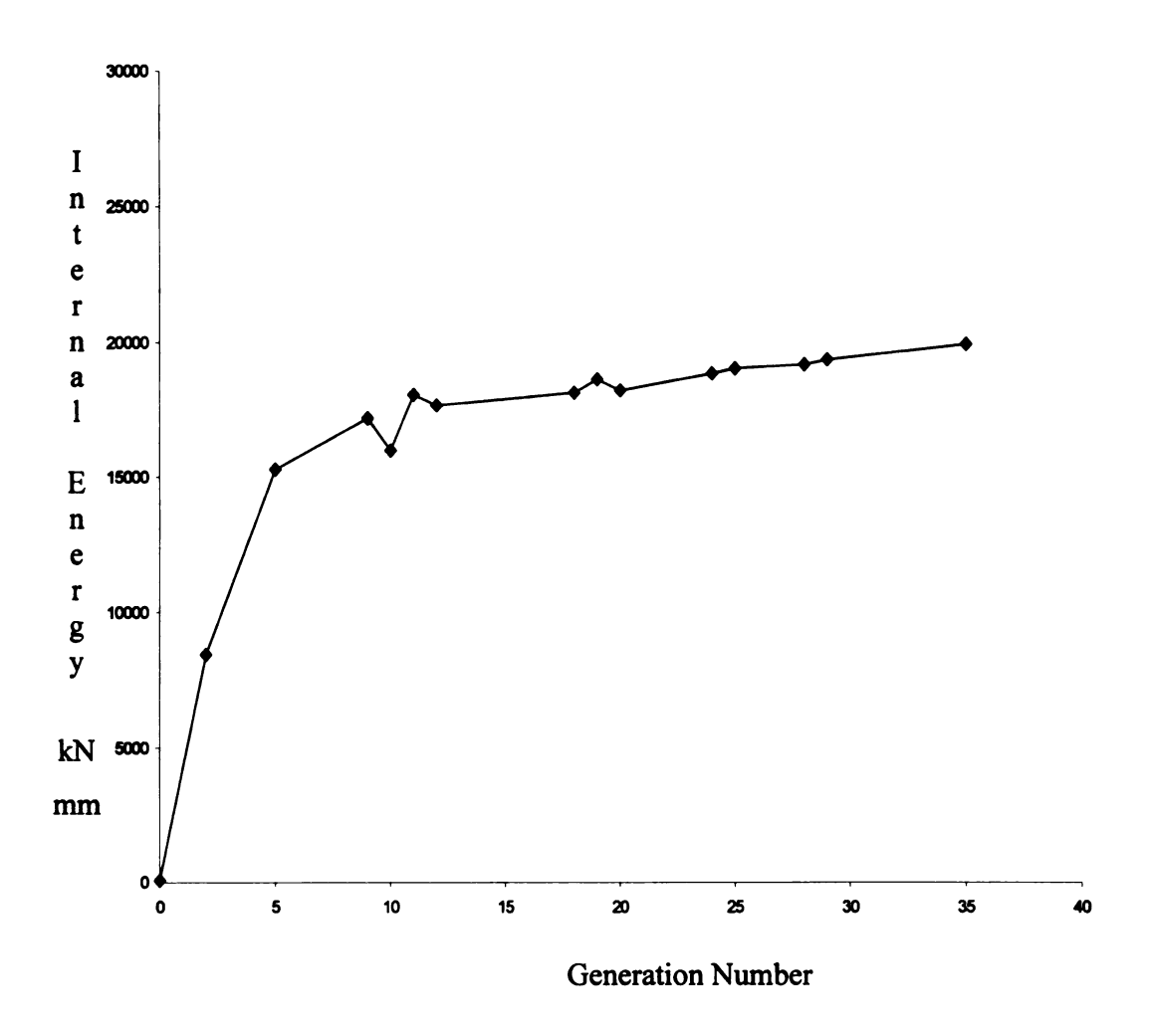


Figure 3.11. Crush zone internal energy as a function of generation number for load case 2, island 18.

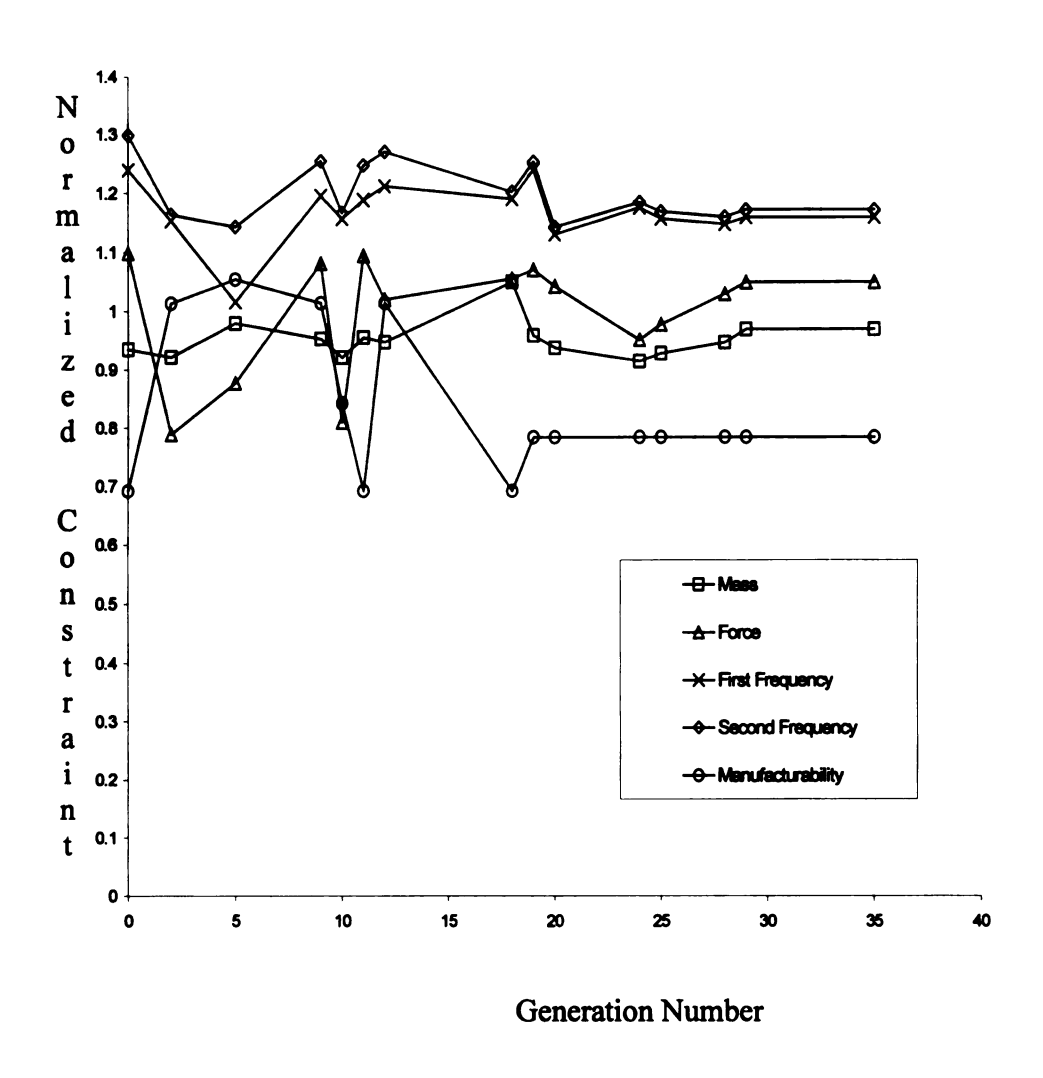


Figure 3.12. Normalized constraints as a function of generation number for island 18. A feasible design has normalized mass, force, and manufacturability constraints which are less than or equal to unity. A feasible design also has normalized first and second modal frequency constraints which are greater than or equal to unity.

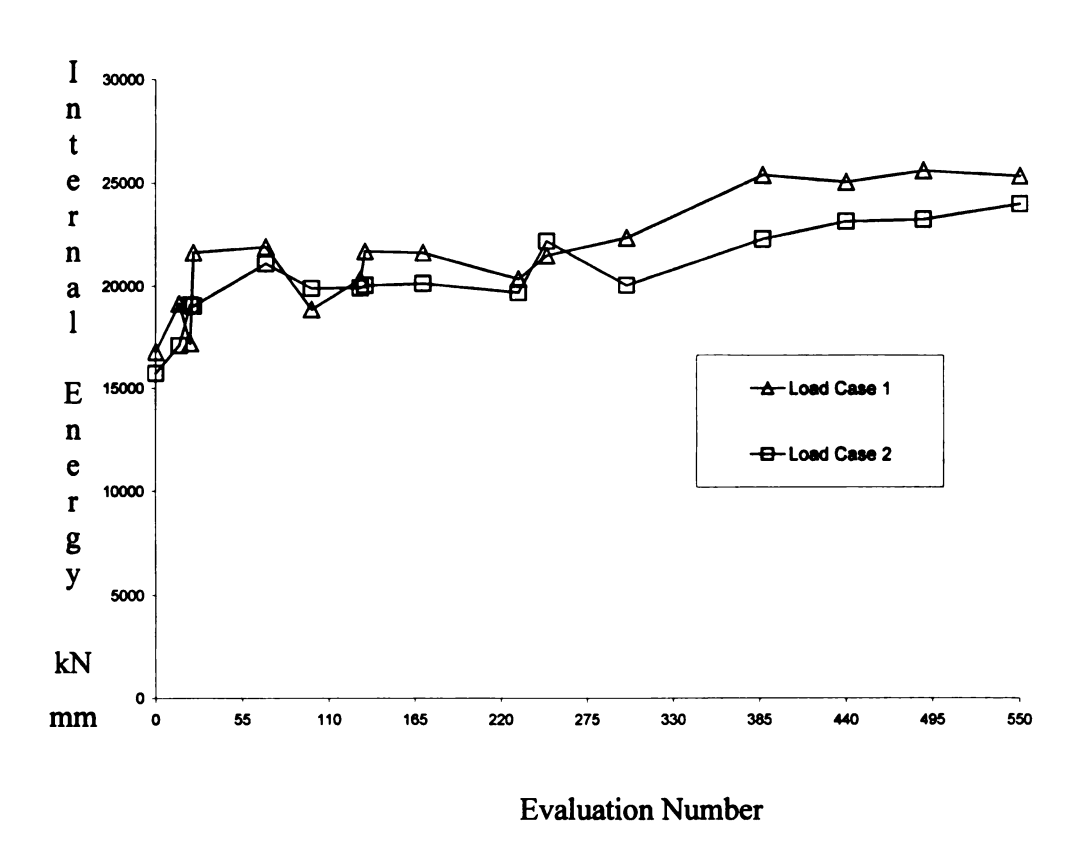


Figure 3.13. Crush zone internal energy as a function of evaluation number for load cases 1 and 2 from monitoring island.

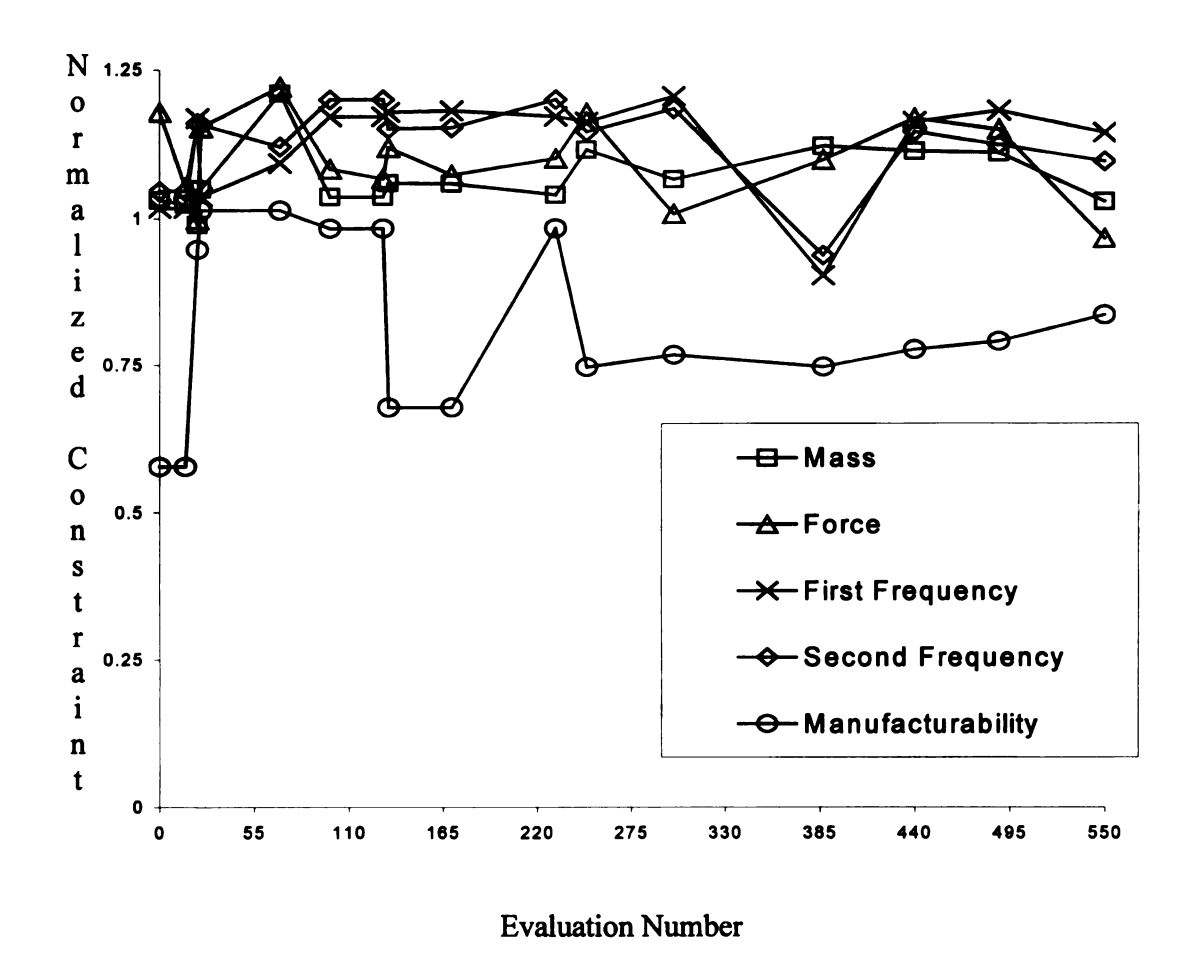


Figure 3.14. Normalized constraints as a function of evaluation number for monitor islands. A feasible design has normalized mass, force, and manufacturability constraints which are less than or equal to unity. A feasible design also has normalized first and second modal frequency constraints which are greater than or equal to unity.

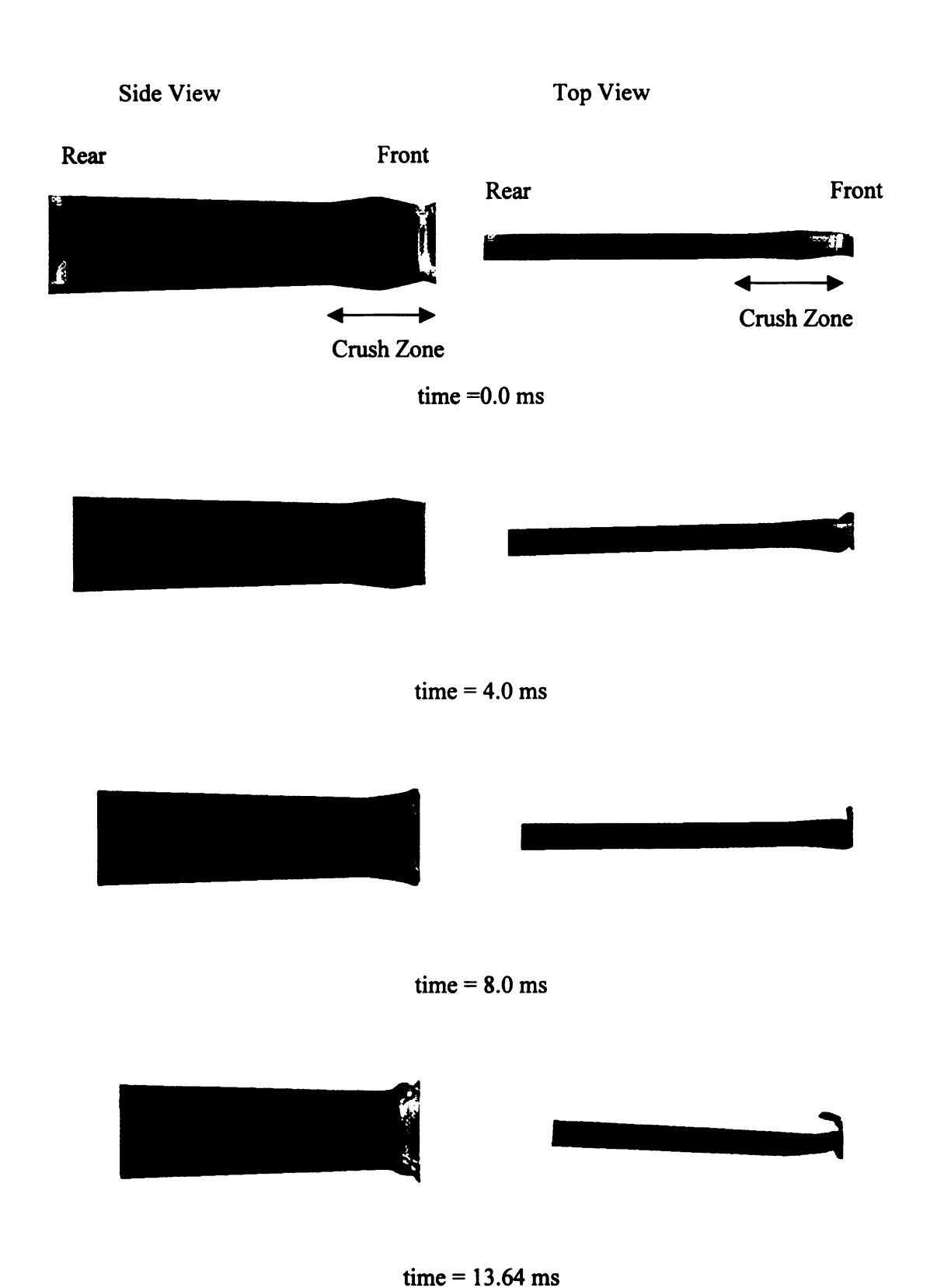


Figure 3.15. Animation of deformation for the best design found (load case 1).

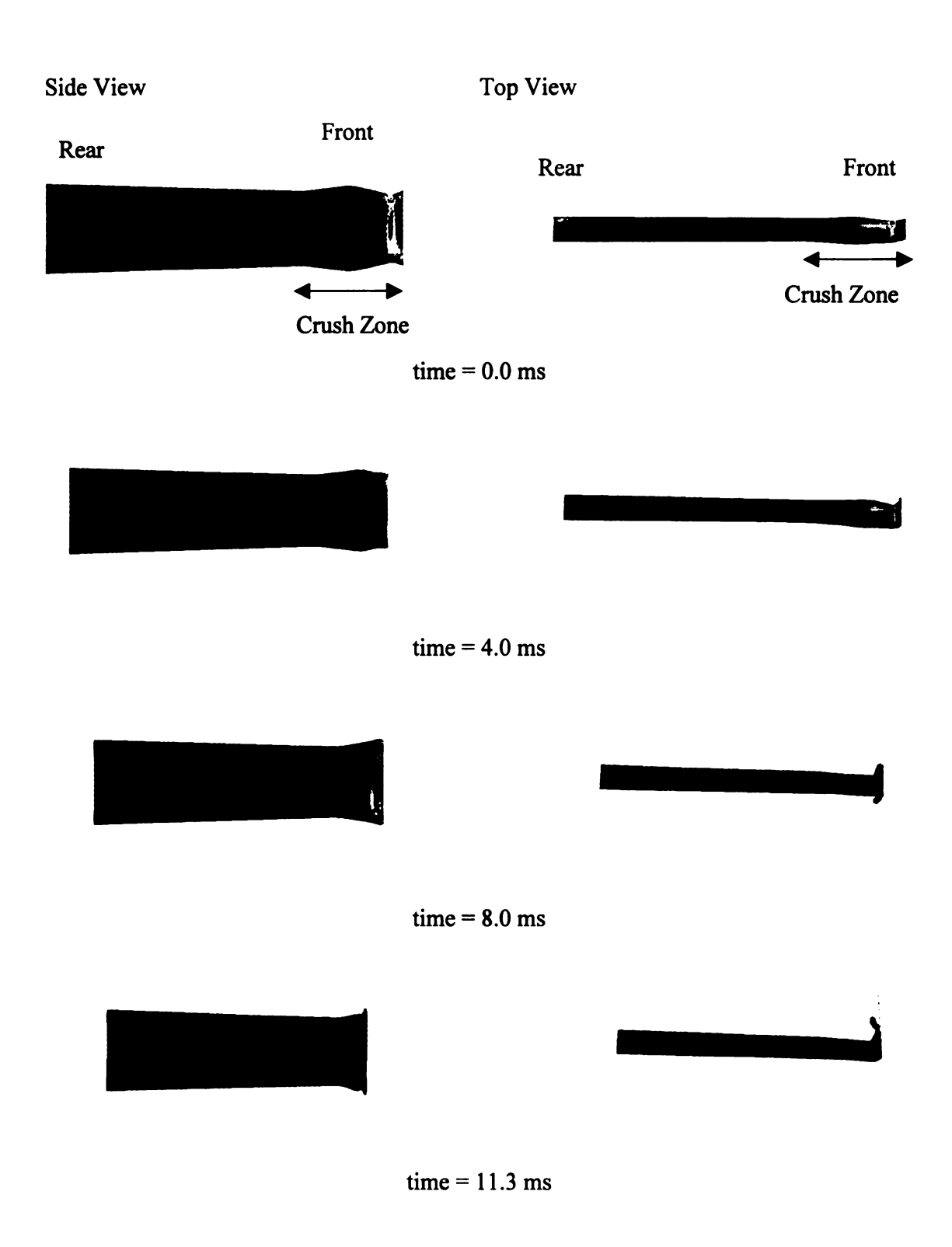
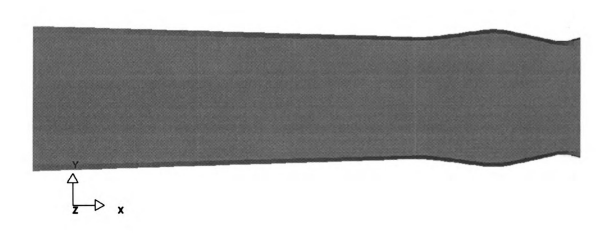


Figure 3.16. Animation of deformation for the best design found (load case 2).



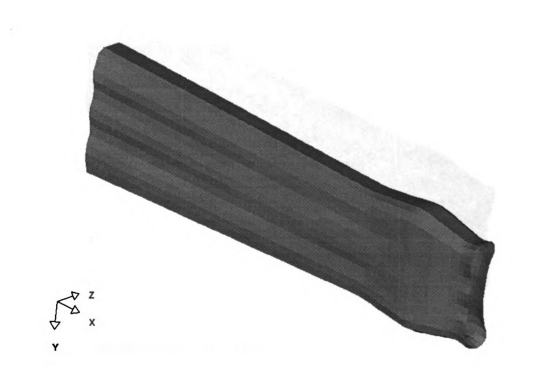


Figure 3.17. Surface models for best design found, run 1.





Figure 3.18. Surface models for best design found, run 2.





Figure 3.19. Surface models for best design found, run 3.

Table 3.1. Target values of inequality constraints for fitness function.

	Q			
C_1	C ₂	C ₃	C ₄	C ₅
120 kN	5.1 kg	75 Hz	115 Hz	0.1

Table 3.2 Weight values used for fitness function.

Α	B_1, E_1-E_4	E ₅	
100000.0	500.0	100.0	

Table 3.3. Genetic operator rate for each island in the island injection Genetic Algorithm.

Island	Crossover	Mutation	Population
Number	Percentage	Percentage	Size
0	75	1.0	80
1	70	1.0	50
2	75	1.0	80
3	70	1.0	80
4	65	1.0	40
5	65	1.0	40
6	65	1.0	40
7	65	1.0	40
8	70	1.0	80
9	65	1.0	80
10	60	1.0	30
11	60	1.0	30
12	60	1.0	30
13	60	1.0	30
14	60	1.0	30
15	60	1.0	30
16	60	1.0	30
17	60	1.0	30
18	65	1.0	80

Table 3.4. Primitive and thickness design variable information.

Island Numbers	Number of thickness choices	Number of Primitive choices	
0 through 2	16	32	
3 through 8	64	128	
9 through 18	128	256	

Table 3.5. Crush evaluation times per island and load case.

Island Numbers	Evaluation Time (Load Case 1)	Evaluation Time (Load Case 2)	
0 through 2	3.84	3.36	
3 through 8	8.4	7.35	
9 through 18	12.36	10.82	

Table 3.6. Number of full and partial design evaluations.

Island Number	Full Crush Evaluation	Partial Evaluation
0	645	1671
1	515	1500
2	780	1732
3	520	1148
4	501	1321
5	487	1433
6	530	1398
7	571	1451
8	563	1423
9	442	1451
10	431	1202
11	402	1176
12	478	1098
13	398	1254
14	421	1176
15	443	1205
16	436	1187
17	389	1132
18	404	1265

Table 3.7. Thickness design variables for each best design.

Run Number	First Thickness (mm)	Second Thickness (mm)	Third Thickness (mm)	Fourth Thickness (mm)
1	5.34	5.00	3.98	3.85
2	5.50	4.75	4.15	3.90
3	5.25	4.85	4.05	4.00

Table 3.8. Objective and constraint data for the best design found in three different independent runs.

Run #	Internal Energy Load Case 1 (kN- mm)	Internal Energy Load Case 2 (kN- mm)	Mass (kg)	Peak Force (kN)	First Modal Resp. (Hz)	Second Modal Resp. (Hz)	Manuf.
1	25298.6	24527.1	5.12	123.0	82.1	126.0	0.8
2	25611.2	24201.4	5.05	125.1	84.0	125.8	0.74
3	25010.6	24727.6	5.08	119.5	83.5	124.9	0.70

Table 3.9. Stochastic variability of internal energy for the best designs found (20 independent evaluations) with respect to thickness.

Run #	Average Internal Energy Load Case 1 (kN-mm)	Standard Dev. Internal Energy Load Case 1 (kN-mm)	Average Internal Energy Load Case 2 (kN-mm)	Standard Dev. Internal Energy Load Case 1 (kN-mm)
1	24981.6	405.1	24305.4	601.9
2	25111.2	367.1	24150.3	613.2
3	25310.6	503.5	23891.1	643.1

Chapter 4

DEVELOPMENT OF A GEOMETRICALLY NONLINEAR ZIG-ZAG FINITE ELEMENT MODEL

4.1 Introduction

Analysis of laminated composites and sandwich panels often requires a compromise between accuracy/complexity and efficiency/simplicity. While first-order shear deformation theory (Yang, et al., 1966) and higher order theories (see Reddy, 1990) are able to predict the overall structural response of most relatively thin laminated structures, these theories often poorly predict the magnitudes and distributions of local strains and stresses. In sandwich panels, these theories, as well as more specialized but traditional sandwich theories (see Vinson, 1999; Zenkert, 1997), fail to properly predict core shear and compressive stresses, cannot be applied to the full range of core densities and types, and cannot handle the extremes of skin thicknesses and moduli. At the other end of the spectrum, fully three-dimensional finite element models typically require significant through-thickness discretization (e.g., one element per layer), involving large computing power and an onerous model development effort. The above issues are further exacerbated whenever a nonlinear analysis is required.

The goal of most new laminate modeling approaches is to increase accuracy while decreasing modeling effort and/or computational cost. Toward this goal, a new technical theory and associated finite element model have been developed for analysis of thick or thin laminated composite and sandwich panels (Cho and Averill, 2000). The theory employs the sublaminate concept such that

each computational layer contains several physical layers. Within each sublaminate, an accurate approximation of the displacement field accounts for discrete layer effects without increasing the number of degrees of freedom as the number of layers is increased. This is accomplished by analytically satisfying the continuity of transverse shear stresses at layer interfaces. Because the resulting through-thickness variation of "in-plane" displacements takes the form of a piecewise linear function, the theory is often called zig-zag theory. Depending on the laminate layup and the type of global and/or local response measures that are sought, the optimal number of sublaminate approximations required for accurate analysis of thick multilayered composite laminates or sandwich panels is far less than the number of layers in the laminate. Often, only one sublaminate is required.

This model has been cast in a form that is very convenient for use in finite element analysis, namely, eight-noded brick and six-noded wedge three-dimensional elements have been developed that behave very much like plate elements, but have nearly all of the advantages of traditional three-dimensional elements (Cho and Averill, 2000). In particular, these layered solid elements can be stacked in the thickness direction of a laminate, allowing any desired degree of through-thickness discretization. Further, these elements may have very large aspect ratios without exhibiting shear locking or Poisson ratio locking. The three-dimensional zig-zag sublaminate finite elements contain only the typical five engineering degrees-of-freedom (i.e., three translations and two rotations) at

each node, so they are compatible with the requirements of most commercial finite element packages.

The first-order zig-zag sublaminate theory and its associated finite elements have been shown to be very accurate and robust for predicting the linear structural response of a wide range of laminated composite and sandwich panels. However, the effectiveness of this model in predicting nonlinear response has not been thoroughly investigated. The zig-zag sublaminate approach seems to have great promise for predicting progressive failure, sandwich skin buckling. and other nonlinear structural behaviors. Hence, recent attention has been given to the development of geometrically nonlinear zig-zag models. Geometrically nonlinear models of various forms of the zig-zag plate theory have been developed by several investigators (Yip. 1996; Lee, 1998; DiSciuva, 1996, 1997). The combination of accuracy and simplicity of the first-order zig-zag sublaminate model makes it more convenient for general purpose use compared to the available higher-order zig-zag type models. Thus, in the present work the firstorder zig-zag model (Cho and Averill, 2000) is extended to account for geometric nonlinearity due to moderate rotations of the plate reference surface. Such an extension is motivated by the need to simulate nonlinear phenomena such as those mentioned above. Here, the new nonlinear model is developed and validated.

4.2 Basic Ingredients Needed For The First-order Zig-Zag Plate Theory

In this section a brief description of the geometrically nonlinear first-order zig-zag sublaminate plate theory is provided. Many details related to the mathematical development of the zig-zag coefficients are neglected, and attention is focused on the extension of the model to account for moderately large rotations. For a complete description of the geometrically linear theory and the associated numerical validation studies, the reader is referred to (Cho and Averill, 2000).

It is assumed that the laminate is composed of N_T perfectly bonded layers. The thickness and material stiffness properties may vary arbitrarily from layer to layer. The laminate is modeled as M sublaminates, with each sublaminate containing N_m layers, where m is the sublaminate number. Mathematically, this is represented as:

$$N_T = \sum_{m=1}^{M} N_m \tag{4.1}$$

In order to facilitate the development of the theory, all expressions in the following derivation pertain to the m-th sublaminate. The sublaminate number designation m is omitted for brevity. The reference surface of the m-th sublaminate is assumed to be the bottom surface of the sublaminate, as shown in Figure 4.1.

The global X_3 -axis is taken perpendicular to the in-plane X_1 , X_2 coordinate axes and has its origin at the bottom of the laminate, while x_3 is a local

sublaminate coordinate in the direction of X_3 with its origin at the bottom of the sublaminate (See Figure 4.1).

The constitutive relations for a three-dimensional stress state in the k-th layer of the m-th sublaminate can be written as:

$$\begin{bmatrix}
S_{11}^{(k)} \\
S_{22}^{(k)} \\
S_{33}^{(k)} \\
S_{23}^{(k)} \\
S_{13}^{(k)} \\
S_{12}^{(k)}
\end{bmatrix} = \begin{bmatrix}
C_{11}^{(k)} & C_{12}^{(k)} & C_{13}^{(k)} & 0 & 0 & C_{16}^{(k)} \\
C_{12}^{(k)} & C_{22}^{(k)} & C_{23}^{(k)} & 0 & 0 & C_{26}^{(k)} \\
C_{13}^{(k)} & C_{23}^{(k)} & C_{33}^{(k)} & 0 & 0 & C_{36}^{(k)} \\
0 & 0 & 0 & C_{44}^{(k)} & C_{45}^{(k)} & 0 \\
0 & 0 & 0 & C_{45}^{(k)} & C_{55}^{(k)} & 0 \\
C_{16}^{(k)} & C_{26}^{(k)} & C_{36}^{(k)} & 0 & 0 & C_{66}^{(k)}
\end{bmatrix} \begin{pmatrix}
\varepsilon_{11}^{(k)} \\
\varepsilon_{22}^{(k)} \\
\varepsilon_{33}^{(k)} \\
\gamma_{23}^{(k)} \\
\gamma_{13}^{(k)} \\
\gamma_{12}^{(k)}
\end{bmatrix}$$

$$(4.2.)$$

where $S_{ij}^{(k)}$ are the components of the second Piola-Kirchhoff stress tensor and $\varepsilon_{ij}^{(k)}$ are the components of the Green strain tensor. For most practical laminated composites, the 13 coefficients of the material stiffness matrix are obtained from 9 independent material constants and a transformation law (see Jones, 1999).

If strains are small compared to unity but rotations of the plate reference surface are moderate, then the Green strain tensor can be degenerated to a simplified form commonly referred to as the von Karman strain tensor, defined in vector format as:

$$\begin{cases}
\mathcal{E}_{11}^{(k)} \\
\mathcal{E}_{22}^{(k)} \\
\mathcal{E}_{33}^{(k)} \\
\gamma_{23}^{(k)} \\
\gamma_{13}^{(k)} \\
\gamma_{12}^{(k)}
\end{cases} = \begin{cases}
u_{1,1}^{(k)} \\
u_{2,2}^{(k)} \\
u_{3,3}^{(k)} \\
u_{2,3}^{(k)} + u_{3,2}^{(k)} \\
u_{1,3}^{(k)} + u_{3,1}^{(k)} \\
u_{1,2}^{(k)} + u_{2,1}^{(k)}
\end{cases} + \begin{cases}
\frac{1}{2} (u_{3,1}^{(k)})^2 \\
\frac{1}{2} (u_{3,2}^{(k)})^2 \\
0 \\
0 \\
0 \\
u_{3,1}^{(k)} u_{3,2}^{(k)}
\end{cases}$$

$$(4.3)$$

where $u_i^{(k)}$ is the displacement of a point in the x_i direction and $()_{,j}$ implies differentiation with respect to x_i .

The sublaminate displacement fields are initially assumed in the following form:

$$u_{1}^{(k)}(x_{1}, x_{2}, x_{3}, t) = u_{b} + x_{3} \cdot \Psi_{1} + \sum_{i=1}^{k-1} (x_{3} - x_{3i}) \cdot \xi_{i}$$

$$u_{2}^{(k)}(x_{1}, x_{2}, x_{3}, t) = v_{b} + x_{3} \cdot \Psi_{2} + \sum_{i=1}^{k-1} (x_{3} - x_{3i}) \cdot \eta_{i}$$

$$u_{3}^{(k)}(x_{1}, x_{2}, x_{3}, t) = w_{b} \cdot \left(1 - \frac{x_{3}}{h}\right) + w_{i} \cdot \left(\frac{x_{3}}{h}\right)$$

$$(4.4)$$

where t represents time, h is the thickness of the sublaminate, u_b and v_b are the axial displacements in x_1 and x_2 directions, respectively, at $x_3 = 0$, Ψ_1 and Ψ_2 are rotations of the normal at $x_3 = 0$, and w_b and w_i are the transverse deflections of the bottom and top surfaces, respectively, of the m-th sublaminate. Thus, it is assumed that $u_1^{(k)}$ and $u_2^{(k)}$ vary in a piecewise linear fashion throughthe-thickness of a sublaminate and $u_3^{(k)}$ varies linearly through-the-thickness. The parameters ξ_i and η_i in equation 4.4 are eliminated by enforcing continuity of transverse shear stress at each ply interface (Cho and Averill, 2000; DiSciuva, 1997). The shear stress continuity conditions at the k-th interface can be expressed as:

$$S_{23}^{(k)} = S_{23}^{(k+1)}, \quad S_{13}^{(k)} = S_{13}^{(k+1)}$$
 (4.5)

Assuming that infinitesimal strain theory holds for the transverse shear strain components, the form of the assumed displacement fields in equation 4.5 is such that the in-plane displacements $u_1^{(k)}$ and $u_2^{(k)}$ contribute only constant terms to

the transverse shear stresses, $S_{13}^{(k)}$ and $S_{23}^{(k)}$. For consistency, then, the transverse displacement $u_3^{(k)}$ should also contribute only constant terms to these stress components. In order to achieve this consistency, terms in the transverse shear strain expressions that involve the transverse displacement variables are evaluated at the midplane of the sublaminate, thereby taking a thickness averaged value of these terms. Substituting equations 4.3 and 4.4 into equation 4.5 and solving for ξ_i and η_i , it can be seen that ξ_i and η_i depend on the ratios of shear properties between adjacent layers and on the shear deformation in each sublaminate. If either of these quantities are small, then discrete-layer effects will also be small.

The rotational variables Ψ_1 and Ψ_2 in the displacement field are now eliminated by introducing the variables u_t and v_t (the in-plane translations at the top surface of the sublaminate) in order to expedite the development of versatile finite element models. Thus, rather than describing the in-plane displacement field by a translation and rotation at one point, it can more conveniently be described here by the translation at two points.

The displacement fields must be further manipulated in order to develop a C^0 finite element. Because the derivatives of transverse deflections $(\frac{\partial w_b}{\partial x_1}, \frac{\partial w_t}{\partial x_1}, \frac{\partial w_b}{\partial x_2})$ and $\frac{\partial w_t}{\partial x_2}$ and $\frac{\partial w_t}{\partial x_2}$ appear in the displacement field, their second derivatives will be present in the strain energy functional. C^1 continuity of w_b and w_t is thus required. It is desirable to alleviate such a requirement by introducing new rotational degrees of freedom as follows:

$$\frac{\partial w_b}{\partial x_1} = -\theta_{2b}, \quad \frac{\partial w_t}{\partial x_1} = -\theta_{2t}, \quad \frac{\partial w_b}{\partial x_2} = \theta_{1b}, \quad \frac{\partial w_t}{\partial x_2} = \theta_{1t}$$
 (4.6)

These relationships will be constrained in the strain energy via a combination of the interdependent interpolation and the penalty method. The displacement fields can now be written using indicial notation as follows:

$$u_1^{(k)} = \overline{u}_{\alpha\beta} \cdot \Phi_{\alpha\beta}^{(k)}, \quad u_2^{(k)} = \overline{u}_{\alpha\beta} \cdot \Psi_{\alpha\beta}^{(k)}, \quad u_3^{(k)} = w_\beta \cdot \Omega_\beta \qquad \alpha = 1...4; \quad \beta = 1,2 \quad (4.7)$$

where the index β is used to denote the top and bottom of the sublaminate with 1: bottom and 2: top, and $\Phi_{\alpha\beta}^{(k)}, \Psi_{\alpha\beta}^{(k)}$ and Ω_{β} are shape functions in the thickness direction (see Cho and Averill, 2000). Unless noted otherwise, summation on repeated indices is implied. The variables $\overline{u}_{\alpha\beta}$ are:

$$\overline{u}_{1\beta} = u_{\beta}, \quad \overline{u}_{2\beta} = v_{\beta}, \quad \overline{u}_{3\beta} = \theta_{1\beta}, \quad \overline{u}_{4\beta} = \theta_{2\beta}$$
 (4.8)

The transverse normal strain arising from the assumed displacement field (4.7) is constant through-the-thickness of a sublaminate and takes the value $(w_i - w_b)/h$. This assumption may generate substantial errors in composites that have a soft core or layer, such as in sandwich panels, laminates containing damage, or adhesive layers. It is desirable to improve the distribution of the transverse normal strain through-the-thickness. The improvement can be achieved by assuming a constant transverse normal stress, \bar{S}_{33} through-the-thickness of a sublaminate. \bar{S}_{33} can be determined using Reissner's mixed variational principle (Reissner, 1986). From equation 4.2, the transverse normal strain is obtained as:

$$\overline{\varepsilon}_{33}^{(k)} = \frac{1}{C_{13}^{(k)}} \left(\overline{S}_{33} - C_{13}^{(k)} \varepsilon_{11}^{(k)} - C_{23}^{(k)} \varepsilon_{22}^{(k)} - C_{36}^{(k)} \gamma_{12}^{(k)} \right) \tag{4.9}$$

 \overline{S}_{33} is then determined analytically from the following relation:

$$0 = \sum_{k=1}^{N} \int_{x_{3(k-1)}}^{x_{3(k)}} \left(\overline{\varepsilon}_{33}^{(k)} - \frac{w_t - w_b}{h} \right) dx_3$$
 (4.10)

The constant transverse normal stress \bar{S}_{33} is found to be:

$$\overline{S}_{33} = f_1(\overline{u}_{\alpha\beta}, W_{\beta}, \Phi_{\alpha\beta}^{(k)}, \Psi_{\alpha\beta}^{(k)}, \Omega_{\alpha\beta}^{(k)})$$

$$\tag{4.11}$$

Now, the newly defined transverse normal strain can be written as:

$$\bar{\varepsilon}_{33}^{(k)} = f_2(\bar{u}_{\alpha\beta}, w_{\beta}, \Phi_{\alpha\beta}^{(k)}, \Psi_{\alpha\beta}^{(k)}, \Omega_{\alpha\beta}^{(k)})$$
(4.12)

The functions f_1 and f_2 are defined in (Cho and Averill, 2000) for small displacement analysis. For the purpose of calculating \overline{S}_{33} , the von Karman nonlinear strain terms must be included in equation 4.9 to ensure accuracy of the solution for all types of laminates.

4.3. Virtual Work

The equations of motion, the essential and natural boundary conditions, as well as the displacement-based finite element model can be developed from the principle of virtual work. Again, attention will be limited to a single sublaminate. The work functional is modified here to include the imposition of the constraints in Equation 4.6 via the penalty method. The total work performed by internal and external forces on a sublaminate is:

$$W = W_I + W_E \tag{4.13}$$

For linear elastic material behavior, the internal work is:

$$W_I = \frac{1}{2} \int SE \, dV \tag{4.14}$$

where E and S are vector representations of the Green's strain and the second Piola-Kirchhoff stress states. W_E is the work of the external forces performed on the sublaminate:

$$W_{E} = -\int \mathbf{b}^{T} \mathbf{u} dV - \int \mathbf{t}^{T} \mathbf{u} d\Gamma$$
 (4.15)

where u is a vector of displacements, b is a vector of body forces and t is a vector of tractions on the surface Γ .

The work functional defined by equation 4.13 will be subject to the four constraints in equation 4.6, which can be represented as:

$$G_i(u,u')=0$$
 $i=1,2,3,4$ (4.16)

We now introduce a modified work functional:

$$W_{M} = W_{L} + W_{E} + W_{P} \tag{4.17}$$

If the constraints (6) are enforced using the penalty method, then:

$$W_{P} = \sum_{i=1}^{4} \frac{\gamma}{2} \int_{\Omega} G_{i}^{2} d\Omega \qquad (4.18)$$

where γ is the penalty parameter, Ω is the domain upon which the constraints

are to be enforced,
$$G_1 = \frac{\partial w_b}{\partial x_1} + \theta_{2b}$$
, $G_2 = \frac{\partial w_t}{\partial x_1} + \theta_{2t}$, $G_3 = \frac{\partial w_b}{\partial x_2} - \theta_{1b}$, and

$$G_4 = \frac{\partial w_t}{\partial x_2} - \theta_{1t}.$$

The total virtual work performed on a sublaminate is now defined by the first infinitesimal variation of the modified work functional:

$$\delta W_{M} = \delta W_{F} + \delta W_{F} + \delta W_{P} = 0 \tag{4.19}$$

δW_I is the virtual work resulting from internal forces:

$$\delta W_I = \left[\mathbf{S} \, \delta \mathbf{E} \, dV \right] \tag{4.20}$$

 δW_E is the virtual work resulting from external forces:

$$\delta W_E = -\left[\mathbf{b}^T \delta \mathbf{u} dV - \left[\mathbf{t}^T \delta \mathbf{u} d\Gamma\right]\right] \tag{4.21}$$

 δW_P is the virtual work resulting from violation of the equality constraints:

$$\delta W_{P} = \sum_{i=1}^{N} \gamma \int \left[\delta G_{i}(u, u') G_{i}(u, u') \right] dV$$
 (4.22)

As the penalty parameter γ becomes larger, violation of the equality constraints is minimized in a least squares sense. The governing equations, finite element model and boundary conditions can be derived directly from equation 4.19. The details of this procedure are omitted for brevity.

4.4 Finite Element Formulation

The standard form of the finite element approximation is:

$$\mathbf{u} = \mathbf{N}\overline{\mathbf{u}} \tag{4.23}$$

where N is a matrix of element interpolation functions and $\overline{\mathbf{u}}$ is a vector of nodal degrees of freedom.

Green's strain can be written as the sum of linear and nonlinear parts:

$$\mathbf{E} = \varepsilon_L + \varepsilon_{NL} \tag{4.24}$$

The linear portion of the Green's strain is:

$$\varepsilon_{t} = \mathbf{L}\mathbf{u} = \mathbf{L}\mathbf{N}\overline{\mathbf{u}} = \mathbf{B}_{t}\overline{\mathbf{u}} \tag{4.25}$$

where L is a matrix of linear differential operators and B_L is a matrix containing gradients of the interpolation functions. All coefficients needed to formulate B_L can be found in (Cho and Averill, 2000). The nonlinear portion of the Green's strain is:

$$\varepsilon_{\scriptscriptstyle NL} = \frac{1}{2} \mathbf{A}(\theta) \theta(\mathbf{u}) \tag{4.26}$$

where $\theta(\mathbf{u})$ is a vector of displacement gradients and $\mathbf{A}(\theta)$ is a matrix composed of the vector $\theta(\mathbf{u})$. Green's strain can then be written as:

$$\mathbf{E} = \mathbf{B}_{L}\overline{\mathbf{u}} + \frac{1}{2}\mathbf{A}(\theta)\theta(\overline{\mathbf{u}}) = \hat{\mathbf{B}}\overline{\mathbf{u}}$$
 (4.27)

and the first infinitesimal variation of Green's strain is:

$$\delta \mathbf{E} = \mathbf{B}_{L} \delta \overline{\mathbf{u}} + \frac{1}{2} \left(\delta \mathbf{A}(\theta) \theta(\overline{\mathbf{u}}) + \mathbf{A}(\theta) \delta \theta(\overline{\mathbf{u}}) \right) \tag{4.28}$$

To simplify the definition of the first variation of Green's strain we note that:

$$\delta \mathbf{E} = \mathbf{B}_{L} \delta \overline{\mathbf{u}} + \frac{1}{2} \left(\mathbf{A} (\delta \theta) \theta(\overline{\mathbf{u}}) + \mathbf{A} (\theta) \delta \theta(\overline{\mathbf{u}}) \right)$$
(4.29)

and:

$$\delta\theta(\overline{\mathbf{u}}) = \theta(\overline{\mathbf{u}})\delta\overline{\mathbf{u}} \tag{4.30}$$

so that:

$$\delta \mathbf{E} = \mathbf{B}_{1} \delta \overline{\mathbf{u}} + \mathbf{A}(\theta) \theta(\overline{\mathbf{u}}) \delta \overline{\mathbf{u}}$$
 (4.31)

The first variation of the Green's strain can now be written as:

$$\delta \mathbf{E} = \mathbf{B}_{L} \delta \overline{\mathbf{u}} + \mathbf{A}(\theta) \theta(\overline{\mathbf{u}}) \delta \overline{\mathbf{u}} = (\mathbf{B}_{L} + \mathbf{A}(\theta)\mathbf{G}) \delta \overline{\mathbf{u}} = \overline{\mathbf{B}} \delta \overline{\mathbf{u}}$$
(4.32)

where G is a matrix of nodal shape function gradients.

The virtual work can now be written as:

$$\delta W_{M} = \delta \overline{\mathbf{u}}^{T} \left(\int \overline{\mathbf{B}}^{T} \mathbf{S} dV + \gamma \int \mathbf{p}^{T} \mathbf{p} \overline{\mathbf{u}} d\Omega - \int \mathbf{b}^{T} \mathbf{N} dV - \int \mathbf{t}^{T} \mathbf{N} d\Gamma \right) = 0$$
 (4.33)

where **p** is a vector containing nodal shape functions used to define the penalty constraints. This relation is valid for an arbitrary variation of the element nodal degrees of freedom, thus:

$$\mathbf{r}(\overline{\mathbf{u}}) = \int \overline{\mathbf{B}}^{T} \mathbf{S} dV + \gamma \int \mathbf{p}^{T} \mathbf{p} \overline{\mathbf{u}} d\Omega - \int \mathbf{b}^{T} \mathbf{N} dV - \int \mathbf{t}^{T} \mathbf{N} d\Gamma = 0$$
 (4.34)

In general, an exact solution to equation 4.34 will not be attained, so the residual $r(\overline{u})$ will be non-zero. The residual is often called the out-of-balance forcing vector since it represents the amount that the current solution is "out of equilibrium."

Equation 4.34 is typically written in the form:

$${}^{D}\mathbf{K}\overline{\mathbf{u}} = \mathbf{f} \tag{4.35}$$

where the direct stiffness matrix (including the penalty term) is written as:

$${}^{D}\mathbf{K} = \int \overline{\mathbf{B}}^{T} \mathbf{D} \hat{\mathbf{B}} dV + \gamma \int_{\Omega} \mathbf{p}^{T} \mathbf{p} d\Omega$$
 (4.36)

and the forcing vector is written as:

$$\mathbf{f} = (\mathbf{b}^{\mathsf{T}} \mathbf{N} dV + (\mathbf{t}^{\mathsf{T}} \mathbf{N} d\Gamma)$$
 (4.37)

It should be noted that direct iteration of equation 4.35 can be performed by constructing, inverting and iterating upon the unsymmetric direct stiffness matrix, but this leads to high computational costs and slow convergence rates. Instead, we employ the Newton-Raphson solution technique that uses a

symmetric tangent stiffness matrix to iterate until a sufficiently accurate solution is obtained.

4.5 Newton-Raphson Method

To define the tangent stiffness matrix ^TK, we expand the residual in a Taylor series expansion about the current equilibrium configuration (denoted by the subscript o):

$$\mathbf{r}(\overline{\mathbf{u}}) = \mathbf{r}_o + \frac{\partial \mathbf{r}_o}{\partial \overline{\mathbf{u}}} \delta \overline{\mathbf{u}} + \frac{1}{2!} \delta \overline{\mathbf{u}}^T \frac{\partial^2 \mathbf{r}_o}{\partial \overline{\mathbf{u}}^2} \delta \overline{\mathbf{u}} + \cdots$$
 (4.38)

Higher order terms in the Taylor Series expansion are assumed to be small when compared to the constant and linear terms. We wish to minimize the residual $r(\overline{u})$ so equation 4.38 becomes:

$$\mathbf{0} = \mathbf{r}_o + \frac{\partial \mathbf{r}_o}{\partial \overline{\mathbf{u}}} \delta \overline{\mathbf{u}} \tag{4.39}$$

The first variation of nodal degrees of freedom about the current configuration is:

$$\delta \overline{\mathbf{u}} = -\left(\frac{\partial \mathbf{r}_o}{\partial \overline{\mathbf{u}}}\right)^{-1} \mathbf{r}_o = -\left({}^{\tau} \mathbf{K}\right)^{-1} \mathbf{r}_o \tag{4.40}$$

For complex formulations such as the current one, direct application of equation 4.40 can be cumbersome. Alternatively, but equivalently, the tangent stiffness can be formed by taking the second infinitesimal variation of the modified functional (see Crisfield, 1991). The tangent stiffness can then be defined as:

$$\delta(\delta W_{M}) = \delta \mathbf{r}_{o}(\overline{\mathbf{u}}) = \delta \overline{\mathbf{u}}^{T} \left(\frac{\partial \mathbf{r}_{o}}{\partial \overline{\mathbf{u}}}\right) \delta \overline{\mathbf{u}} = \delta \overline{\mathbf{u}}^{T} (^{T} \mathbf{K}) \delta \overline{\mathbf{u}}$$
(4.41)

We can express the first infinitesimal variation of the residual $\mathbf{r}_{o}(\overline{\mathbf{u}})$ as:

$$\delta \mathbf{r}_{o}(\overline{\mathbf{u}}) = \delta \overline{\mathbf{u}}^{T} \left\{ \left[\left(\delta \overline{\mathbf{B}}^{T} \mathbf{S} + \overline{\mathbf{B}}^{T} \delta \mathbf{S} \right) dV + \gamma \left[\left(\mathbf{p}^{T} \mathbf{p} \right) d\Omega \delta \overline{\mathbf{u}} \right] \right\}$$
(4.42)

The first term in (42) can be written as:

$$\delta \overline{\mathbf{u}}^{T} \left[\delta \overline{\mathbf{B}}^{T} \mathbf{S} dV = \delta \overline{\mathbf{u}}^{T} \left[\left(\delta \mathbf{A}(\theta) \mathbf{G} \right)^{T} \mathbf{S} dV \right] \right]$$
(4.43)

which can be rearranged and manipulated (due to the symmetry of the second Piola-Kirchhoff stress tensor) to form:

$$\delta \overline{\mathbf{u}}^{T} \left[\mathbf{G}^{T} (\delta \mathbf{A}(\theta))^{T} \mathbf{S} dV = \delta \overline{\mathbf{u}}^{T} \left[\mathbf{G}^{T} \hat{\mathbf{S}} \delta \mathbf{A}(\theta) dV \right] \right]$$
(4.44)

where $\hat{\mathbf{S}}$ is a matrix of second Piola-Kirchoff stresses which gives rise to the stress stiffening matrix ${}^{\sigma}\mathbf{K}$:

$$\delta \overline{\mathbf{u}}^{T} \left[\mathbf{G}^{T} \hat{\mathbf{S}} \delta \mathbf{A}(\theta) dV = \delta \overline{\mathbf{u}}^{T} \left(\left[\mathbf{G}^{T} \hat{\mathbf{S}} \mathbf{G} dV \right] \delta \overline{\mathbf{u}} \right) = \delta \overline{\mathbf{u}}^{T} \left(\mathbf{K} \right) \delta \overline{\mathbf{u}}$$
(4.45)

The stress stiffening matrix represents structural stiffening effects due to stresses that arise during the nonlinear deformation.

The second term in equation 4.42 can be simplified as:

$$\delta \overline{\mathbf{u}}^{T} \left[\overline{\mathbf{B}}^{T} \delta \mathbf{S} dV = \delta \overline{\mathbf{u}}^{T} \right] \overline{\mathbf{B}}^{T} \mathbf{C} \delta \mathbf{E} dV = \delta \overline{\mathbf{u}}^{T} \left(\left[\overline{\mathbf{B}}^{T} \mathbf{C} \overline{\mathbf{B}} dV \right] \delta \overline{\mathbf{u}} = \delta \overline{\mathbf{u}}^{T} \left(\overline{\mathbf{K}} \right) \delta \overline{\mathbf{u}}$$
(4.46)

The stiffness matrix $\overline{\mathbf{K}}$ represents the combined stiffening effects from large and small displacements.

The last term in equation 4.42 can be represented as:

$$\delta \overline{\mathbf{u}}^{T} \gamma \left(\int_{\Omega} \mathbf{p}^{T} \mathbf{p} d\Omega \right) \delta \overline{\mathbf{u}} = \delta \overline{\mathbf{u}}^{T} \binom{p}{K} \delta \overline{\mathbf{u}}$$
 (4.47)

The penalty stiffness matrix ${}^{P}\mathbf{K}$ represents the stiffness required to enforce the linear equality constraints in a least square sense.

Finally, the tangent stiffness matrix is:

$${}^{T}\mathbf{K} = {}^{\sigma}\mathbf{K} + \overline{\mathbf{K}} + {}^{P}\mathbf{K} \tag{4.48}$$

The solution at the i-th iteration of the n-th time increment is obtained using:

$$\begin{bmatrix} {}^{T}\mathbf{K} \end{bmatrix}_{i}^{"} \{ \Delta \overline{\mathbf{u}} \}_{i+1}^{"} = \{ \mathbf{F} \}_{i}^{"} - \begin{bmatrix} {}^{D}\mathbf{K} \end{bmatrix}_{i}^{"} \{ \overline{\mathbf{u}} \}_{i}^{"}$$
(4.49)

and:

$$\{\overline{\mathbf{u}}\}_{i=1}^n = \Delta \{\overline{\mathbf{u}}\}_{i=1}^n + \{\overline{\mathbf{u}}\}_i^n \tag{4.50}$$

where $\{\overline{\mathbf{u}}\}_{i+1}^n$ and $\Delta\{\overline{\mathbf{u}}\}_{i+1}^n$ are the total and incremental displacements at iteration i+1 for the n-th time increment. The equations 4.49 and 4.50 are solved iteratively until $\Delta\{\overline{\mathbf{u}}\}_{i+1}^n$ is sufficiently small.

4.6 Finite Element Approximations

The first-order zig-zag sublaminate finite element model formulation for linear strain theory was developed by Cho and Averill (2000). These elements are based on a formulation that involves sublaminate surface variables, which facilitates the development of a three-dimensional finite element model. Each node contains five degrees of freedom – three translations and two rotations. Both an eight-noded brick and a six-noded wedge finite element have been developed (see Figure 4.2). For the geometrically nonlinear model formulated here, a similar approach is used. For brevity, only the eight-noded brick element is discussed.

The in-plane displacement and rotational degrees of freedom are approximated by bilinear Lagrange interpolation functions:

$$u_b = \sum_{i=1}^n \overline{u}_{bi} N_i \qquad u_t = \sum_{i=1}^n \overline{u}_{ii} N_i \qquad (4.51)$$

$$v_b = \sum_{i=1}^n \overline{v}_{bi} N_i \qquad v_i = \sum_{i=1}^n \overline{v}_{ii} N_i \qquad (4.52)$$

$$\theta_{xb} = \sum_{i=1}^{n} \overline{\theta}_{xbi} N_{i} \qquad \theta_{xt} = \sum_{i=1}^{n} \overline{\theta}_{xti} N_{i} \qquad (4.53)$$

$$\theta_{yb} = \sum_{i=1}^{n} \overline{\theta}_{ybi} N_{i} \qquad \theta_{yt} = \sum_{i=1}^{n} \overline{\theta}_{yti} N_{i} \qquad (4.54)$$

where N_i are bilinear Lagrange interpolation functions and n is the number of nodes that define either the top or the bottom surface of the element. For the eight-noded brick element, n=4.

An interdependent interpolation scheme is used for the transverse deflection degrees of freedom. The interdependent interpolation scheme reduces the effects of locking and facilitates the satisfaction of the constraints in equation 4.6. The interdependent interpolation concept was first developed by Tessler and Hughes (1983). This scheme does not require additional degrees of freedom and it improves element accuracy and efficiency. The interdependent interpolation scheme couples the transverse deflection degrees of freedom with the rotational degrees of freedom, as follows:

$$w_{\beta} = \sum_{i=1}^{n} \left(N_{i} \overline{w}_{\beta i} + \hat{N}_{i} \overline{\theta}_{x \beta i} + \hat{N}_{i} \overline{\theta}_{y \beta i} \right) \tag{4.55}$$

where N_i are the bilinear Lagrange interpolation functions, \hat{N}_i are special quadratic functions, β ranges from 1 to 2 (1= bottom, 2=top), and n=4 is the number of nodes on the top or bottom surface.

While the interdependent interpolation scheme alleviates some of the shear locking in the element, it does not eliminate it completely. A locking-free element is obtained by enforcing both field and edge consistency conditions, as

Si

shown by Prathap and Somashekar (1988). These concepts have been applied to the current element (Cho and Averill, 2000) to make it robust for application to both very thin and very thick laminated plates.

Appendix A defines all matrices needed to form the direct and tangent stiffness matrices for the geometrically nonlinear first-order zig-zag sublaminate finite element model accounting for moderately large displacements and moderate rotations. The current geometrically nonlinear finite element model has been implemented as a user element subroutine within the commercial finite element code ABAQUS (Hibbit, et al., 1997). This approach takes advantage of the efficient iterative solution algorithm native to ABAQUS and allows attention to be focused on development and testing of the new nonlinear zig-zag sublaminate theory and its associated finite element model. All numerical results in the following section were obtained using the present model as a user element subroutine within ABAQUS.

4.6 Numerical Results

In this section, sample numerical results obtained from the first-order geometrically nonlinear zig-zag model are compared with available experimental results (see Zaghloul and Kennedy, 1975; cited in Ochoa and Reddy, 1992) for bending of square, symmetrically laminated, simply-supported and clamped composite panels subjected to a uniform transverse pressure load. Since the geometrically nonlinear response of composite plates is highly dependent upon the lamination scheme and boundary conditions, it is essential to faithfully

S 0. la Th to m pla

> fig firs

19

of

cur squ represent the lamination scheme and boundary conditions in the experiment if numerical and experimental results are to be compared. The numerical replication of the experimental setup can often be accomplished to a satisfactory level of accuracy, but usually cannot be replicated exactly. In order to illustrate the importance of zig-zag effects in nonlinear analysis of laminated structures, numerical results are also presented for bending of a square, symmetrically laminated, simply-supported sandwich composite panel subjected to a uniform transverse pressure load.

The first laminate studied is a simply supported, single-layer orthotropic square plate with in-plane dimensions of 12 by 12 inches and a thickness of 0.138 inches. Material properties of this panel are given in Table 4.1. The second laminate studied is a clamped square cross-ply laminate with a (0/90/90/0) layup. This panel has the same in-plane dimensions as the first example, but it has a total thickness of 0.096 inches. Table 4.2 contains the stiffness properties of the material used in this second panel. Due to symmetry of the panels, only a quarter plate model was developed, with meshes in the quarter region as given in the figures (e.g., 4x4x1). Along the simply-supported edges of the plate model in the first example, simply-supported boundary conditions were imposed at the bottom of the laminate to best represent the experimental setup (Zaghloul and Kennedy, 1975).

Figures 4.3 and 4.4 contain the experimental and predicted load-deflection curves for the square simply supported single-layer orthotropic plate and the square clamped cross-ply laminate (0/90/90/0), respectively. Numerical results

ar ar m

> th b

Si re

b

th

pi th

nı di:

ar

th

are presented for both the first-order zig-zag sublaminate finite element model and the S4R shell element available in ABAQUS. For the first-order zig-zag model predictions, results are given for various levels of in-plane and throughthickness mesh refinement. Both plates stiffen significantly due to the coupling of bending and membrane stresses. Figures 4.3 and 4.4 show excellent correlation between results obtained from the geometrically nonlinear first-order zig-zag sublaminate model, numerical results using ABAQUS, and the experimental results. The small differences in the solution predicted by the S4R element and the first-order zig-zag element can most likely be attributed to the slightly different boundary conditions utilized. In the S4R element, boundary displacement constraints are imposed at the plate mid-surface, as is common practice for shelltype finite elements. On the other hand, boundary displacement constraints in the three-dimensional first-order zig-zag element are imposed at the bottom surface for the simply-supported case and at both top and bottom surfaces for the clamped case. Based on the results using the first-order zig-zag sublaminate model, it is clear that through-thickness refinement does not improve the predictions of global response for either of these panels. The correlation between the two numerical solutions is better than the correlation between either of the numerical solutions and the experimental results. For both cases considered, discrepancies between the computational results and the experimental results are likely due to differences in boundary conditions and material properties.

The final numerical example was constructed to compare the predicted through-thickness variation of displacements and stresses using the

su

pr in

pl

ce la

> qı pi th

th sh

SI PI

de

Sa Zi

su

tra red

ac

geometrically nonlinear zig-zag model. The laminate considered here is a simply supported sandwich panel with a compliant core, which has been studied previously (Cho and Averill, 2000). The plate has in-plane dimensions 10 x 10 inches and a total thickness of 1 inch, so the aspect ratio of the plate is ten. The plate is loaded by a uniform pressure applied on 4 x 4 inch square patch at the center of the plate. Tables 4.3 and 4.4 contain the material properties and lamination scheme, respectively, of the sandwich panel. Due to symmetry, only a quarter of the plate was modeled with a uniform 5x5 finite element mesh in the plane of the laminate and with a varying number of elements through-thethickness. For example, when three elements are used through-the-thickness of the plate the total thicknesses of the bottom face sheet, the core and the top face sheet were each represented by one element. As in the first example, simple supports were imposed along the bottom edge of the panel. The results of the present model are compared to predictions of the ABAQUS layered solid element denoted as C3D8I, which uses incompatible modes to overcome locking.

Figure 4.5 displays the predicted load-deflection curves (at center of the sandwich panel) obtained by the linear and the geometrically nonlinear first-order zig-zag element and the ABAQUS C3D8I element at the *top* of the simply supported sandwich panel. It can be seen that the ABAQUS element requires three elements through-the-thickness to achieve a converged solution for the transverse deflection at the top of the panel, while the first-order zig-zag model requires only a single element through-the-thickness to attain a similar level of accuracy.

sa zi

st

tr.

fir

Fi

00

fir tra

g

Se.

Al Ta

for of

in

Figure 4.6 displays the predicted load-deflection curves (at center of the sandwich panel) obtained by the linear and the geometrically nonlinear first-order zig-zag element and the ABAQUS C3D8I element at the **bottom** of the simply supported sandwich panel. It can be seen that the ABAQUS element requires three elements through-the-thickness to achieve a converged solution for the transverse deflection. The deflection at the bottom of the panel decreases as the number of first-order zig-zag elements is increased through-the-thickness. Figure 4.5 depicts very little change in deflection at the top of the panel as the number of first-order zig-zag elements is increased through-the-thickness. Together, Figures 4.5 and 4.6 show an increase in nominal transverse normal strain as the number of first-order zig-zag elements is increased through-the-thickness. This occurs due to the compliant core of the sandwich panel. For this problem, three first-order zig-zag elements through-the-thickness are required to capture the transverse "squashing" of the core. To determine if the core is "squashing" due to geometrically nonlinear through-thickness refinement effects, a set of small displacement analyses were conducted with first-order zig-zag and ABAQUS C3D8I elements. Table 4.5 contains the deflections at the bottom and top of the sandwich panel assuming small displacements using the first-order zig-zag and ABAQUS elements with one, two and three elements through-the-thickness. Table 4.5 shows the deflection of the top of the panel remaining nearly constant for the first-order zigzag finite element model, while the deflection at the bottom of the panel decreases as the number of elements through-the-thickness is increased. The "squashing" of the core is captured as the number of elements

thro

dis

su

the ce

thi an

pla

agı

in-

inte trar

finit

ABA bott

by i

ABA

Withi

through-the-thickness is increased, even though small displacements are assumed.

For an applied load of 9.5 ksi, Figures 4.7 and 4.8 display the predicted through-thickness variation of in-plane displacements. The in-plane displacements from ABAQUS and the first-order zig-zag element agree with sufficient refinement (three elements through-the-thickness).

Figures 4.9 and 4.10 display the predicted through-thickness variation of the in-plane Cauchy bending stresses at the nearest integration points to the center of the plate for an applied load of 9.5 ksi for various levels of through-thickness refinement. For clarity, Figures 4.11 and 4.12 compare the ABAQUS and first-order zig-zag model prediction of through-thickness variation of the in-plane Cauchy bending stresses within the top "skin" of the sandwich panel. The in-plane bending stresses from ABAQUS and the first-order zig-zag element agree with sufficient refinement (three elements through-the-thickness).

Figure 4.13 displays the transverse normal Cauchy stress at the integration points closest to the center of the plate. Due to the assumed constant transverse normal Cauchy stress, each sublaminate of the first-order zig-zag finite models will have a constant through-thickness normal Cauchy stress. The ABAQUS and first-order zig-zag predictions differ significantly in the top and bottom "skins" of the sandwich panel in Figure 4.13. This can be accounted for by inspecting the kinematic assumptions of each finite element model. The ABAQUS finite element model assumes that the displacements vary linearly within an element. This enforces the strains to be continuous at each layer

in e s CI n tr in interface within an element. This implies that the stresses are discontinuous at each layer interface due the abrupt changes in material properties within a single ABAQUS element. Conversely, the first-order zig-zag element assumes that the stresses are continuous at each layer interface within a sublaminate. For this reason, the first-order zig-zag element is expected to yield higher accuracy when compared to the simple linear ABAQUS element.

Figure 4.14 displays the transverse normal strain at the integration points closest to the center of the plate. Due to the assumed constant transverse normal Cauchy stress, the transverse normal strains vary linearly within each layer of the first-order zig-zag finite model. As the number of sublaminates (or elements) is increased through-the-thickness, a larger amount of nominal transverse strain is predicted. Figure 4.14 depicts the previously discussed transverse "squashing" of the core conveyed in Figures 4.5 and 4.6.

Figures 4.15 and 4.16 display the predicted through-thickness variation of the transverse Cauchy shear stresses for the first-order zig-zag model and simple linear ABAQUS element for various levels of transverse refinement. The difference in kinematic assumptions for the first-order zig-zag and linear ABAQUS finite element explains the discrepancies in the through-thickness variation of the transverse Cauchy shear stresses within the bottom and top "skins" of the panel. The linear ABAQUS element assumes a constant state of strain within an element, thus the stresses have double values at each layer interface within an element. The first-order zig-zag finite element model assumes

pa de W a piecewise linear variation of in-plane displacements through-the-thickness of the sublaminate while satisfying continuity of inter-laminar stresses.

Figure 4.17 depicts the predicted through-thickness variation of the inplane Cauchy shear stress for the first-order zig-zag model and simple linear ABAQUS element for various levels of transverse refinement. Both elements predict similar through-thickness variation of in-plane Cauchy shear stress.

Differences between the first-order zig-zag and linear ABAQUS solutions can be attributed to the different kinematic assumptions used in the models, with the zig-zag element being expected to yield higher accuracy than the simple linear model employed in the C3D8I element. For clarity, Figure 4.18 depicts the measurement points of the in-plane displacements, stresses and strains.

4.8 Conclusions

A new geometrically nonlinear first-order zig-zag sublaminate plate theory and finite element model have been formulated, implemented and validated against existing experimental and numerical results for laminated composite panels. This model is accurate for a wide range of laminated panel applications including very thin laminated panels up to very thick laminated and sandwich panels. Further, this model is cast in a form that facilitates its use within commercial finite element packages. Namely, the finite element models developed take the form of a three-dimensional eight-noded brick or six-noded wedge element with the usual five engineering degrees-of-freedom per node.

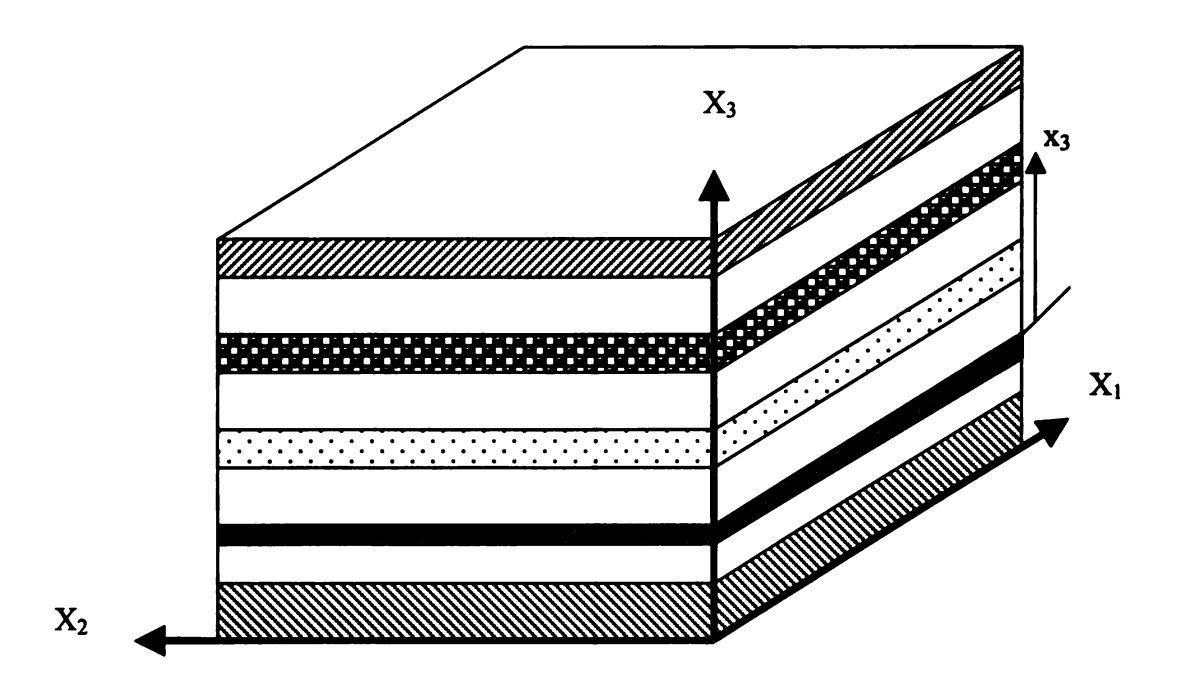


Figure 4.1. Schematic of ply stacking and coordinate system used in first order sublaminate theory.

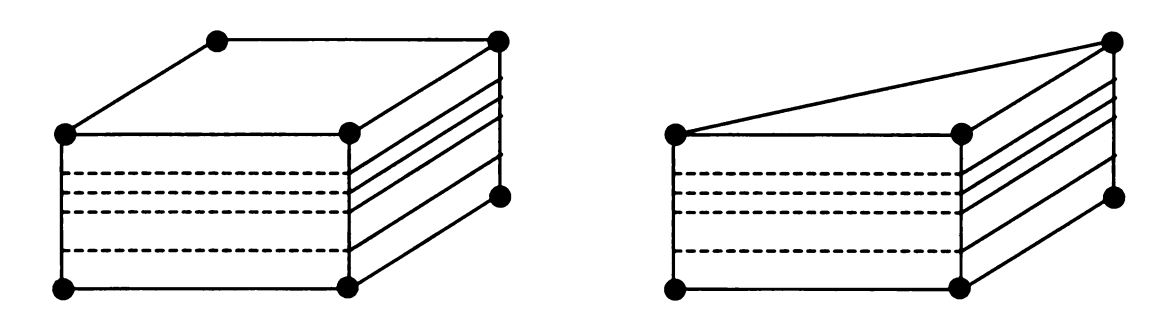


Figure 4.2. Element topology for the eight-noded brick and the six-noded wedge finite elements based on first order zig-zag sublaminate theory.

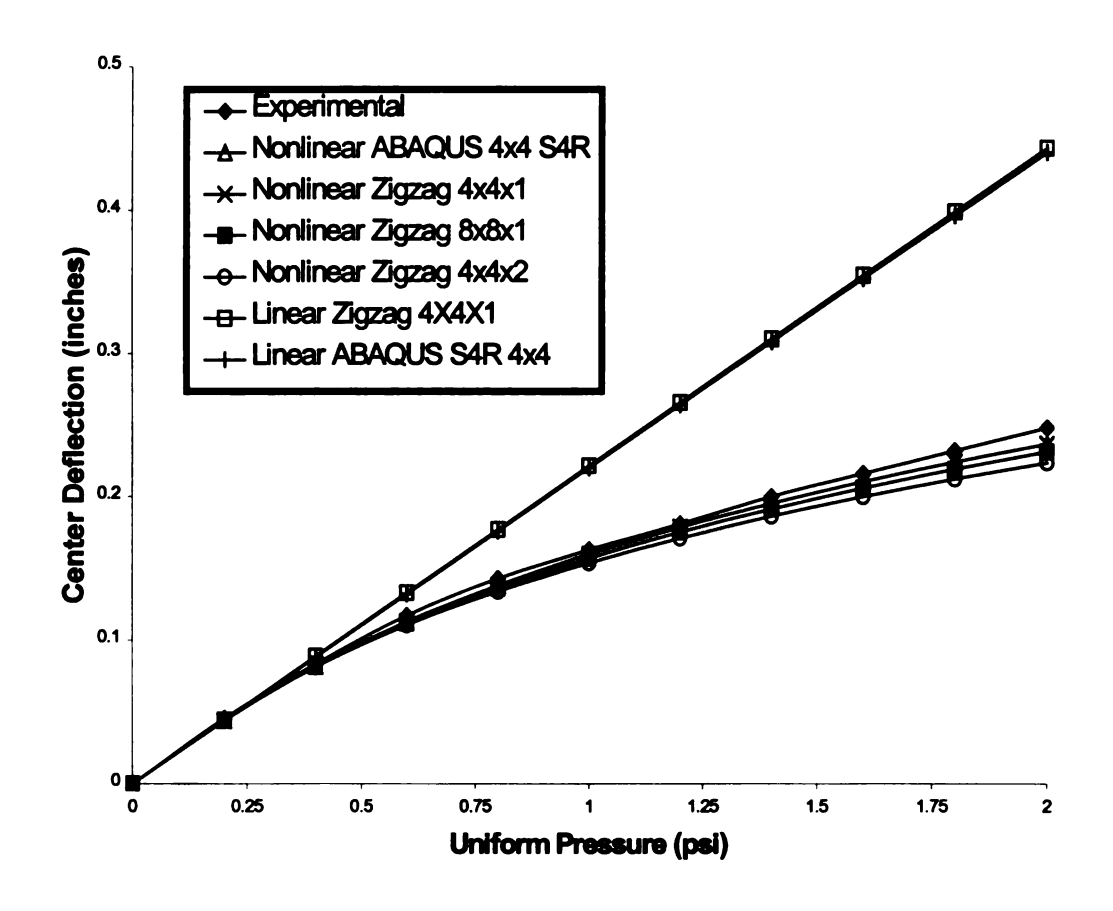


Figure 4.3. Load versus deflection for a square simply-supported single-layer orthotropic plate under uniform pressure at various levels of in-plane and through-thickness refinement.

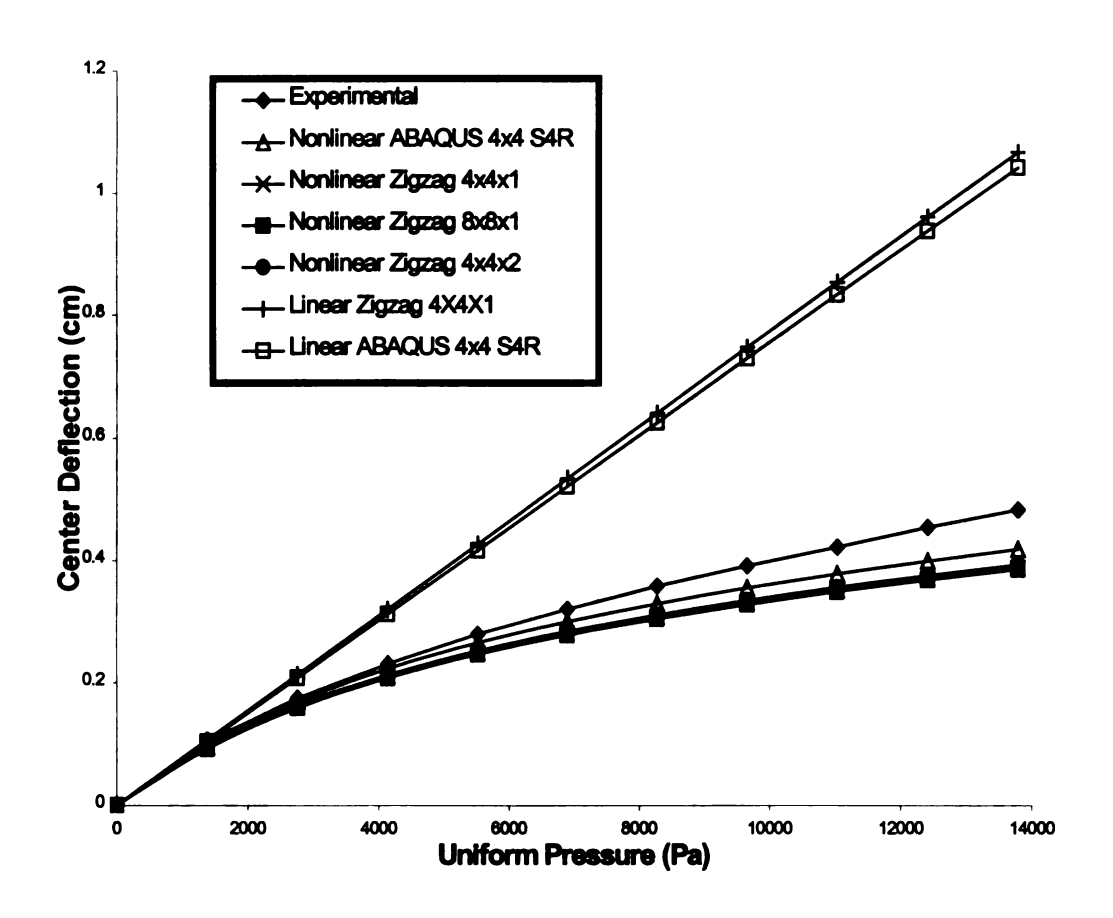


Figure 4.4 Load-deflection curves for the clamped square cross ply plate (0/90/90/0) under uniform pressure at various levels of in-plane and through-thickness refinement.

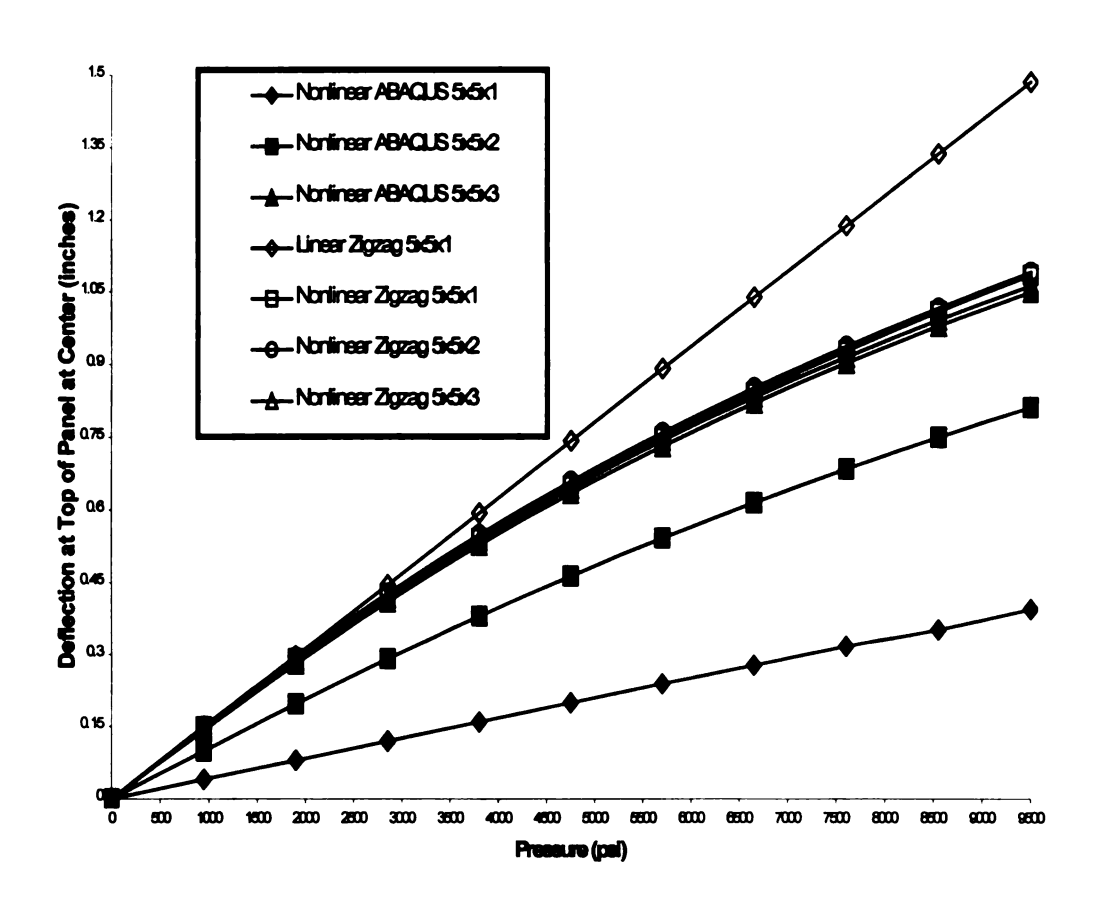


Figure 4.5. Linear and nonlinear load versus deflection at the top of a simply-supported square sandwich panel under uniform pressure using first-order zigzag sublaminate theory.

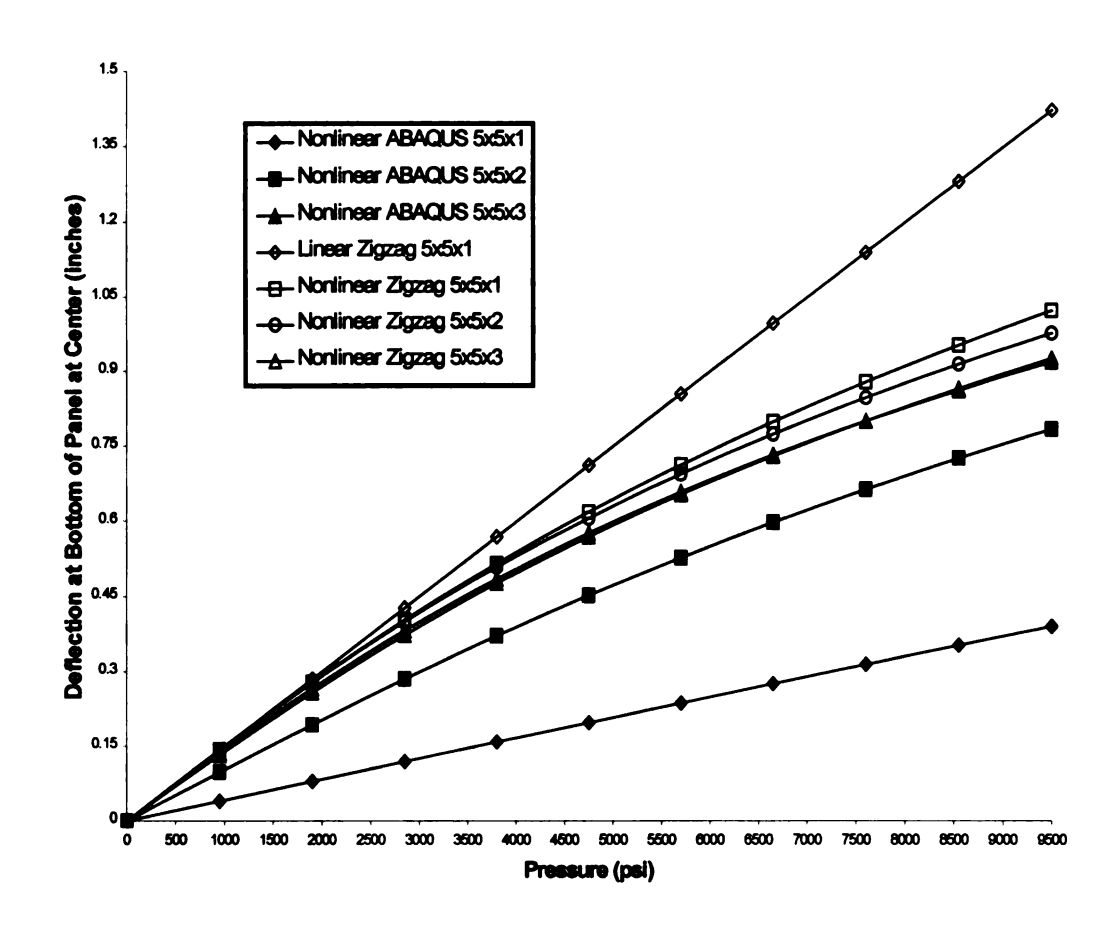


Figure 4.6. Linear and nonlinear load versus deflection at the bottom of a simply-supported square sandwich panel under uniform pressure using first-order zigzag sublaminate theory.

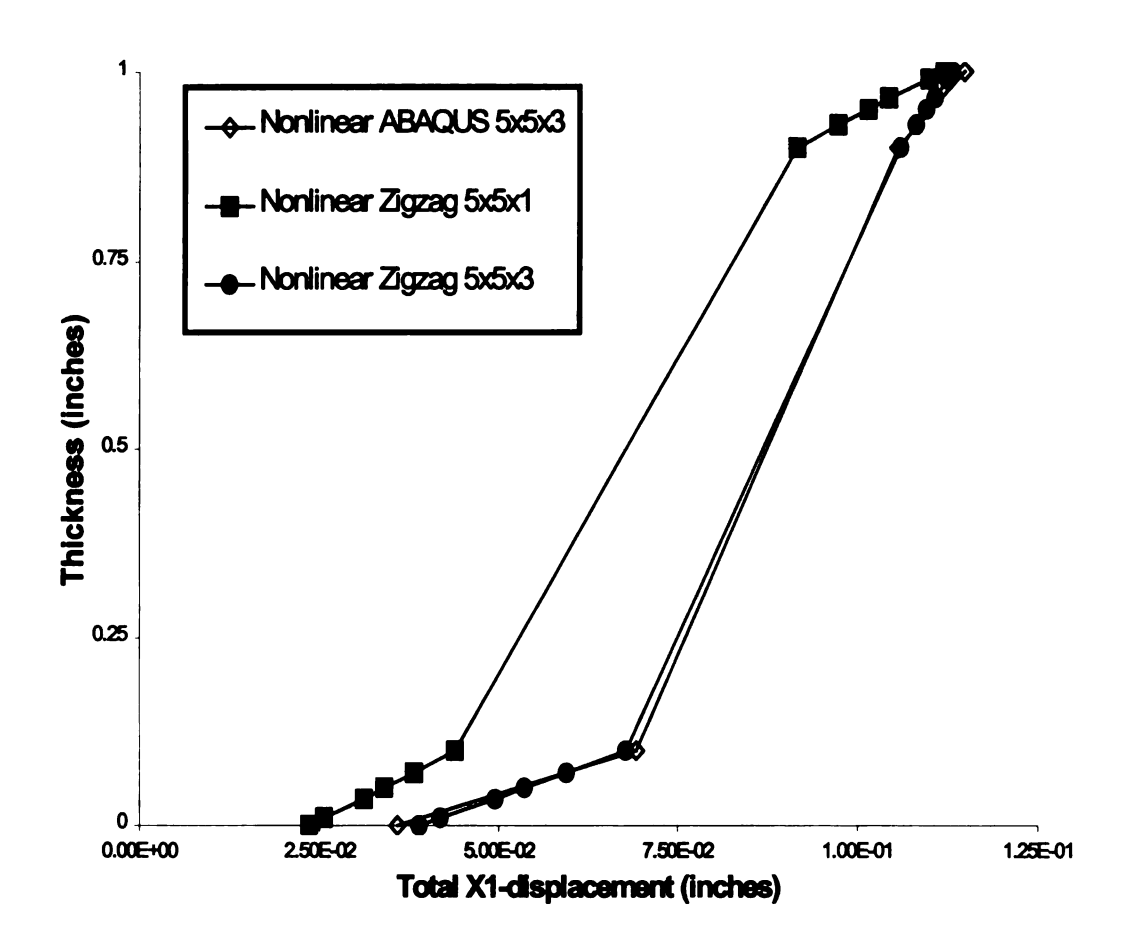


Figure 4.7. Through-thickness variation of total X1-displacement at the plate midspan and X1=0.

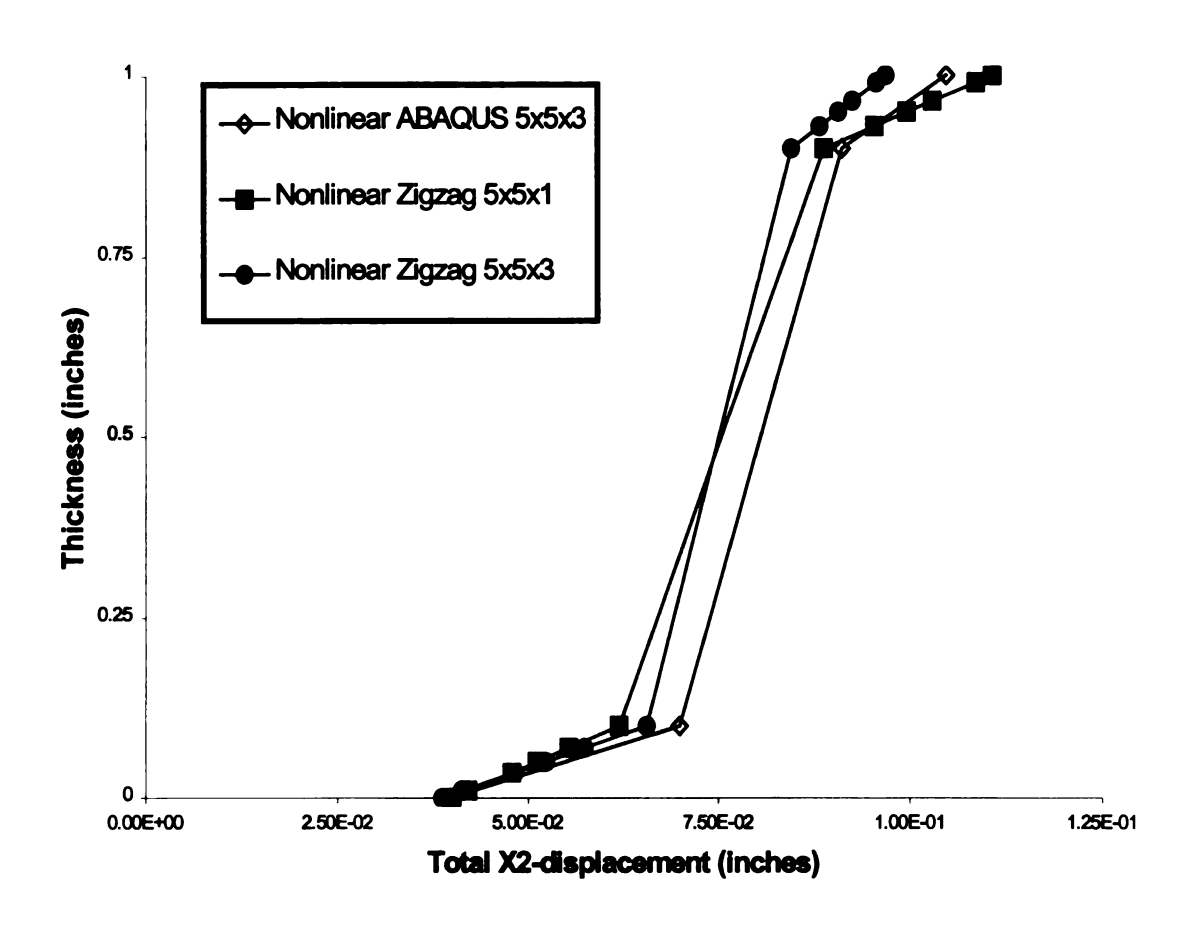


Figure 4.8. Through-thickness variation of total X2-displacement at the plate midspan and X2=0.

Figure at the

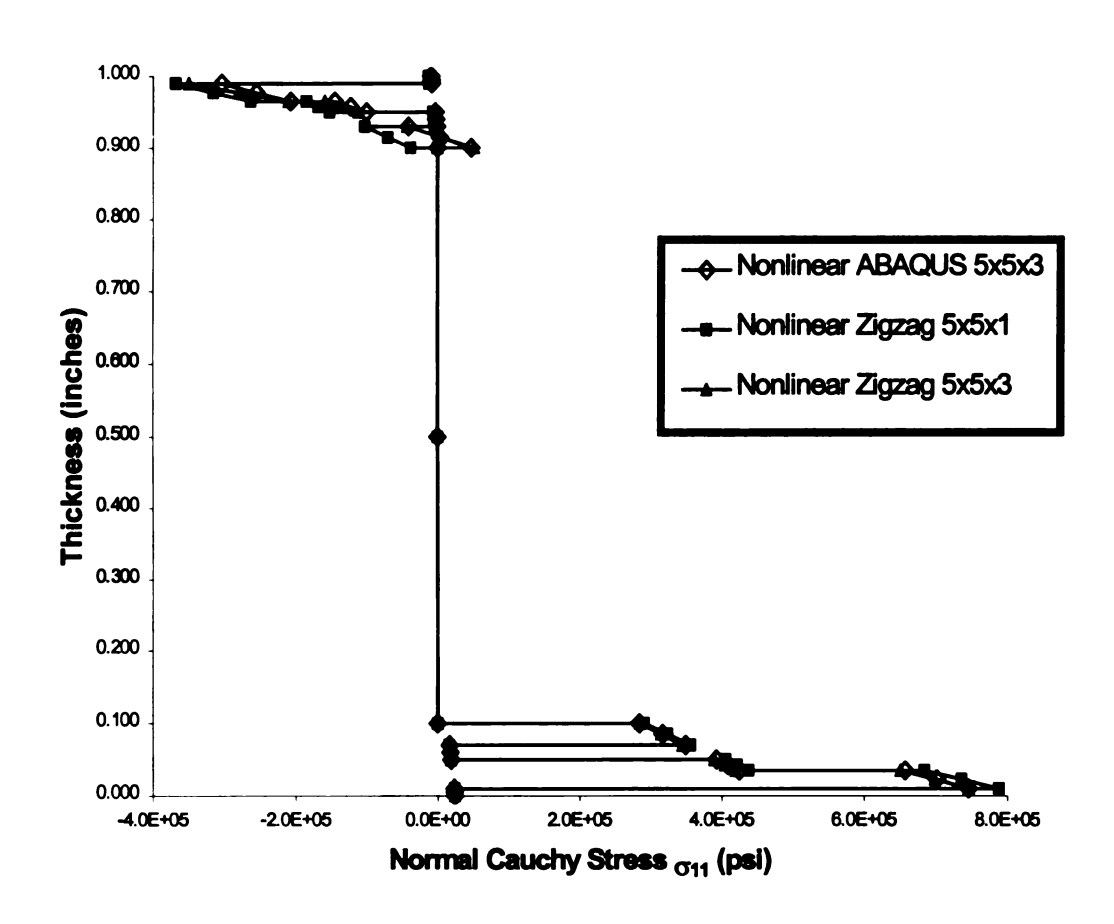


Figure 4.9. Through-thickness variation of the normal Cauchy stress (in the X1-direction) at the Gauss points nearest to the center of the plate.

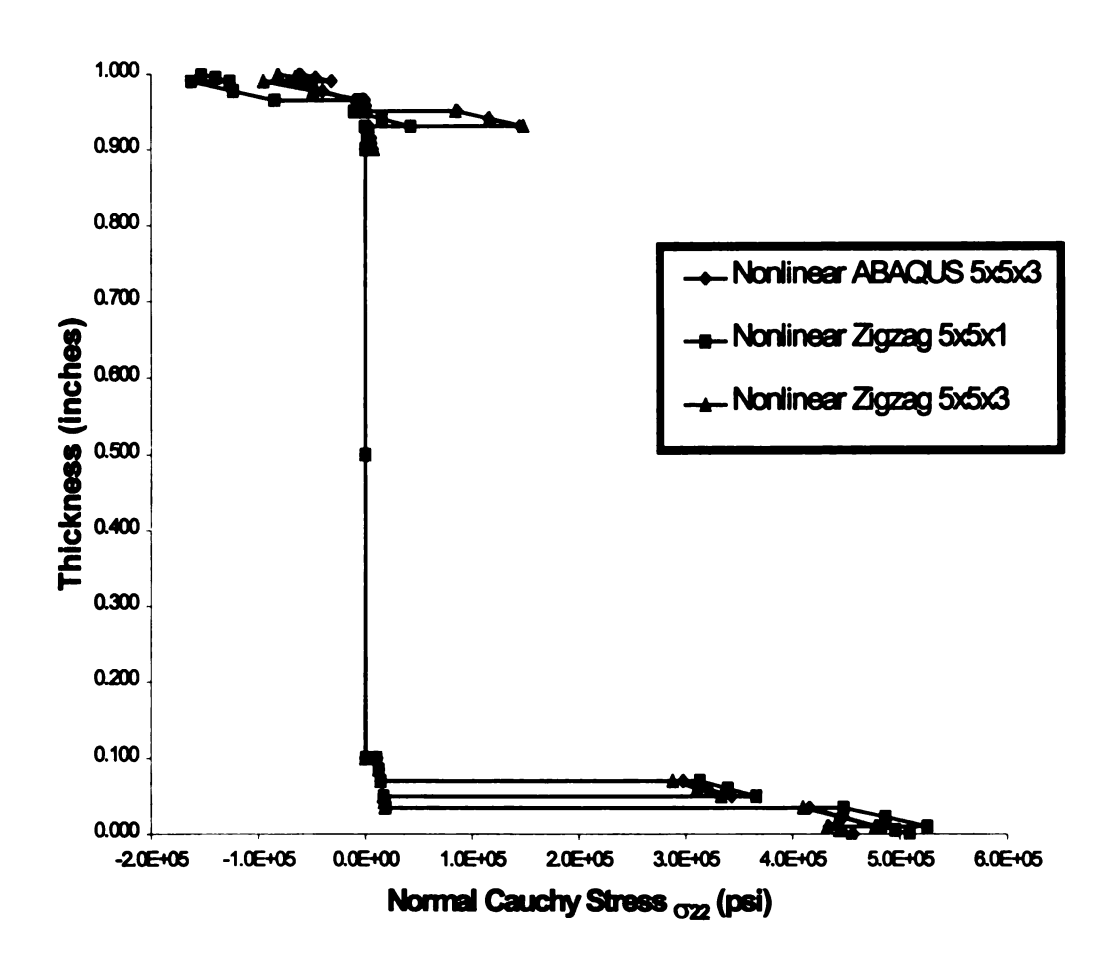


Figure 4.10. Through-thickness variation of the normal Cauchy stress (in the X2-direction) at the Gauss points nearest to the center of the plate.

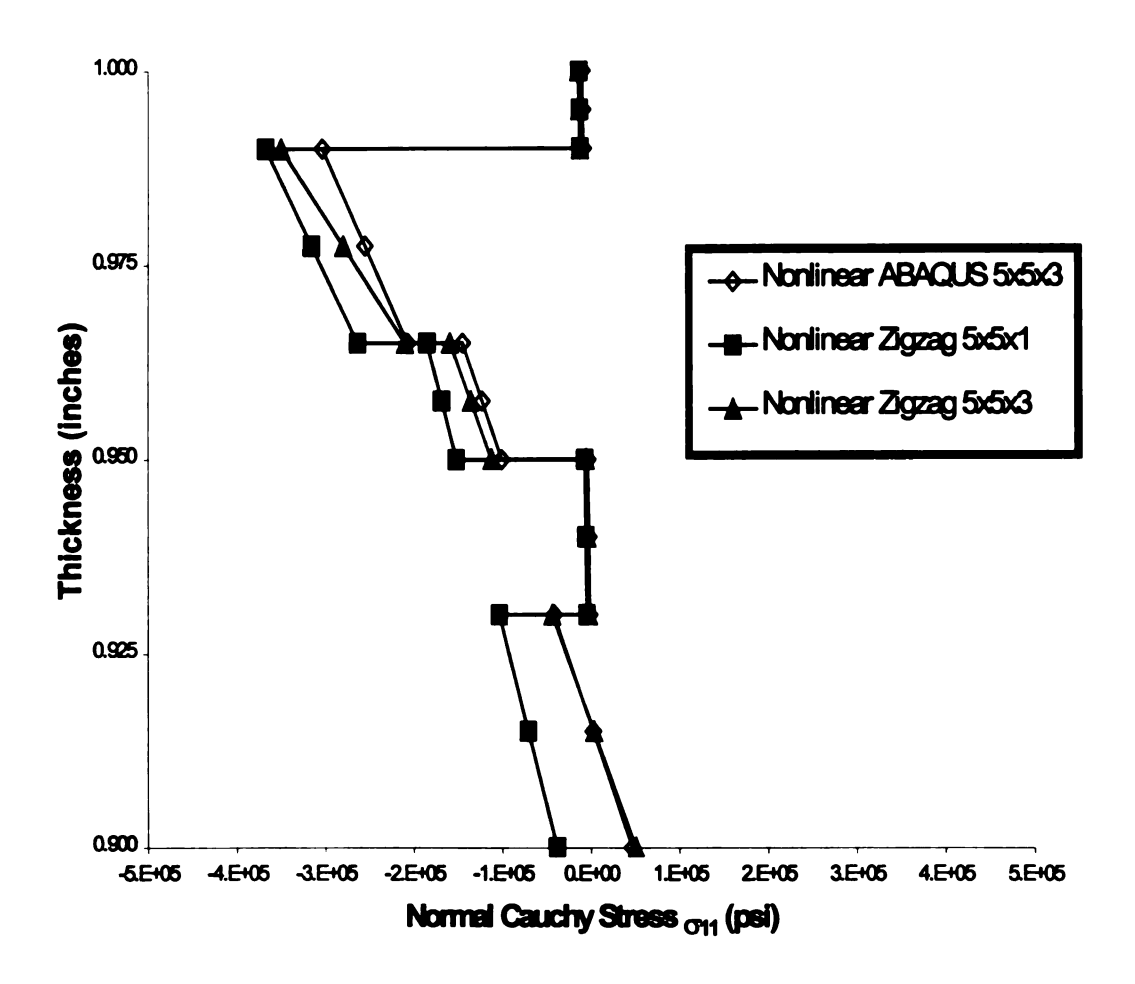


Figure 4.11. Through-thickness variation of the normal Cauchy stress (in the X1-direction) for the top five layers of the sandwich panel at the Gauss points nearest to the center of the plate.

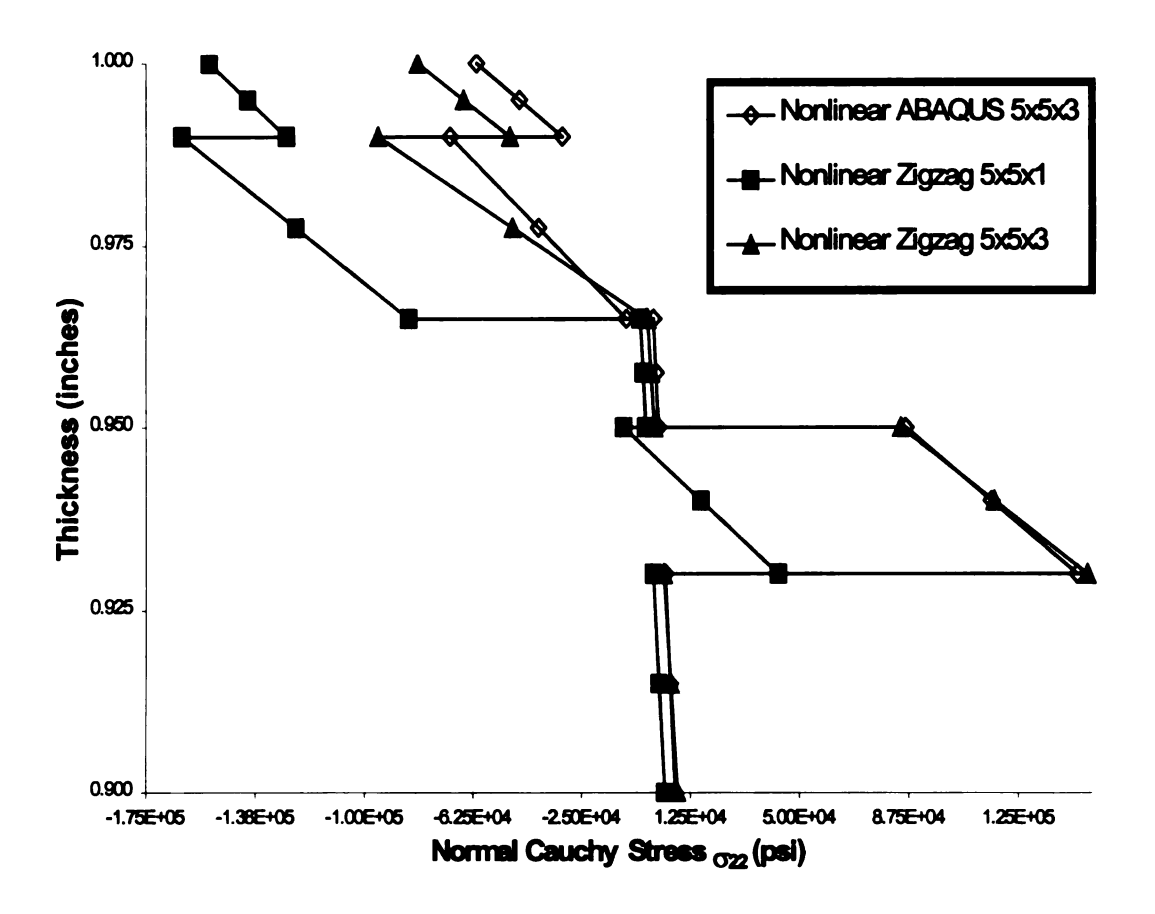


Figure 4.12. Through-thickness variation of the normal Cauchy stress (in the X2-direction) for the top five layers of the sandwich panel at the Gauss points nearest to the center of the plate.

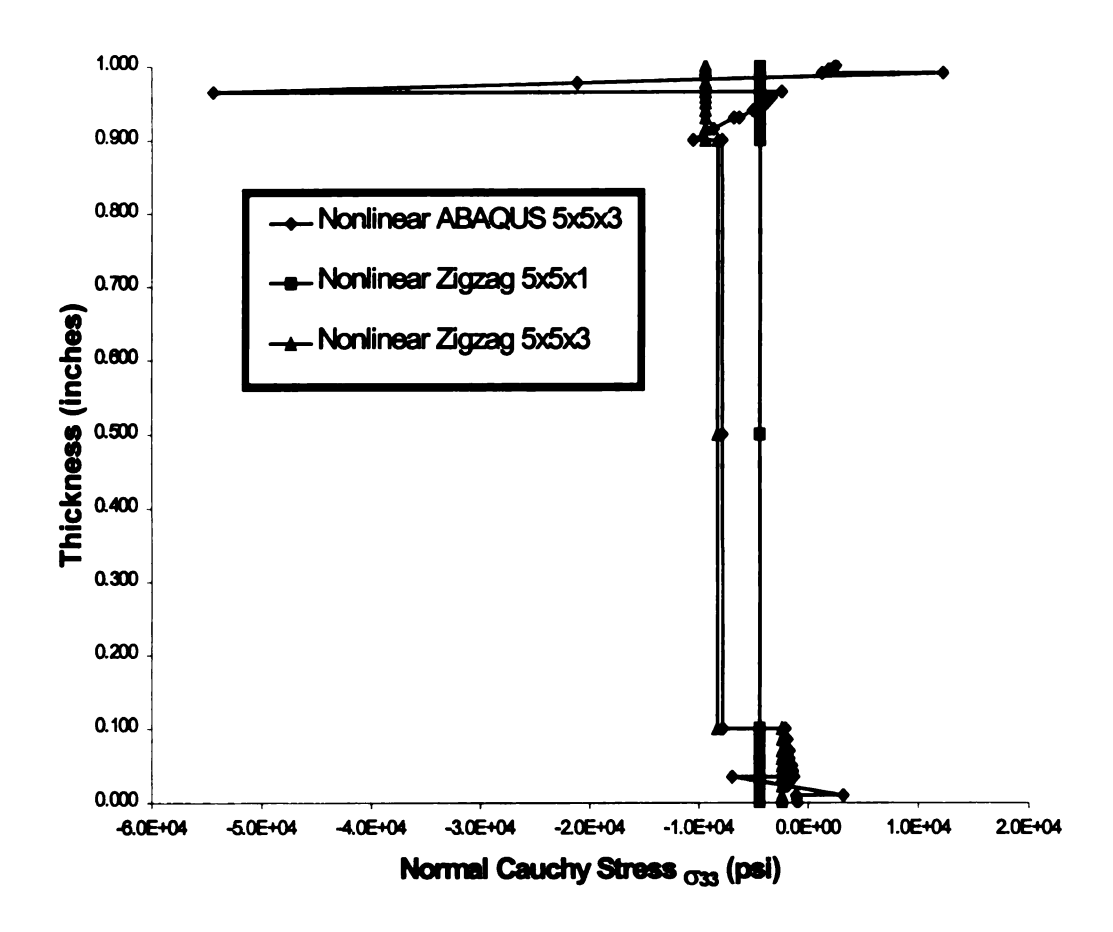


Figure 4.13. Through-thickness variation of the normal Cauchy stress (in the X3-direction) at the Gauss points nearest to the center of the plate.

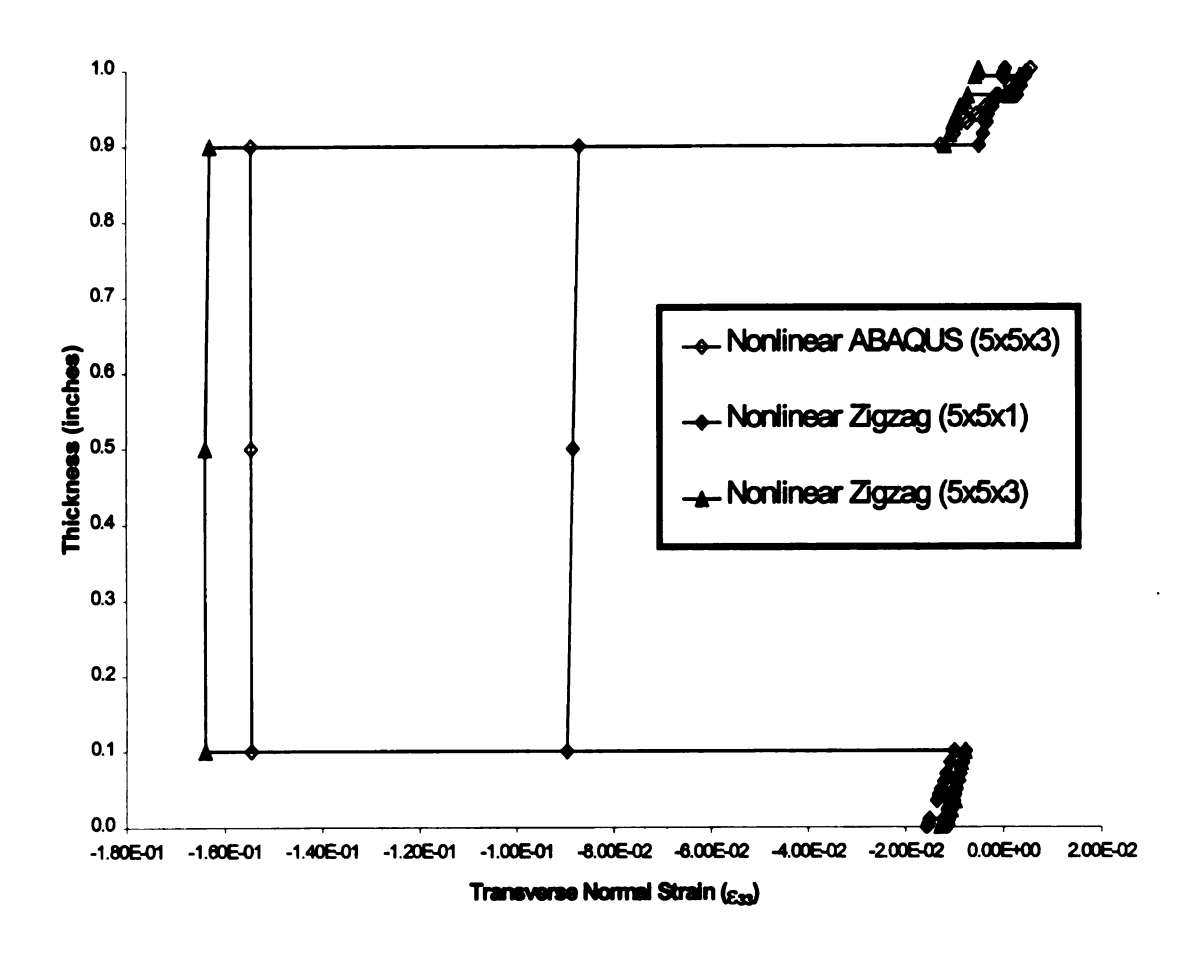


Figure 4.14. Through-thickness variation of transverse normal strain (ϵ_{33}) at the Gauss points nearest to the center of the plate.

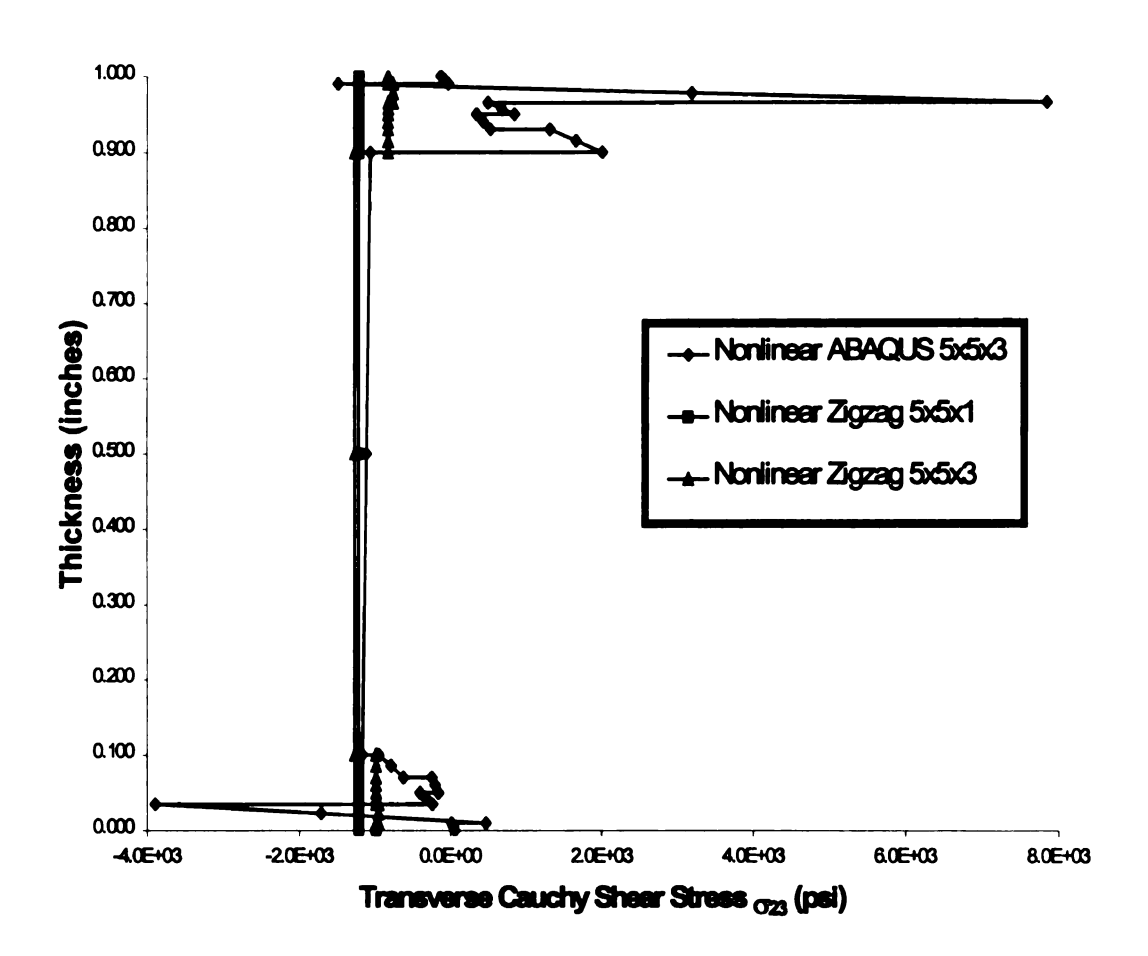


Figure 4.15. Through-thickness variation of the transverse Cauchy stress (σ_{23}) at the Gauss points nearest to the center of the plate.

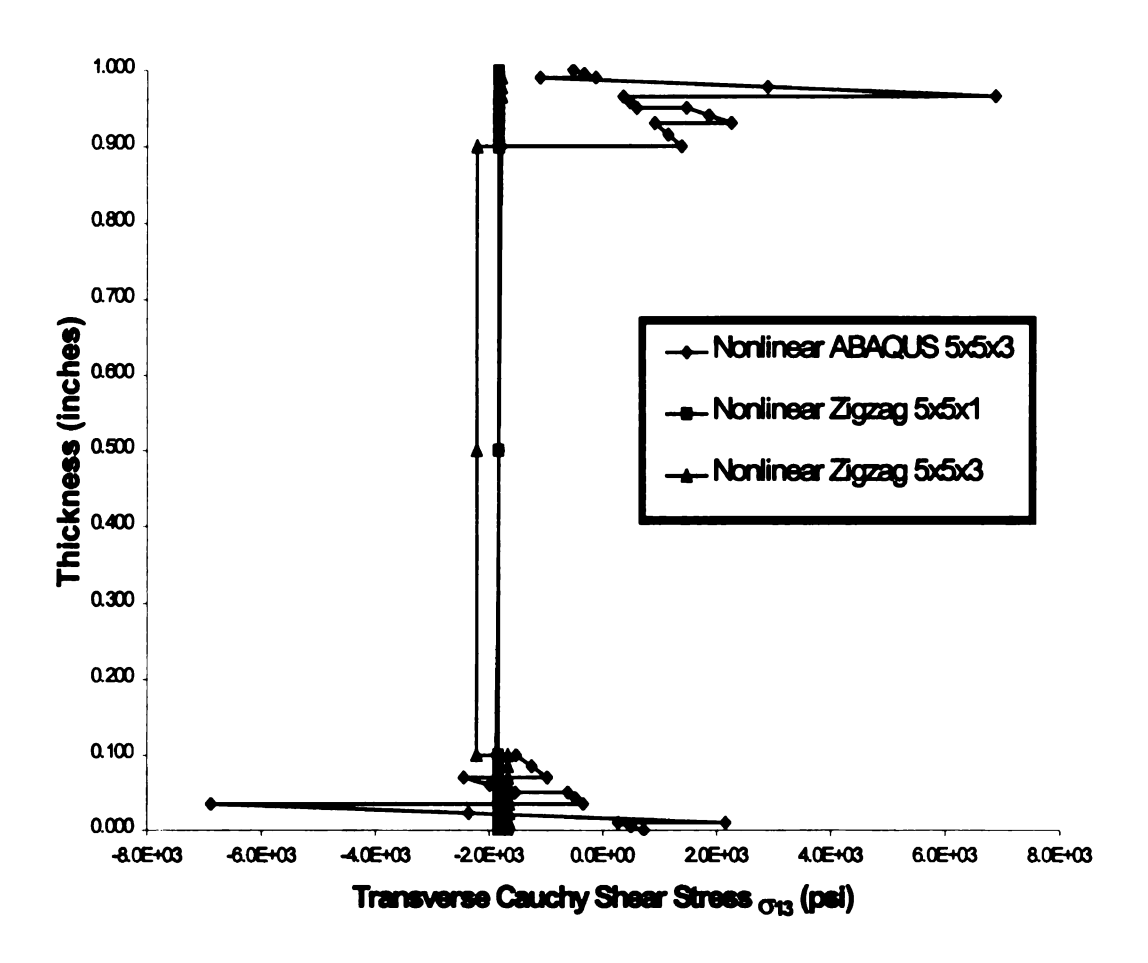


Figure 4.16. Through-thickness variation of the transverse Cauchy stress (σ_{13}) at the Gauss points nearest to the center of the plate.

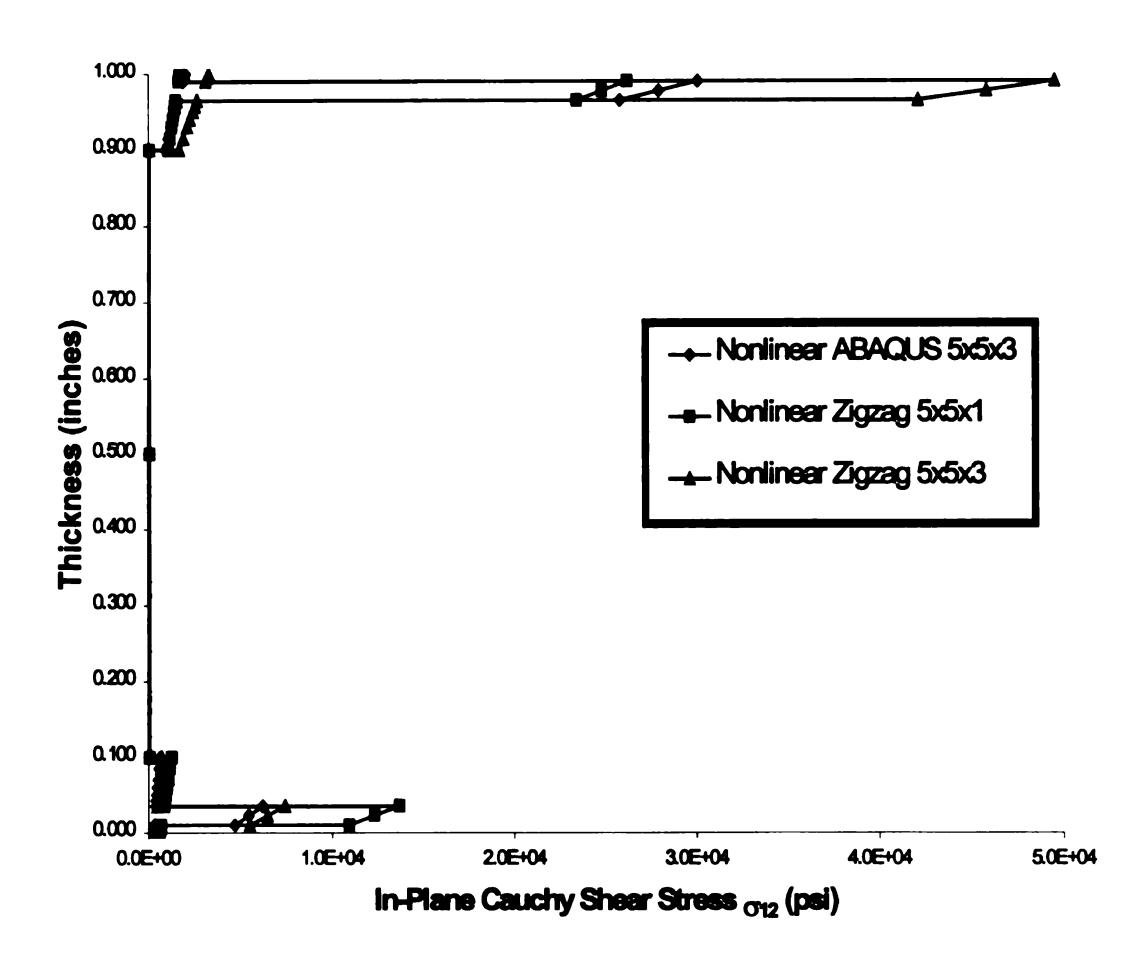


Figure 4.17. Through-thickness variation of the in-plane Cauchy stress (σ_{12}) at the Gauss points nearest to the center of the plate.

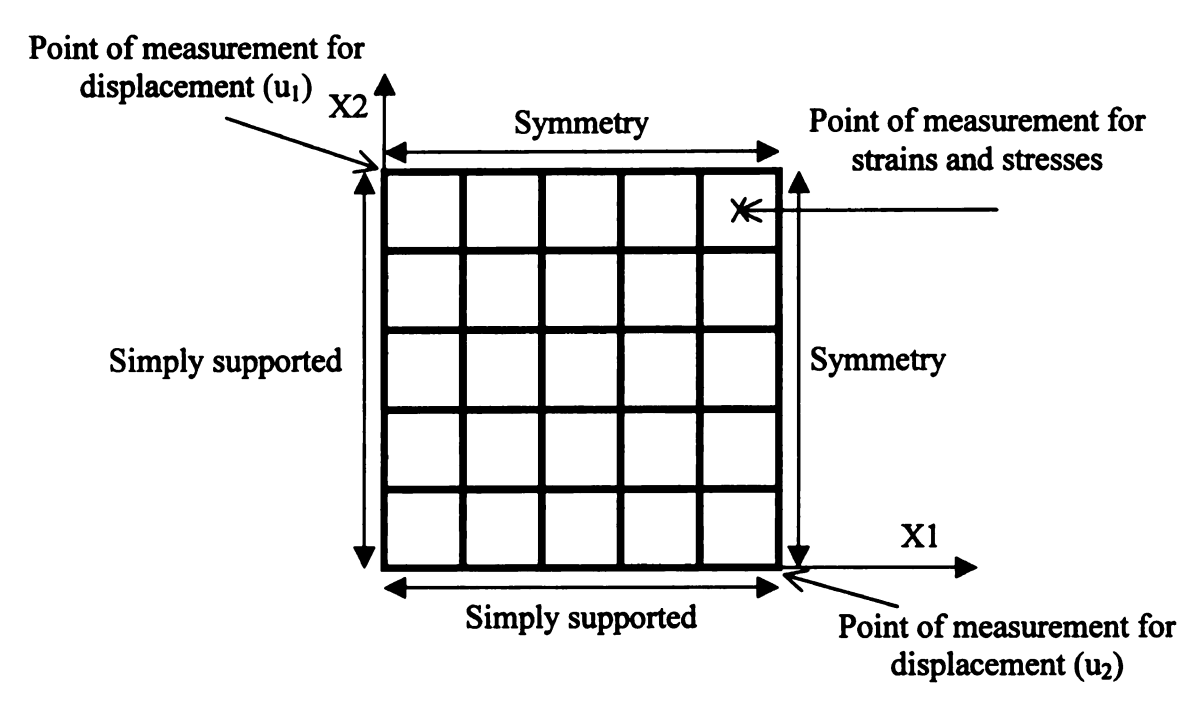


Figure 4.18. Measurement points for the displacements, strains, and stresses for the sandwich panel.

Table 4.1. Material properties for square single-layer orthotropic plate.

E_{11} =3.00E6 psi	E_{22} =1.30E6 psi	E_{33} =3.00E6 psi
$v_{12}=0.32$	$_{V23}=0.32$	_{V13} =0.32
G_{12} =0.36E6 psi	G_{23} =0.36E6 psi	G_{13} =0.36E6 psi

Table 4.2. Material properties for square cross-ply laminated plate (0/90/90/0).

$E_{11}=1.82E6 \text{ psi}$	$E_{22}=1.82E6 \text{ psi}$	E_{33} =1.82E6 psi
{V12} =0.2395	${V23}$ =0.2395	_{V13} =0.2395
G_{12} = 0.31E6 psi	G_{23} =0.31E6 psi	G_{13} =0.31E6 psi

Table 4.3. Material properties for sandwich panel.

	Material 1	aterial 1 Material 2		Core	
E_{11} (10 ⁶ psi)	1	33	25	0.05	
E ₂₂ (10 ⁶ psi)	25	21	1	0.15	
E ₃₃ (10 ⁶ psi)	1	21	1	0.05	
ν ₁₂	0.01	0.25	0.25	0.01	
V 23	0.25	0.25	0.25	0.15	
ν ₁₃	0.25	0.25	0.25	0.15	
G ₁₂ (10 ⁶ psi)	0.5	8	0.5	0.02	
G ₂₃ (10 ⁶ psi)	0.5	8	0.5	0.04	
G ₁₃ (10 ⁶ psi)	0.2	8	0.5	0.02	

Table 4.4. Lamination scheme for sandwich panel.

Layer No.	Material	Thickness (inches)
I	1	0.001
2	2	0.025
3	3	0.015
4	1	0.020
5	3	0.030
6	Core	0.800
7	3	0.030
8	1	0.020
9	3	0.015
10	2	0.025
II	1	0.010

Table 4.5. The effect of transverse refinement considering small displacements.

Number of	ABAQUS:	ABAQUS:	FZZ:	FZZ:
elements	Displacement	Displacement	Displacement	Displaceme
through- thickness	at bottom (inches)	at top (inches)	at bottom (inches)	nt at top (inches)
1	0.3950	0.3978	1.422	1.484
2	0.9757	1.027	1.425	1.496
3	1.317	1.401	1.375	1.449

Chapter 5

OPTIMIZATION OF SANDWICH PANELS USING GENETIC ALGORITHMS

5.1 Introduction

Optimization problems are encountered on an hourly basis in the everyday life of an engineer. For example, we will review a typical optimization problem posed by a naval engineer. The goal of the optimization problem is to find a sandwich panel design with minimal mass while simultaneously satisfying stiffness and stress constraints applying state equations that are governed by the geometrically nonlinear (moderately large displacements and moderate rotations) equations of motion. The sandwich panel designs found with a simple Genetic Algorithm will be contrasted to an existing "baseline" sandwich panel design in terms of its design variables, objectives and constraints.

5.2 Sandwich Panel Optimization Problem Statement

All optimization problems can be defined as finding a set of bounded design variables to minimize objective(s) while satisfying all constraints. We will follow in similar fashion by describing the design variables, the objective and constraints for the sandwich panel optimization problem statement.

Typically, sandwich panel designs are constructed of layered composite materials on the top and bottom of the panel (referred to as the bottom and top skin). The center of most sandwich panels is composed of lighter materials (often called the core). The skins of a classic sandwich panel design are meant

to carry the bulk of the bending stresses while the light weight core experiences most of the shear stresses. With this in mind, the simple GA was allowed to vary the number of layers in the bottom skin, top skin and core of the sandwich panel. The bottom and top skins of the sandwich panel were independently required to each have at least two, but no more than eight plies. The core of the sandwich panel was required to have at least one, but no more than three layers. The bounds on the number of layers in the bottom skin, core and top skin of the sandwich panel were chosen to satisfy manufacturability requirements. The GA could change each ply orientation ranging from 0 to 180 degrees with a 15 degree increment. The choice of ply orientation was discretized in such a manner to meaningfully reflect a realistic manufacturing increment. The GA chose each ply material from a discrete set of materials given in Table 5.1. For each layer in the core, the GA could change the core layer thickness ranging from ¼ to 1¼ inches with a 1/4 inch increment. The thickness of each layer within the core was discretized to reflect a meaningful manufacturing increment. The GA chose each core material from a discrete set of materials given in Table 5.2.

The representation of the design variables along the chromosome was set up in an order that staggered the number of plies in the top, core layers and number of plies in the bottom with material choice, orientation direction and thickness to reflect their physical location on the sandwich panel. This choice was made according to the principal of keeping related physical entities close to each other on the chromosome, which has been known to aid search within a GA (see Holland, 1975, Goldberg, 1988). The first discrete variable on the

chromosome was the number of plies on the bottom skin of the panel. Next, a discrete ply material choice and orientation choice was staggered on the chromosome for each bottom ply. The discrete number of layers in the core was followed by a core material choice for each possible layer in the core. The next discrete variable on the chromosome was the number of plies on the top skin of the panel. A discrete ply material choice and orientation choice was then staggered on the chromosome for each top ply. The simple GA had a population size of 50, 70% crossover rate and 1% mutation rate per field.

The objective of the sandwich panel optimization problem was to minimize mass. Inequality constraints were placed on the maximum transverse displacement and on the maximum value for a set of failure indices. The first set of failure indices was defined as the ratio of the inplane stresses to inplane strengths of each ply and core layer. An additional failure index was defined by the ratio of the shear strength to shear stress of each layer in the core. A failure index greater than unity indicates initiation of material failure. It was assumed that a suitable factor of safety was included in the definition of the loads, so no additional factor of safety was used in the displacement or stress failure constraints. The in-plane and shear strengths are listed in Tables 5.1 and 5.2 for each material choice.

The state equations were the geometrically nonlinear static equations of motion evaluated with the first order zigzag finite element model developed in Chapter 4 of this dissertation. The finite element mesh and boundary conditions are displayed in Figure 5.1. The sandwich panel was considered to be clamped

on all edges with no pressure applied on the front half of the panel. A 220psi transverse pressure load is applied at the middle of the panel at a 45 degree angle over a six inch band and a 30psi transverse pressure load is applied on the rear half of the panel. The model was meant to represent a section of boat hull under pressure loadings that occur during extreme usage. All finite element meshes of the boat hull referenced in this paper contained a 14 by 6 in-plane discretization with a single element through the thickness. The finite element mesh was constructed to align the pressure loads with the finite element discretization.

The baseline sandwich panel design was a symmetric layup composed of two plies in the bottom skin, a single core layer and two plies in the top skin. The orientations of all plies were aligned with the global coordinate system. Starting from the bottom of the sandwich panel, the first and second plies were composed of materials CM-1808 and XM-1808, found in Table 5.1. The baseline sandwich panel core material had properties given by material A550 in Table 5.2, with a thickness of 1.340 inches.

The baseline sandwich panel weighs 18.47 pounds with a maximum transverse displacement of 0.73 inches and failure index of 3.14 when evaluated with the geometrically nonlinear first order zig-zag finite element model developed in Chapter 4 of this dissertation. The maximum transverse displacement and failure index occur at the center of the panel within the high pressure strip. The baseline design is infeasible in terms of the inequality constraints placed on the maximum failure index.

5.3 Results

Two independent simple GA runs were performed. The two best designs obtained using a simple GA were unsymmetrical layups. Figure 5.2 displays the mass of the best design as a function of generation number for the first simple GA run. At first, the mass is much larger than the baseline design, but eventually converges to a design which is slightly lighter. Figure 5.3 displays the normalized constraint of the best design found as a function of the generation number for the first simple GA run. Initially, the stress constraint is severely violated, but it eventually converges to a feasible final design. Tables 5.3 displays the baseline and simple GA sandwich panel designs in terms their design variables, objectives and constraints for two independent runs. The simple GA designs have nearly identical masses compared to the baseline design while faintly violating the displacement constraint. The maximum failure indices for the simple GA sandwich panel designs are below the enforced failure constraint bound. The two independent runs produced two distinct final designs, indicating the simple GA prematurely converged to at least one suboptimal design. Each simple GA run lasted 5 days on a single 550 MHz cpu; each nonlinear finite element evaluation took about 3 minutes. As demonstrated on this problem, a simple GA tends to converge to suboptimal solutions while requiring large overall run times.

Figure 5.4 displays the force deflection response of the simple GA designs and baseline designs, showing significant stiffening due to geometric nonlinearities. Whereas the baseline design is stiffer at small loads when

compared to the simple GA designs, the stiffnesses for all designs are identical at large loads. The GA has discovered designs which take advantage of the geometrically nonlinear behavior of sandwich panels. The ply layup scheme and the core of the simple GA designs develop smaller stresses by carrying larger membrane stresses which help reduce stresses associated with bending while maintaining the appropriate geometrically nonlinear stiffness. Load that is transferred through bending causes a significant increase in overall stress when compared to load that is transferred through membrane effects. If the state equations had ignored geometric nonlinearities, the best designs found by the simple GA could have been considered to be infeasible designs with respect to the stiffness inequality constraint.

5.4 Conclusions

The design space of an optimization problem involving geometric nonlinear response of sandwich panels was searched with a simple GA. The simple GA found designs that outperformed the original baseline design. The original baseline design satisfied the displacement inequality constraint, but harshly violated the inequality constraint placed on the failure index. Both simple GA designs satisfy all constraints with nearly identical mass to that of the baseline design. The simple GA designs are more compliant at small loadings (compared to the baseline design), but are specifically constructed to significantly stiffen at larger loads, due to geometric nonlinearities, while maintaining feasible stresses.

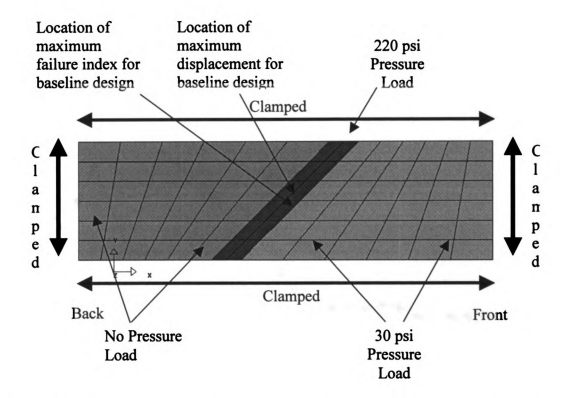


Figure 5.1. Finite element mesh including applied boundary conditions. Location of maximum transverse displacement and failure index. The sandwich panel is 24 inches wide and 84 inches long.

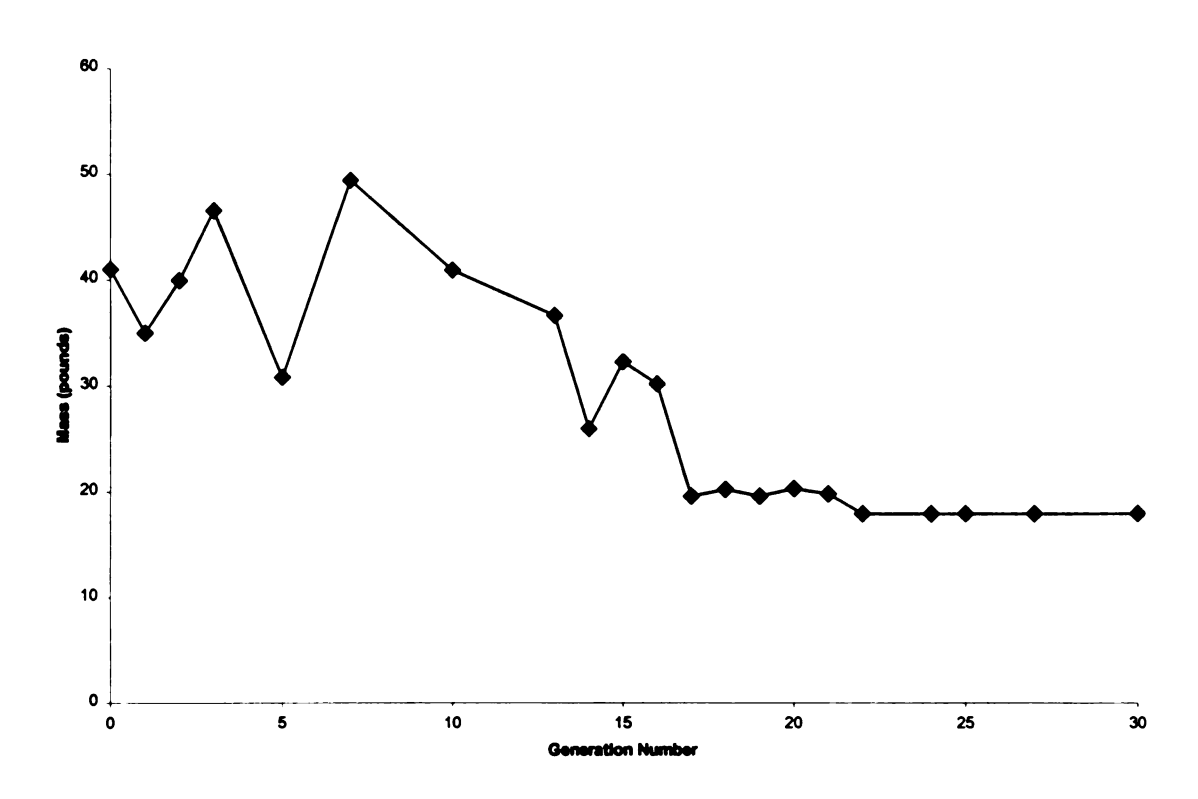


Figure 5.2. The mass of the best design found as a function of generation number.

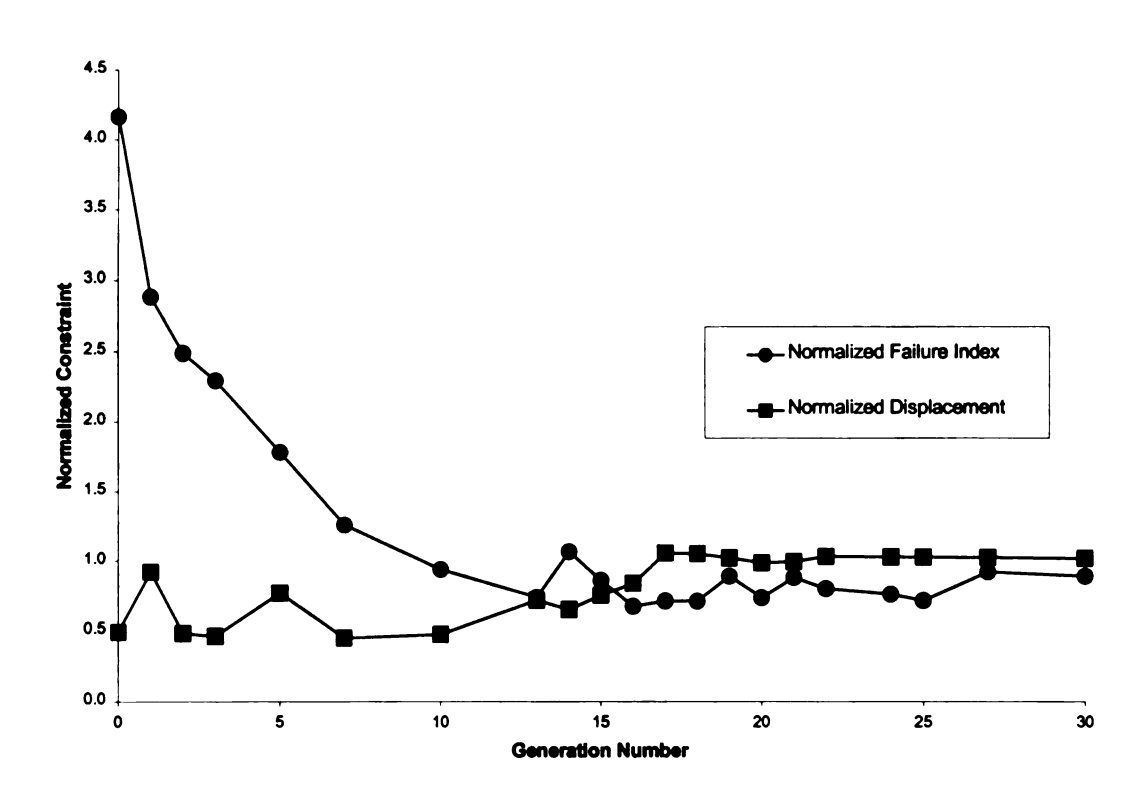


Figure 5.3. Normalized constraints of the best design found as a function of generation number.

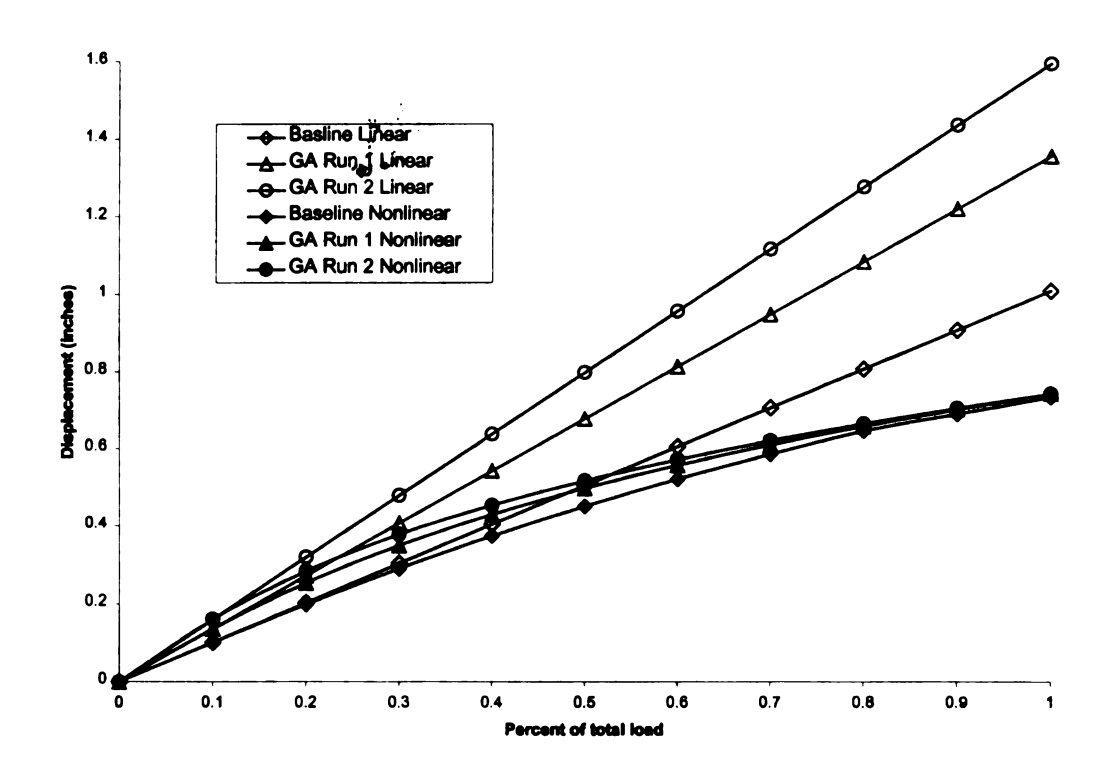


Figure 5.4. Linear and geometrically nonlinear load deflection response curves for the baseline and simple GA optimized sandwich panels.

Table 5.1. Ply material properties.

Material Name	E1 (msi)	E2 (msi)	E3 (msi)	v	Fiber Weight (oz/yd²)	Thickness (mils)	Longt. Strength (ksi)	Trans. Strength (ksi)
CM-1208	2.17	1.66	1.34	0.3	18.9	37	36.76	14.13
CM-1215	1.86	1.33	1.34	0.3	25.6	37	23	14.13
CM-1608	2.13	2.07	1.22	0.3	22.5	44	24.75	13.17
CM-1615	1.77	1.87	1.22	0.3	29	56	22	13.63
CM-1808	2.59	1.74	1.19	0.3	24.4	43	35.27	13.34
CM-1815	2.2	1.82	1.15	0.3	31.2	57	28.48	15
CM-2308	2.37	2.28	1.36	0.3	29	53	29.9	13.86
CM-2315	1.85	1.79	1.18	0.3	36.7	73	26.33	13.07
CM-3308	2.38	2.52	1.18	0.3	36.7	61	41.19	13.07
CM-3415	1.98	2.01	1.1	0.3	36.7	80	25.46	11.65
CM-3610	2.17	2.27	1.1	0.3	36.7	76	29.86	11.65
XM-1208	1.3	1.33	2.03	0.3	19.2	39	13.59	27.04
XM-1215	1.2	1.02	2.19	0.3	26	47	15.68	27
XM-1708	1.31	1.25	2.05	0.3	24.4	44	14.26	31.82
XM-1715	1.36	1.35	2.25	0.3	31.1	51	16.2	31.49
XM-2408	1.14	1.34	2.05	0.3	31	50	10.58	31.82
XM-2415	1.22	1.62	2.19	0.3	37.8	66	13.53	24.99
XM-1305	1.85	2	2.1	0.3	24	26	8	18
XM-1308	1.85	2	2.1	0.3	24	29	8	18
XM-1708	1.5	2.2	2.1	0.3	24	48	13.6	18
XM-1808	1.5	2.2	2.1	0.3	24.8	48	13.6	23.4
XM-1808B	1.5	2.2	2.1	0.3	24.8	48	13.6	23.4
XM-2408	1.55	2.2	2.2	0.3	30.8	56	14.2	33.2
XM-2415	1.5	2.1	3.1	0.3	37.5	71	11.5	39.8

Table 5.2. Core material properties.

Core Material Name	E1 (psi)	v	Density (lb/ft ³)	Shear Strength (psi)	Compressive Strength (psi)
A400	4.998e3	0.3	4.0	125.0	80.0
A450	6.5000e3	0.3	4.5	135.0	95.0
A500	8.4440e3	0.3	5.0	142.0	115.0
A550	8.8000e3	0.3	5.7	166.0	142.0
A600	9.2170e3	0.3	6.3	191.0	165.0
A650	9.8850e3	0.3	8.0	241.0	210.0

Table 5.3. Baseline and optimized sandwich panel design variables. All material names are in reference to Tables 1 and 2.

	Baseline	Opt. Run 1	Opt. Run 2
# of plies in bottom skin	2	3	3
# of core layer(s)	1	1	1
# of plies in top skin	2	2	4
Orientation of bottom plies (degrees)	0.0, 0.0	30, 150, 60	0, 75, 120
Orientation of top plies (degrees)	0.0, 0.0	45, 75	0, 150, 135, 60
Bottom ply materials	XM-1808, CM-1808	CM-2315, CM-1208, CM-3610	XM-1708, CM-1208, CM-1208
Core material(s)	A550	A400	A400
Core thickness (inches)	1.340	1.0	0.625
Top ply materials	CM-1808, XM-1808	CM-3610, CM-1808	XM-1808B, XM-1208, CM-1608, CM-2315

Table 5.4. Baseline and GA optimized sandwich panel objectives and constraints.

	Ineq. Constraint	Baseline	Opt. Run 1	Opt. Run 2
Mass (lbs)		18.47	17.88	18.94
Transverse	0.73	0.73	0.74	0.74
displacement (inches)				
Max. failure indicy	1.0	3.14	0.92	0.87

Chapter 6

SUMMARY AND CONCLUSIONS

This dissertation addressed three major areas: multi-objective optimization of crashworthiness, geometrically nonlinear analysis of laminated composite materials and optimization of laminated composite sandwich panels considering geometrically nonlinear response. Each area of research in this dissertation contributed unique accomplishments within their field.

The shortcomings of available optimization techniques were overcome by developing an approach that allows for concurrent multi-objective optimization of structures with an island injection Genetic Algorithm for: 1) crash energy management, 2) modal vibration frequency response, 3) peak crush force, 4) weight reduction, and 5) manufacturability while considering stochastic variability of design variables and loading conditions. Existing automated design technology has never simultaneously addressed all these competing mechanisms. Three independent runs converged to nearly identical designs. This result does not guarantee that the global optimum was found; rather it indicates that a similar search of the design space was completed for each run, from different initial populations, making it at lease possible that a relatively thorough search was conducted (noting that if radically different designs had resulted, this claim could not be made).

A new geometrically nonlinear first-order zig-zag sublaminate plate theory and finite element model was formulated and implemented. The new

geometrically nonlinear first-order zig-zag sublaminate plate theory and finite element model was validated against existing experimental and numerical results for laminated composite panels. This model is accurate for a wide range of laminated panel applications including very thin laminated panels up to very thick laminated and sandwich panels. The model is cast in a form that facilitates its use within commercial finite element packages. The finite element models developed take the form of a three-dimensional eight-noded brick or six-noded wedge element with the usual five engineering degrees-of-freedom per node.

Finally, an optimization problem was considered involving geometric nonlinear response of sandwich panels with a simple GA. The simple GA designs were compliant at small loadings, but were specifically constructed to significantly stiffen at larger loads due to geometric nonlinearities, while maintaining feasible stresses. This was accomplished by the ply layup scheme and the core of the simple GA designs, which develop smaller overall stresses by carrying more load through membrane effects.

APPENDIX A

The displacement fields for the first order zig-zag theory can be expressed in indicial notation as:

$$u_{x_{1}}^{(k)} = \overline{u}_{\alpha\beta} \Phi_{\alpha\beta}^{(k)}$$

$$u_{x_{2}}^{(k)} = \overline{u}_{\alpha\beta} \Psi_{\alpha\beta}^{(k)} \qquad \alpha = 1...4; \beta = 1,2$$

$$u_{x_{1}}^{(k)} = w_{\beta} \Omega_{\beta}$$
A.(1)

where the index β is used to denote the top and bottom of the sublaminate with 1:bottom and 2:top, and $\Phi_{\alpha\beta}^{(k)}$, $\Psi_{\alpha\beta}^{(k)}$ and Ω_{β} are shape functions in the thickness direction (see Cho and Averill, 2000). Summation on repeated indices is implied unless otherwise noted. The variables $\overline{u}_{\alpha\beta}$ are:

$$\overline{u}_{1\beta} = u_{\beta}$$
, $\overline{u}_{2\beta} = v_{\beta}$, $\overline{u}_{3\beta} = \theta_{x\beta}$, $\overline{u}_{4\beta} = \theta_{y\beta}$ A.(2)

Green's strain can be written as the sum of linear and nonlinear parts:

$$\mathbf{E} = \mathbf{\varepsilon}_L + \mathbf{\varepsilon}_{NL} \tag{3}$$

The linear portion of the Green's strain is:

$$\varepsilon_{L} = \mathbf{L}\mathbf{u} = \mathbf{L}\mathbf{N}\overline{\mathbf{u}} = \mathbf{B}_{L}\overline{\mathbf{u}}$$
 A.(4)

Since $\Phi_{\alpha\beta}^{(k)}$, $\Psi_{\alpha\beta}^{(k)}$ and Ω_{β} are functions of the through-thickness direction only, two dimensional shape functions (equations 4.51 – 4.54) can approximate the nodal variables $\overline{u}_{\alpha\beta}$. The linear strains are first approximated as:

$$\mathcal{E}_{11\ L}^{(k)} = \overline{u}_{\alpha\beta,x_{1}} \Phi_{\alpha\beta}^{(k)}
\mathcal{E}_{22\ L}^{(k)} = \overline{u}_{\alpha\beta,x_{2}} \Psi_{\alpha\beta}^{(k)}
\mathcal{E}_{33\ L}^{(k)} = w_{\beta} \Omega_{\beta,x_{3}}
\gamma_{23\ L}^{(k)} = \overline{u}_{\alpha\beta} \Psi_{\alpha\beta,x_{3}}^{(k)} + w_{\beta,x_{2}} \Omega_{\beta} \Big|_{z=\frac{h}{2}}
\gamma_{13\ L}^{(k)} = \overline{u}_{\alpha\beta} \Psi_{\alpha\beta,x_{3}}^{(k)} + w_{\beta,x_{1}} \Omega_{\beta} \Big|_{z=\frac{h}{2}}
\gamma_{12\ L}^{(k)} = \overline{u}_{\alpha\beta,x_{3}} \Phi_{\alpha\beta}^{(k)} + \overline{u}_{\alpha\beta,x_{3}} \Psi_{\alpha\beta}^{(k)}$$

$$A.(5)$$

where tensor notations are implied and a comma denotes partial differentiation. The contribution of the transverse deflection to the transverse shear strains $\gamma_{23}^{(k)}$ and $\gamma_{13}^{(k)}$ are evaluated at the at the middle of the sublaminate to obtain constant shear stresses through-the-thickness of the sublaminate.

A constant transverse normal strain may give rise to substantial errors in composites which have a soft core or layer (see Cho and Averill, 2000). An improvement in the through-thickness description of deformation can be found by assuming a constant transverse normal stress which can be obtained using Reissner's mixed variational principal (see Reissner, 1986). The newly defined transverse normal strain for small displacements can be written as:

$$\mathcal{E}_{33}^{-(k)} = \overline{u}_{\alpha\beta,x_1} \lambda_{x_1\alpha\beta}^{(k)} + \overline{u}_{\alpha\beta,x_2} \lambda_{x_2\alpha\beta}^{(k)} + w_{\beta} \chi_{\beta}$$
 A.(6)

The coefficients $\lambda_{x_1\alpha\beta}^{(k)}$, $\lambda_{x_2\alpha\beta}^{(k)}$ and χ_{β} are defined in Cho (1997).

For an eight noded brick element, \mathbf{B}_{L} can be defined as:

$$\begin{split} B_L^{(k)}(1,i1) &= \Phi_{11}^{(k)} N_{i,x} \\ B_L^{(k)}(1,i2) &= \Phi_{21}^{(k)} N_{i,x} \\ B_L^{(k)}(1,i2) &= 0 \\ B_L^{(k)}(1,i4) &= \Phi_{31}^{(k)} N_{i,x} \\ B_L^{(k)}(1,i5) &= \Phi_{41}^{(k)} N_{i,x} \\ B_L^{(k)}(1,i6) &= \Phi_{12}^{(k)} N_{i,x} \\ B_L^{(k)}(1,i7) &= \Phi_{22}^{(k)} N_{i,x} \\ B_L^{(k)}(1,i8) &= 0 \\ B_L^{(k)}(1,i9) &= \Phi_{32}^{(k)} N_{i,x} \\ B_L^{(k)}(1,i10) &= \Phi_{42}^{(k)} N_{i,x} \\ B_L^{(k)}(1,i10) &= \Phi_{42$$

$$\begin{split} B_L^{(k)}(2,i1) &= \Psi_{11}^{(k)} N_{i,y} \\ B_L^{(k)}(2,i2) &= \Psi_{21}^{(k)} N_{i,y} \\ B_L^{(k)}(2,i3) &= 0 \\ B_L^{(k)}(2,i4) &= \Psi_{31}^{(k)} N_{i,y} \\ B_L^{(k)}(2,i5) &= \Psi_{41}^{(k)} N_{i,y} \\ B_L^{(k)}(2,i6) &= \Psi_{12}^{(k)} N_{i,y} \\ B_L^{(k)}(2,i7) &= \Psi_{22}^{(k)} N_{i,y} \\ B_L^{(k)}(2,i7) &= 0 \\ B_L^{(k)}(2,i9) &= \Psi_{32}^{(k)} N_{i,y} \\ B_L^{(k)}(2,i10) &= \Psi_{42}^{(k)} N_{i,y} \\ B_L^{(k)}(2,i10) &= \Psi_{42$$

$$B_{L}^{(k)}(3,i1) = \lambda_{x11}^{(k)} N_{i,x} + \lambda_{y11}^{(k)} N_{i,y}$$

$$B_{L}^{(k)}(3,i2) = \lambda_{x21}^{(k)} N_{i,x} + \lambda_{y21}^{(k)} N_{i,y}$$

$$i = 1...4$$

$$i1 = (i-1)*5+1$$

$$i2 = (i-1)*5+2$$

$$i3 = (i-1)*5+3$$

$$i4 = (i-1)*5+4$$

$$i5 = (i-1)*5+4$$

$$i5 = (i-1)*5+2$$

$$i6 = (i-1)*5+2$$

$$i6 = (i-1)*5+2$$

$$i7 = (i-1)*5+2$$

$$i8 = (i-1)*5+2$$

$$i9 = (i-1)*5+2$$

$$i19 = (i-1)*5+2$$

$$i10 = (i-1)*5+2$$

$$\begin{split} B_L^{(k)}(4,i1) &= \Psi_{11,z}^{(k)} N_i \\ B_L^{(k)}(4,i2) &= \Psi_{21,z}^{(k)} N_i \\ B_L^{(k)}(4,i3) &= -\Omega_1^{(k)} \big|_{z=h/2} \hat{N}_{i,y} \\ B_L^{(k)}(4,i4) &= \Psi_{31,z}^{(k)} N_i \\ B_L^{(k)}(4,i5) &= \Psi_{41,z}^{(k)} N_i \\ B_L^{(k)}(4,i6) &= \Psi_{12,z}^{(k)} N_i \\ B_L^{(k)}(4,i7) &= \Psi_{22,z}^{(k)} N_i \\ B_L^{(k)}(4,i8) &= \Omega_2^{(k)} \big|_{z=h/2} \hat{N}_{i,y} \\ B_L^{(k)}(4,i9) &= \Psi_{32,z}^{(k)} N_i \\ B_L^{(k)}(4,i10) &= \Psi_{43,z}^{(k)} N_i \\ \end{split}$$

$$\begin{split} B_L^{(k)}(5,i1) &= \Psi_{11,z}^{(k)} N_i \\ B_L^{(k)}(5,i2) &= \Psi_{21,z}^{(k)} N_i \\ B_L^{(k)}(5,i3) &= -\Omega_1^{(k)} \big|_{z=h/2} \hat{N}_{i,x} \\ B_L^{(k)}(5,i4) &= \Psi_{31,z}^{(k)} N_i \\ B_L^{(k)}(5,i5) &= \Psi_{41,z}^{(k)} N_i \\ B_L^{(k)}(5,i6) &= \Psi_{12,z}^{(k)} N_i \\ B_L^{(k)}(5,i7) &= \Psi_{22,z}^{(k)} N_i \\ B_L^{(k)}(5,i8) &= \Omega_2^{(k)} \big|_{z=h/2} \hat{N}_{i,x} \\ B_L^{(k)}(5,i9) &= \Psi_{32,z}^{(k)} N_i \\ B_L^{(k)}(5,i10) &= \Psi_{42,z}^{(k)} N_i \\ \end{split}$$

$$\begin{split} B_L^{(k)}(6,i1) &= \Phi_{11}^{(k)} N_{i,y} + \Psi_{11}^{(k)} N_{i,x} \\ B_L^{(k)}(6,i2) &= \Phi_{21}^{(k)} N_{i,y} + \Psi_{21}^{(k)} N_{i,x} \\ B_L^{(k)}(6,i3) &= 0 \\ B_L^{(k)}(6,i4) &= \Phi_{31}^{(k)} N_{i,y} + \Psi_{31}^{(k)} N_{i,x} \\ B_L^{(k)}(6,i5) &= \Phi_{41}^{(k)} N_{i,y} + \Psi_{41}^{(k)} N_{i,x} \\ B_L^{(k)}(6,i6) &= \Phi_{12}^{(k)} N_{i,y} + \Psi_{12}^{(k)} N_{i,x} \\ B_L^{(k)}(6,i7) &= \Phi_{22}^{(k)} N_{i,y} + \Psi_{22}^{(k)} N_{i,x} \\ B_L^{(k)}(6,i8) &= 0 \\ B_L^{(k)}(6,i9) &= \Phi_{32}^{(k)} N_{i,y} + \Psi_{32}^{(k)} N_{i,x} \\ B_L^{(k)}(6,i10) &= \Phi_{42}^{(k)} N_{i,y} + \Psi_{42}^{(k)} N_{i,x} \\ B_L^{(k)}(6,i10) &= \Phi_{$$

It should be noted that the through-thickness shearing strains represented here are in their original form. Cho and Averill enforced field consistency, consistent penalty constraints and edge consistency to define alternate through-thickness shearing strains which alleviated locking. All coefficients needed to formulate **B**_L can be found in Cho, 1997.

The nonlinear portion of the Green's strain is:

$$\varepsilon_{NL} = \frac{1}{2} \mathbf{A}(\theta) \mathbf{\theta}(\mathbf{u})$$
 A.(13)

where $\theta(\mathbf{u})$ is a vector of displacement gradients and $\mathbf{A}(\theta)$ is a matrix composed of the vector $\theta(\mathbf{u})$. For this element formulation, equation A.(13) can be written in compact vector form as:

$$\begin{cases}
\mathcal{E}_{11}^{(k)} \\
\mathcal{E}_{22}^{(k)} \\
\mathcal{E}_{33}^{(k)} \\
\gamma_{13}^{(k)} \\
\gamma_{12}^{(k)}
\end{cases}_{NL} = \begin{cases}
\frac{1}{2} \Omega_{\rho} u_{3\beta,x_{1}} \Omega_{\alpha} u_{3\alpha,x_{1}} \\
\frac{1}{2} \Omega_{\rho} u_{3\beta,x_{2}} \Omega_{\alpha} u_{3\alpha,x_{2}} \\
0 \\
0 \\
0 \\
\Omega_{\rho} u_{3\beta,x_{1}} \Omega_{\alpha} u_{3\alpha,x_{2}}
\end{cases} \qquad \alpha = 1,2 \\
\beta = 1,2$$
A.(14)

$$\Omega_b = 1 - \frac{x_3}{h} \qquad \qquad \Omega_t = \frac{x_3}{h} \qquad \qquad \text{A.(15)}$$

where h is the height of the sublaminate, while b and t denote the bottom and top of the sublaminate. The one-dimensional shape functions are evaluated at the mid-plane of the sublaminate to ensure that transverse shear strain expressions only contribute constant terms to the transverse stresses $S_{23}^{(k)}$ and $S_{13}^{(k)}$, to maintain consistency with the terms in the in-plane displacements $u_1^{(k)}$ and $u_2^{(k)}$ (equation 4.4).

The von Karman strain terms are present in the transverse normal strain due to the constant transverse normal stress assumption. The nonlinear contribution of the transverse normal strain for the kth layer is:

$$\bar{\varepsilon}_{33}^{(k)}_{NL} = \frac{1}{C_{33}^{(k)}} \left(\bar{S}_{33NL} - C_{13}^{(k)} \varepsilon_{11NL}^{(k)} - C_{23}^{(k)} \varepsilon_{22NL}^{(k)} - C_{36}^{(k)} \gamma_{12NL}^{(k)} \right)$$
 A.(16)

 $\overline{S}_{_{33_{ML}}}$ is then determined analytically from Reissner's mixed variational principle (equation 4.10) to obtain the following relation:

$$\overline{S}_{33_{NL}} = A_1 \sum_{i=1}^{N} \int_{x3_{i,1}}^{x3_i} \left[C_{13}^{(i)} \varepsilon_{11}^{(i)} + C_{23}^{(i)} \varepsilon_{22}^{(i)} + C_{36}^{(i)} \gamma_{12}^{(i)} \right] dx_3 \qquad A.(17)$$

where N is the number of layers in the sublaminate and the coefficient A₁ is:

$$A_{1} = \sum_{i=1}^{N} 1 / \left[\frac{\left(x_{3_{i}} - x_{3_{i-1}} \right)}{C_{33}^{(i)}} \right]$$
 A.(18)

Each nonlinear strain term in equation A.(17) is a function of the through the thickness coordinate (x_3) . After substituting the one-dimensional throughthickness shape functions (equations A.(15)) into equation A.(17) and integrating, the analytical form of the geometrically nonlinear through-thickness constant normal stress within a sublaminate (equation A.(17)) is:

$$\overline{S}_{33_{NL}} = \frac{1}{2} w_{\beta,x_1} w_{\alpha,x_1} \Delta 13_{\alpha\beta} + \frac{1}{2} w_{\beta,x_2} w_{\alpha,x_2} \Delta 23_{\alpha\beta} + w_{\beta,x_1} w_{\alpha,x_2} \Delta 36_{\alpha\beta} \qquad A.(19)$$

where a comma denotes partial differentiation, while α and β are used in tensor form, and the coefficients $\Delta 13_{\alpha\beta}$, $\Delta 23_{\alpha\beta}$, and $\Delta 36_{\alpha\beta}$ are:

$$\Delta 13_{\alpha\beta} = A_1 \sum_{i=1}^{N} r_{13}^{i} \kappa_{\alpha\beta}^{i} \qquad \Delta 23_{\alpha\beta} = A_1 \sum_{i=1}^{N} r_{23}^{i} \kappa_{\alpha\beta}^{i} \qquad \Delta 36_{\alpha\beta} = A_1 \sum_{i=1}^{N} r_{36}^{i} \kappa_{\alpha\beta}^{i} \qquad A.(20)$$

and:

$$\kappa_{\alpha\beta}^{i} = \int_{x_{3_{i-1}}}^{x_{3_{i}}} \Omega_{\alpha} \Omega_{\beta} dx_{3}$$
 A.(21)

The gradients of the transverse displacement with respect to the in-plane directions (x_1 and x_2) are:

$$W_{\alpha,\xi} = \sum_{i=1}^{4} \left(W_{\alpha_i} N_{i,\xi} + \theta_{x\alpha_i} \hat{N}_{i,\xi} + \theta_{y\alpha_i} \hat{N}_{i,\xi} \right) \xi = x_1, x_2 \quad \alpha = 1,2 \quad A.(22)$$

where a comma denotes partial differentiation, $N_{i,\xi}$ are the gradients of the bilinear Lagrange interpolation functions and $\hat{N}_{i,\xi}$ are the gradients of the shape functions obtained from the interdependent interpolation scheme as found in Cho, 1997.

The analytical form of the geometrically nonlinear through-thickness normal strain for the kth layer in a sublaminate can be found by substituting equations A.(15) and A.(17) into equation A.(16) to obtain:

$$\overline{\varepsilon}_{33}^{(k)}_{NL} = \frac{1}{C_{33}^{(k)}} \begin{cases} \frac{1}{2} w_{\beta,x_1} w_{\alpha,x_1} \Delta 13_{\alpha\beta} + \frac{1}{2} w_{\beta,x_2} w_{\alpha,x_2} \Delta 23_{\alpha\beta} \\ + w_{\beta,x_1} w_{\alpha,x_2} \Delta 36_{\alpha\beta} \end{cases} \\
- \begin{cases} \frac{1}{2} r_{13}^{(k)} \Omega_{\beta} w_{\beta,x_1} \Omega_{\alpha} w_{\alpha,x_1} + \frac{1}{2} r_{23}^{(k)} \Omega_{\beta} w_{\beta,x_2} \Omega_{\alpha} w_{\alpha,x_2} \\ + r_{36}^{(k)} \Omega_{\beta} w_{\beta,x_1} \Omega_{\alpha} w_{\alpha,x_2} \end{cases} \right|_{z=h/2} A.(23)$$

where a comma denotes partial differentiation, while lpha and eta are used in tensor form.

Now that the constant transverse normal stress and transverse normal strain have been defined including the von Karman strains, we can move on to the first infinitesimal variation of the nonlinear strain as defined in equation 4.31:

$$\delta \varepsilon_{NL} = \mathbf{A}(\theta) \mathbf{\theta}(\overline{\mathbf{u}}) \delta \overline{\mathbf{u}}$$
 A.(24)

Let $\theta(\mathbf{u})$ be defined as a vector containing all the nonlinear coefficients:

$$\Theta(u) = \left\{ w_{b,x_1} \quad w_{t,x_1} \quad w_{b,x_2} \quad w_{t,x_2} \right\}^T$$
 A.(25)

 $A(\theta)$ was developed by taking the first variation of the von Karman strains in equation A.(14) including the geometrically nonlinear through-thickness normal strain as defined by equation A.(23). For the k^{th} layer in a sublaminate $A(\theta)$ is:

$$\mathbf{A}(1,1)^{(k)} = \left(\Omega_{b}\Omega_{\alpha}w_{\alpha,x_{1}}\right)\Big|_{z=h/2}$$

$$\mathbf{A}(1,2)^{(k)} = \left(\Omega_{t}\Omega_{\alpha}w_{\alpha,x_{1}}\right)\Big|_{z=h/2}$$

$$\mathbf{A}(2,3)^{(k)} = \left(\Omega_{b}\Omega_{\alpha}w_{\alpha,x_{2}}\right)\Big|_{z=h/2}$$

$$\mathbf{A}(2,4)^{(k)} = \left(\Omega_{t}\Omega_{\alpha}w_{\alpha,x_{2}}\right)\Big|_{z=h/2}$$

$$\mathbf{A}(3,1)^{(k)} = \frac{1}{C_{13}^{(k)}}\left(w_{\alpha,x_{1}}\Delta 13_{b\alpha} + w_{\alpha,x_{2}}\Delta 36_{b\alpha}\right)$$

$$-\left(r_{13}^{(k)}\Omega_{b}\Omega_{\alpha}w_{\alpha,x_{1}} + r_{34}^{(k)}\Omega_{b}\Omega_{\alpha}w_{\alpha,x_{2}}\right)\Big|_{z=h/2}$$

$$\mathbf{A}(3,2)^{(k)} = \frac{1}{C_{33}^{(k)}}\left(w_{\alpha,x_{1}}\Delta 13_{t\alpha} + w_{\alpha,x_{2}}\Delta 36_{t\alpha}\right)$$

$$-\left(r_{13}^{(k)}\Omega_{t}\Omega_{\alpha}w_{\alpha,x_{1}} + r_{34}^{(k)}\Omega_{t}\Omega_{\alpha}w_{\alpha,x_{2}}\right)\Big|_{z=h/2}$$

$$\mathbf{A}(3,3)^{(k)} = \frac{1}{C_{33}^{(k)}}\left(w_{\alpha,x_{2}}\Delta 23_{b\alpha} + w_{\alpha,x_{1}}\Delta 36_{b\alpha}\right)$$

$$-\left(r_{13}^{(k)}\Omega_{b}\Omega_{\alpha}w_{\alpha,x_{2}} + r_{34}^{(k)}\Omega_{b}\Omega_{\alpha}w_{\alpha,x_{1}}\right)\Big|_{z=h/2}$$

$$\mathbf{A}(26)$$

$$\mathbf{A}(3,4)^{(k)} = \frac{1}{C_{33}^{(k)}} \left(w_{\alpha,x_{2}} \Delta 23_{t\alpha} + w_{\alpha,x_{1}} \Delta 36_{t\alpha} \right) - \left(r_{23}^{(k)} \Omega_{t} \Omega_{\alpha} w_{\alpha,x_{2}} + r_{36}^{(k)} \Omega_{t} \Omega_{\alpha} w_{\alpha,x_{1}} \right) \Big|_{z=h/2}$$

$$\mathbf{A}(6,1)^{(k)} = \left(\Omega_{b} \Omega_{\alpha} w_{\alpha,x_{2}} \right) \Big|_{z=h/2}$$

$$\mathbf{A}(6,2)^{(k)} = \left(\Omega_{t} \Omega_{\alpha} w_{\alpha,x_{1}} \right) \Big|_{z=h/2}$$

$$\mathbf{A}(6,3)^{(k)} = \left(\Omega_{b} \Omega_{\alpha} w_{\alpha,x_{1}} \right) \Big|_{z=h/2}$$

$$\mathbf{A}(6,4)^{(k)} = \left(\Omega_{t} \Omega_{\alpha} w_{\alpha,x_{1}} \right) \Big|_{z=h/2}$$

where α is summed from bottom to top. All other positions of the $\mathbf{A}(\theta)$ matrix are homogeneous.

The stress stiffening matrix \hat{S} was found from the relationship:

$$\delta \mathbf{A}^{\mathsf{T}} \mathbf{S} = \hat{\mathbf{S}} \delta \mathbf{\Theta}$$
 A.(27)

For the k^{th} layer within the suiblaminate, \hat{S} can be defined by:

$$\hat{S}(1,1)^{(k)} = \left[S_{11} \Omega_b \Omega_b + \left(\frac{\Delta 13_{bb}}{C_{33}^{(k)}} - r_{13}^{(k)} \Omega_b \Omega_b \right) \overline{S}_{33} \right]_{z=h/2}
\hat{S}(1,2)^{(k)} = \left[S_{11} \Omega_b \Omega_t + \left(\frac{\Delta 13_{bt}}{C_{33}^{(k)}} - r_{13}^{(k)} \Omega_b \Omega_t \right) \overline{S}_{33} \right]_{z=h/2}
\hat{S}(1,3)^{(k)} = \left[S_{12} \Omega_b \Omega_b + \left(\frac{\Delta 36_{bb}}{C_{33}^{(k)}} - r_{36}^{(k)} \Omega_b \Omega_b \right) \overline{S}_{33} \right]_{z=h/2}
\hat{S}(1,4)^{(k)} = \left[S_{12} \Omega_b \Omega_t + \left(\frac{\Delta 36_{bt}}{C_{33}^{(k)}} - r_{36}^{(k)} \Omega_b \Omega_t \right) \overline{S}_{33} \right]_{z=h/2}
\hat{S}(2,2)^{(k)} = \left[S_{11} \Omega_t \Omega_t + \left(\frac{\Delta 13_{tt}}{C_{33}^{(k)}} - r_{13}^{(k)} \Omega_t \Omega_t \right) \overline{S}_{33} \right]_{z=h/2}$$

$$\hat{\mathbf{S}}(2,3)^{(k)} = \left[S_{12} \Omega_b \Omega_t + \left(\frac{\Delta 36_{bt}}{C_{33}^{(k)}} - r_{36}^{(k)} \Omega_b \Omega_t \right) \overline{S}_{33} \right]_{z=h/2} \\
\hat{\mathbf{S}}(2,4)^{(k)} = \left[S_{12} \Omega_t \Omega_t + \left(\frac{\Delta 36_{tt}}{C_{33}^{(k)}} - r_{36}^{(k)} \Omega_t \Omega_t \right) \overline{S}_{33} \right]_{z=h/2} \\
\hat{\mathbf{S}}(3,3)^{(k)} = \left[S_{22} \Omega_b \Omega_b + \left(\frac{\Delta 23_{bb}}{C_{33}^{(k)}} - r_{23}^{(k)} \Omega_b \Omega_b \right) \overline{S}_{33} \right]_{z=h/2} \\
\hat{\mathbf{S}}(3,4)^{(k)} = \left[S_{22} \Omega_b \Omega_t + \left(\frac{\Delta 23_{tb}}{C_{33}^{(k)}} - r_{23}^{(k)} \Omega_b \Omega_t \right) \overline{S}_{33} \right]_{z=h/2} \\
\hat{\mathbf{S}}(4,4)^{(k)} = \left[S_{22} \Omega_t \Omega_t + \left(\frac{\Delta 23_{tb}}{C_{33}^{(k)}} - r_{23}^{(k)} \Omega_t \Omega_t \right) \overline{S}_{33} \right]_{z=h/2} \\
\hat{\mathbf{S}}(4,4)^{(k)} = \left[S_{22} \Omega_t \Omega_t + \left(\frac{\Delta 23_{tb}}{C_{33}^{(k)}} - r_{23}^{(k)} \Omega_t \Omega_t \right) \overline{S}_{33} \right]_{z=h/2} \\
\hat{\mathbf{S}}(4,4)^{(k)} = \left[S_{22} \Omega_t \Omega_t + \left(\frac{\Delta 23_{tb}}{C_{33}^{(k)}} - r_{23}^{(k)} \Omega_t \Omega_t \right) \overline{S}_{33} \right]_{z=h/2} \\
\hat{\mathbf{S}}(4,4)^{(k)} = \left[S_{22} \Omega_t \Omega_t + \left(\frac{\Delta 23_{tb}}{C_{33}^{(k)}} - r_{23}^{(k)} \Omega_t \Omega_t \right) \overline{S}_{33} \right]_{z=h/2} \\
\hat{\mathbf{S}}(4,4)^{(k)} = \left[S_{22} \Omega_t \Omega_t + \left(\frac{\Delta 23_{tb}}{C_{33}^{(k)}} - r_{23}^{(k)} \Omega_t \Omega_t \right) \overline{S}_{33} \right]_{z=h/2} \\
\hat{\mathbf{S}}(4,4)^{(k)} = \left[S_{22} \Omega_t \Omega_t - \left(\frac{\Delta 23_{tb}}{C_{33}^{(k)}} - r_{23}^{(k)} \Omega_t \Omega_t \right) \overline{S}_{33} \right]_{z=h/2} \\
\hat{\mathbf{S}}(4,4)^{(k)} = \left[S_{22} \Omega_t \Omega_t - \left(\frac{\Delta 23_{tb}}{C_{33}^{(k)}} - r_{23}^{(k)} \Omega_t \Omega_t \right) \overline{S}_{33} \right]_{z=h/2} \\
\hat{\mathbf{S}}(4,4)^{(k)} = \left[S_{22} \Omega_t \Omega_t - \left(\frac{\Delta 23_{tb}}{C_{33}^{(k)}} - r_{23}^{(k)} \Omega_t \Omega_t \right) \overline{S}_{33} \right]_{z=h/2} \\
\hat{\mathbf{S}}(4,4)^{(k)} = \left[S_{22} \Omega_t \Omega_t - \left(\frac{\Delta 23_{tb}}{C_{33}^{(k)}} - r_{23}^{(k)} \Omega_t \Omega_t \right) \overline{S}_{33} \right]_{z=h/2} \\
\hat{\mathbf{S}}(4,4)^{(k)} = \left[S_{22} \Omega_t \Omega_t - \left(\frac{\Delta 23_{tb}}{C_{33}^{(k)}} - r_{23}^{(k)} \Omega_t \Omega_t \right) \overline{S}_{33} \right]_{z=h/2} \\
\hat{\mathbf{S}}(4,4)^{(k)} = \left[S_{22} \Omega_t \Omega_t - \left(\frac{\Delta 23_{tb}}{C_{33}^{(k)}} - r_{23}^{(k)} \Omega_t \Omega_t \right) \overline{S}_{33} \right]_{z=h/2} \\
\hat{\mathbf{S}}(4,4)^{(k)} = \left[S_{22} \Omega_t \Omega_t - \left(\frac{\Delta 23_{tb}}{C_{33}^{(k)}} - r_{23}^{(k)} \Omega_t \Omega_t \right) \overline{S}_{33} \right]_{z=h/2} \\
\hat{\mathbf{S}}(4,4)^{(k)} = \left[S_{22} \Omega_t \Omega_t - \left(\frac{\Delta 23_{tb}}{C_{33}^{(k)}} - r_{23}^{(k)} \Omega_t \Omega_t \right) \overline{S}_{33} \right]_{z=h/2} \\
\hat{\mathbf$$

Only the upper portion of the stress stiffening matrix \hat{S} is displayed due to symmetry of the second Piola-Kirchhoff stress tensor. Note that all positions in \hat{S} are functions of the newly defined constant geometrically nonlinear transverse normal stress.

Finally, the matrix of nodal shape function gradients **G** is:

$$G(1,i5) = N_{i,x_1} \qquad G(3,i5) = N_{i,x_2}$$

$$G(1,i5+1) = \hat{N}_{i,x_1} \qquad G(3,i5+1) = \hat{N}_{i,x_2}$$

$$G(1,i5+2) = \hat{N}_{i,x_1} \qquad G(3,i5+2) = \hat{N}_{i,x_2} \qquad i = 1...4$$

$$G(2,i5+20) = N_{i,x_1} \qquad G(4,i5+20) = N_{i,x_2} \qquad i5 = 5 * (i-1) + 3$$

$$G(2,i5+21) = \hat{N}_{i,x_1} \qquad G(4,i5+21) = \hat{N}_{i,x_2}$$

$$G(2,i5+22) = \hat{N}_{i,x_1} \qquad G(4,i5+22) = \hat{N}_{i,x_2}$$

All other positions of **G** are zero.

We can define $\hat{\boldsymbol{B}}$ and $\overline{\boldsymbol{B}}$ as:

$$\hat{\mathbf{B}} = \mathbf{B}_L + \frac{1}{2}\mathbf{A}\mathbf{G}$$
 A.(30)

$$\overline{\mathbf{B}} = \mathbf{B}_L + \mathbf{AG}$$
 A.(31)

 $\hat{\bf B}$, $\overline{\bf B}$, $\bf G$, and $\hat{\bf S}$ form the direct stiffness and tangent stiffness matrices as defined in equations (4.36) and (4.45).

REFERENCES

- (1.) ADINA, 1999, "LS-DYNA User's Manual".
- (2.) Averill, R. C. and Reddy, J. N., 1992, "An assessment of Four-Noded Plate Finite Element methods Based on a Generalized Third-Order Theory", Int. Journal for Numerical Methods in Engineering, 33: 1553-1572.
- (3.) Averill, R. C., and Yip, Y., 1996, "Development of Simple, Robust Finite Elements Based on Refined Theories for Thick Laminated Beams", *Computers and Structures*, 59: 529-546.
- (4.) Belegundu A. D. and Zhang S., 1992, "Robustness of Design Through Minimum Sensitivity" *Journal of Mechanical Design*, 114: 213-217.
- (5.) Chapman, C. and Jakiela, M., 1996, "Genetic Algorithm-Based Structural Topology Design with Compliance and Topology Simplification Considerations." *Journal of Mechanical Design*, 118:89-98.
- (6.) Cho, M., and Parmerter, R., 1993, "Efficent higher Order Composite Plate Theory for General Lamination Configurations", *AIAAA Journal*, 31:1299-1306.
- (7.) Cho, Y., 1997, New Zig-Zag Composite Plate theories and 3-D Finite Elements For Static and Explicit Dynamic Analysis of Laminated Composite and Sandwich Panels, Ph.D. Dissertation, Michigan State University, E. Lansing, MI.
- (8.) Cho, Y.B and Averill, R.C., 2000, "First Order Zig-Zag Sublaminate Plate Theory and Finite Element Model for Laminated Composite and Sandwich Panels", to appear in *Composite Structures*.

- (9.) Crisfield, M.A., 1991, *Non-Linear Finite Element Analysis of Solids and Structures*, Vol. 1, John Wiley and Sons, Chichester.
- (10.) DiSciuva M., 1985, "Development of an Anisotropic Multilayered Shear Deformable Rectangular Plate Element", *Computers and Structures*, 47: 91-105.
- (11.) DiSciuva, M., 1993, "A General Quadrilateral Mulit-Layered Plate Element with Continuous Interlaminar Stresses", *Computers and Structures*, 47: 91-105.
- (12.) DiSciuva, M., 1997, "Geometrically Nonlinear Theory of Multilayered Plates with Interlayer Slips," *AIAA Journal*, 35:1753-1759.
- (13.) Eby, D., Averill, R. C., Punch, W. and Goodman, E., 1999, "The Optimization of Flywheels using an Injection Island Genetic Algorithm", *Evolutionary Design by Computers*, edited by P. J. Bentley, Academic Press Ltd.
- (14.) Fabbri, G., 1997, "A Genetic Algorithm for Fin Profile Optimization," Int. J. of Heat and Mass Transfer, 40:2165-2172.
- (15.) Flynn, R., and Sherman, P., 1995, "Multi-Criteria Optimization of Aircraft Panels: Determining Viable Genetic Algorithm Configurations," *International J of Intelligent Systems*, 10: 987-999.
- (16.) Foster, N., and Dulikravich, G., 1997, "Three-Dimensional Aerodynamic Shape Optimization Using Genetic and Gradient Search Algorithms," *Journal of Spacecraft and Rockets*, 34:36-42.
- (17.) Furuya H., and Haftka R. T., 1993, "Locating Actuators for Vibration Suppression on Space Trusses by Genetic Algorithms", *Structures and Controls Optimization*, ASME, AD Col., 38:1-11.
- (18.) Furuya H., and Haftka R., 1995, "Placing Actuators in Space Structures by Genetic Algorithms and Effectiveness Indices", *Structural Optimization*, 9:69-75.

- (19.) Gausser, M., Schueller, G., 1997, "Reliability-Based Optimization of Structural Systems", *Mathematical Methods of Operations Research*, 46: 287-307.
- (20.) Genta, G. and Bassani, D., 1995, "Use of Genetic Algorithms for the Design of Rotors," *Meccanica*, 30: 707-717.
- (21.) Goldberg D. 1988, Genetic Algorithms for Search, Optimization and Machine Learning, New York: Addison-Wesley.
- (22.) Goodman, E., 1996, "GALOPPS, The Genetic Algorithm Optimized for Portability and Parallelism System, User's Guide," Technical Report, Genetic Algorithms Research and Applications Group (GARAGe), Michigan State University, East Lansing, July, 1996.
- (23.) Haftka, R. T., Gurdal, Z. 1993, *Elements of Structural Optimization*, Third Edition, Kluwer Academic Publishers.
- (24.) Gurdal, Z., 1999, Optimal Design, Theory and Applications to Materials and Structures, Technomic Publishing Co., Pennsylvania, Edited by Vasilev, V. V.
- (25.) Hajela P., and Lee, E., 1997, "Topological Optimization of Rotorcraft Subfloor Structures for Crashworthiness Considerations," *Computers and Structures*, 64: 65-76.
- (26.) Haslinger, J. and Jedelsky, D., 1996, "Genetic Algorithms and Fictitious Domain Based Approaches in Shape Optimization," *Structural Optimization*, 12:257-264.
- (27.) Hibbit, Karlsson & Sorensen, 1997 "ABAQUS/Standard User Manual 5.8".
- (28.) Holland J. 1975, *Adaptation in Natural and Artificial Systems*, Ann Arbor: University of Michigan Press.
- (29.) Jones, R. M., 1999, *Mechanics of Composite Materials*, Second Edition, Taylor and Francis, Philadelphia.

- (30.) Keane, A., 1995, "Passive Vibration Control via Unusual Geometries: The Application of Genetic Algorithm Optimization to Structural Design," *Journal of Sound and Vibration*, 185: 441-453.
- (31.) Khot N., and Veley D., 1991, "Use of Robustness Constraints in the Optimum Design of Space Structures", *Journal of Intelligent Material System and Structures*, 2:161-176.
- (32.) Kosigo, N., Watson, L., Gurdal, Z. and Haftka, R., 1993, "Genetic Algorithms with Local Improvement for Composite Laminate Design," *Struct. & Controls Opt.*, ASME, Aero. Div., 38:13-28.
- (33.) Kuschel, N., Rackwitz, R., 1998 "Two Basic Problems in Reliability-Bases Structural Optimization", *Mathematical Methods of Operations Research*, 46: 309-333.
- (34.) Le Riche, T. and Haftka, R., 1993, "Optimization of Laminate Stacking Sequence for Buckling Load Maximization by Genetic Algorithm," *AIAA J* 31:951-956.
- (35.) Lee, C., 1998, "A Continuum-Based Shell Element For Laminated Composites Under Large Deformation", Ph.D. Dissertation, Michigan State University, E. Lansing, MI.
- (36.) Lee, C., 1998, A Continnum-Based Shell Element for Laminated Composites under Large Deformation, Ph.D. Dissertation, Michigan State University, East Lansing, MI.
- (37.) Liu, D., 1988, "Impact-induced Delamination- A View of Bending Stiffness Mismatching", *Journal of Composite Materials*, 30: 1539-1561.
- (38.) LSTC/KBS2, 1999, "LS-DYNA User's Manual".
- (39.) Mallot B., Averill R., Goodman E., Ding Y., and Punch III W., 1996, "Use of Genetic Algorithms for Optimal Design of Laminated Composite Cantilever Sandwich Panels with Bending-Twisting Coupling", presented at *AIAA SDM* (Structures, Dynamics and Materials).

- (40.) Mares, C. and Surace, C., 1996, "An Application of Genetic Algorithms to Identify Damage in Elastic Structures" *Journal of Sound and Vibration*, 195:195-215.
- (41.) Mayer, R., Kukuchi, N., and Scott, R., 1996, "Application of Topological Optimization Techniques to Structural Crashworthiness", *International Journal for Numerical Methods in Engineering*, 39:1383-1403.
- (42.) Nakaishi, Y. and Nakagiri, S., 1996, "Optimization of Frame Topology Using Boundary Cycle and Genetic Algorithm," *JSME International Journal*, 39: 279-285.
- (43.) Ochoa, O.O. and Reddy, J.N., 1992, Finite Element Analysis of Composite Laminates, Kluwer Academic Publishers, Netherlands.
- (44.) Parmee, I. and Vekeria, H., 1997, "Co-Operative Evolutionary Strategies for Single Component Design," *Proc. 7th Int. Conf. on Genetic Algorithms*, T. Baeck, ed., Morgan Kaufmann Publishers, San Francisco, 529-536.
- (45.) Prathap, G. and Somashekar, B. R., 1988, "Field and Edge Consistency Synthesis of a 4-Noded Quadrilateral Plate Bending Element", *Int. J. Num. Meth. Eng.*, 26:1693-1708.
- (46.) Punch, W., Averill, R., Goodman, E., Lin, S.-C. and Ding, Y., 1995, "Design Using Genetic Algorithms Some Results for Laminated Composite Structures," *IEEE Expert*, 10:42-49.
- (47.) Punch, W., Averill, R., Goodman, E., Lin, S.-C., Ding, Y. and Yip, Y., 1994, "Optimal Design of Laminated Composite Structures using Coarse-Grain Parallel Genetic Algorithms," *Computing Systems in Eng.*, 5:414-423.
- (48.) Queipo, N., Devarakonda, R. and Humphrey, J., 1994, "Genetic Algorithms for Thermosciences Research: Application to the Optimized Cooling of Electronic Components," *Int. J. of Heat and Mass Transfer*, 37:893-908.

- (49.) Rajan, S., 1995, "Sizing, Shape and Topology Design Optimization of Trusses using Genetic Algorithms," *Journal of Structural Engineering*, 121:1480-1487.
- (50.) Reddy, J.N., 1990, "A Review of Refined Theories of Laminated Composite Plate", *Shock Vibr. Dig.*, 22:3-17.
- (51.) Reddy, J. N., 1993, *An Introduction to the Finite Element Method,* Second Edition, McGraw-Hill, New York.
- (52.) Reissner, E., 1986, "On a Mixed Variational Theorem and Shear Deformation Rectangular Plate Theory", *Int. J. Num. Meth. Eng.*, 23:93-98.
- (53.) Roux, D., Preez, P., Stander, N., 1996, "Design Optimisation of a Semi-solid Tyre using Response Surface Approximations", *Engineering Computations*, 16: 165-184.
- (54.) Sangren, E., Jensen, E., and Welton, J., 1990, "Topological Design of Structural Components using Genetic Optimization Methods," Sensitivity Analysis and Optimization with Numerical Methods, 115:31-43.
- (55.) Soto, C. and Diaz, A., 1993, "Optimum Layout and Shape of Plate Structures using Homogenization," *Topology Design of Structures*, 31:407-420.
- (56.) Sundaresan S., Ishii K., and Houser D., 1992, "Design Optimization For Robustness Using Performance Simulation Programs", *Engineering Optimization*, 20:163-178.
- (57.) Suzuki, K. and Kikuchi, N., 1990, "Shape and Topology Optimization by a Homogenization Method," Sensitivity Analysis and Optimization with Numerical Methods, 115:15-30.
- (58.) Suzuki, K. and Kikuchi, N., 1991, "A Homogenization Method for Shape and Topology Optimization," Computational Methods in Applied Mechanics in Engineering, 93:291-318.

- (59.) Taguchi, G., 1985, "Quality Engineering in Japan", *Proc. CAD/CAM, Robotics and Automation International Conference*, The University of Arizona, Tucson, AZ.
- (60.) Tessler, A. and Hughes, T.J.R., 1983, "An Improved Treatment of Transverse Shear in Mindlin-Type Four-Node Quadrilateral Element", Computer Method In Applied Mechanics and Eng., 39:311-335.
- (61.) Vietor, T., 1997, "Stochastic Optimization for Mechanical Structures", Mathematical Methods of Operations Research, 46: 377-408.
- (62.) Vinson, J.R., 1999, *The Behavior of Sandwich Structures of Isotropic and Composite Materials*, Technomic Publishing Co., Pennsylvania.
- (63.) Wolfersdorf, J., Achermann, E. and Weigand, B., May 1997, "Shape Optimization of Cooling Channels Using Genetic Algorithms," *J. of Heat Transfer*, 119: 380-388.
- (64.) Yang, P.C., Norris C.H., and Stavsky, Y., 1966, "Elastic Wave Propagation in Heterogeneous Plates", *Int. J. Sol. Structures*, 2:665-684.
- (65.) Yip, Y., 1996, "A 3-D Laminated Plate Finite Element with Zig-Zag Sublaminate Approximations For Composites and Sandwich Panels", Ph.D. Dissertation, Michigan State University, E. Lansing, MI.
- (66.) Yip, Y. C. and Averill, R., 1995, "On Modeling Local Damage in Composite Laminates Using Plate Finite Elements with Zig-Zag Sublaminate Approximations", ASME International Mechanical Engineering Congress & Exposition, San Francisco, CA, November 12-17.
- (67.) Yip, Y.C., 1996, A 3-D Laminated Plate Finite Element with Zig-Zag Sublaminate Approximations for Composites and Sandwich Panels, Ph.D. Dissertation, Michigan State University, East Lansing, MI.
- (68.) Zaghloul, S.A. and Kennedy, J.B., 1975, "Nonlinear Behavior of Symmetrically Laminated Plates," *Journal of Applied Mechanics*, Vol. 42:234-236.

(69.) Zenkert, D., 1997, *An Introduction to Sandwich Construction*, EMAS Publishing, London.



.

